

Testing the use of three-dimensional surface rendering and  
mesh-to-mesh comparisons as a method of pair-matching  
commingled human skeletal remains

by

Kamini Pillay

2373351

A dissertation submitted to the Faculty of Health Sciences, University of the Witwatersrand, Johannesburg, in fulfilment of the requirements for the degree of Master of Science in Medicine.

Supervisors:

Dr Anja Meyer, Mr Renier van der Merwe

Johannesburg, 2023



**PLAGIARISM DECLARATION TO BE SIGNED BY ALL HIGHER DEGREE STUDENTS**

SENATE PLAGIARISM POLICY: APPENDIX ONE

I, **Kamini Pillay** (Student number: **2373351**) am a student registered for the degree of **Master of Science in Medicine** in the academic year **2023**.

I hereby declare the following:

- I am aware that plagiarism (the use of someone else's work without their permission and/or without acknowledging the original source) is wrong.
- I confirm that the work submitted for assessment for the above degree is my own unaided work except where I have explicitly indicated otherwise.
- I have followed the required conventions in referencing the thoughts and ideas of others.
- I understand that the University of the Witwatersrand may take disciplinary action against me if there is a belief that this is not my own unaided work or that I have failed to acknowledge the source of the ideas or words in my writing.
- I have included as an appendix a report from "Turnitin" (or other approved plagiarism detection) software indicating the level of plagiarism in my research document.

Signature: 

Date: 14/06/2023

## **Abstract**

When dealing with mass graves, natural disasters, or mass fatalities, forensic anthropology faces a complex scenario that necessitates specific methods for sorting, matching, and identification. The main aim of dealing with commingled human remains is to sort the remains to identify the minimum number of individuals (MNI). Traditional sorting methods, such as visual-pair-matching, articulation, process of elimination, and taphonomy, are well-documented but subjective and rely heavily on the experience and knowledge of the forensic anthropologist.

The study aimed to evaluate the effectiveness three-dimensional surface renderings of bone and the subsequent comparison of mesh-to-mesh values as a more objective and repeatable method for pair-matching commingled human remains. The Structure-from-Motion (SfM) technique was used to create and render 171 three-dimensional mesh model samples using Agisoft Metashape. These models were used to test the effectiveness of a new digital pair-matching method, the mesh-to-mesh value comparison (MVC) method against a South African populated sample. To generate the mesh-to-mesh values, different softwares were used: Viewbox 4.1, which is proprietary and uses a Trimmed Iterative Closest Point (ICP) algorithm to run the program, and Meshlab 2022.12, an open-source software that does not require a license and uses a general ICP algorithm to run the program. Each software was programmed to generate a root mean square value, which was used as the mesh-to-mesh value required for comparison.

Analysis was performed using two techniques: LCV (Lowest Common Value) mesh-to-mesh comparison using Microsoft Excel and ROC curve analysis performed using MedCalc. The LCV mesh-to-mesh comparison requires the user to filter, sort, and eliminate values based on observation using specific commands on Microsoft Excel until the lowest agreed upon value is found across left-right and right-left. The ROC curve analysis on MedCalc follows the principle stated by Delong et al. (1988), which works with a scoring system. The closer the threshold value is to the top-left corner of the graph, the higher the accuracy of the test being performed.

For the complete cadaveric humeri and femora analysis, both elements performed moderately well with the LCV mesh-to-mesh comparison method, while the ROC curve analysis produced considerably higher results, comparatively. For the complete cadaveric bones, the femur performed better with both softwares when compared to the humerus. Mesh-to-mesh values

obtained through Meshlab and analysed with the ROC curve method generated significantly higher results and were more adept at correctly identifying and distinguishing differences between matches and non-matches. Differences in mesh-to-mesh values between sexes and different population groups were observed.

In the simulated fragmented remains, the distal mesh fragment performed the best with 100% sensitivity for Viewbox, and the shaft performed the best using Meshlab with sensitivity results greater than 79%. For the fragmented remains, the distal mesh fragment and the shaft mesh fragments generated significantly high results when using the values obtained through Viewbox and statistically analysed with the ROC curve method.

The mesh-to-mesh value comparison method was applied to a real-world forensic commingled assemblage with high fragmentation and taphonomically altered bones. The Structure-from-Motion technique was effective in capturing distinct details on bones, aiding in 3D modelling. However, the method failed to identify true positive matches in the humeri bone sample, as there were no individuals matched with visual pair matching in the original case.

In conclusion, the mesh-to-mesh value comparison method has the potential to improve the accuracy and objectivity of forensic anthropology in handling commingled human remains. By utilizing advanced technologies like SfM, ROC curve analysis, and real-world forensic commingled assemblages, this method can be applied to enhance the accuracy and reliability of forensic anthropological research.

## **Acknowledgements**

Funding was received from the National Research Foundation (NRF), General Masters scholarship (IMPC) (reference number: MND210609609559) and from the J.J.J. Smieszek fellowship Scholarship within the School of Anatomical Sciences and the FRC (Faculty Research Committee) grant, both from the University of the Witwatersrand. Funding was used to obtain the camera, tripod, and turntable for the Structure-from-Motion technique.

# Table of Contents

Abstract.....	iii
Acknowledgements .....	v
List of Figures.....	viii
List of Tables .....	x
<b>1 Introduction.....</b>	<b>1</b>
<b>2 Literature Review .....</b>	<b>3</b>
<b>2.1 Different approaches to sorting commingled remains.....</b>	<b>3</b>
2.1.1 Visual pair-matching .....	4
2.1.2 Osteometric analysis .....	5
2.1.3 Mesh-to-mesh value comparison method.....	6
<b>2.2 Different types of three-dimensional (3D) modalities .....</b>	<b>8</b>
<b>3 Materials and Methods.....</b>	<b>12</b>
<b>3.1. Materials.....</b>	<b>12</b>
<b>3.2. Methods.....</b>	<b>14</b>
3.2.1. Structure-from-Motion (SfM) surface modelling .....	14
3.2.2. Simulated ‘sliced’ fragmented remains.....	21
3.2.3. Mirrored image mesh models using Meshlab 2022.2.....	24
3.2.4. Mesh-to-mesh value comparison using Meshlab.....	25
3.2.5. Mesh-to-mesh value comparison and Viewbox 4.1. Beta .....	28
3.2.6. Mesh-to-mesh value comparison analysis.....	30
<b>3.3. Data Analysis.....</b>	<b>31</b>
3.3.1. Intra-observer and Inter-observer error .....	31
3.3.2. Normality and Descriptive Statistic Analysis .....	31
<b>4 Results .....</b>	<b>35</b>
<b>4.1. Intra and Inter-observer error analysis.....</b>	<b>35</b>
4.1.1. LCV mesh-to-mesh comparison femora .....	35
4.1.2. Femora ROC curve intra and inter-observer error analysis.....	37
4.1.3. LCV Humeri.....	41
4.1.4. ROC Humeri .....	43
<b>4.2. Cadaveric Femora Mesh Comparison Sample.....</b>	<b>46</b>
4.2.1. Normality test.....	46
4.2.2. LCV Analysis.....	47
4.2.3. ROC Analysis .....	48

4.2.4. LCV demographical analysis .....	50
4.2.5. ROC demographical analysis.....	52
<b>4.3. Cadaveric Humeri Mesh Comparison Sample.....</b>	<b>54</b>
4.3.1. Normality test.....	55
4.3.2. LCV Analysis.....	55
4.3.3. ROC Analysis .....	56
4.3.4. LCV demographical analysis .....	58
4.3.5. ROC demographical analysis.....	59
<b>4.4. Comparative analysis between femora and humeri results .....</b>	<b>61</b>
<b>4.5. Cadaveric Fragmented Femora Mesh Comparison Sample.....</b>	<b>62</b>
4.5.1. Group 1 - Proximal Mesh Sample .....	63
4.5.2. Group 2 - Distal Mesh Sample .....	65
4.5.3. Group 3 - Shaft only Mesh Sample.....	67
<b>4.6. Cadaveric Fragmented Humeri Mesh Comparison Sample.....</b>	<b>69</b>
4.6.1. Group 1 – Proximal Mesh Sample.....	69
4.6.2. Group 2 – Distal Mesh Sample .....	71
4.6.3. Group 3 – Shaft only Mesh Sample.....	73
<b>4.7. Commingled Forensic Mesh Comparison.....</b>	<b>75</b>
4.7.1. Femora Mesh .....	76
4.7.2. Humeri Mesh .....	77
<b>5 Discussion.....</b>	<b>79</b>
<b>5.1. Comparative analysis of the three-dimensional femora and humeri models created using Structure-from-Motion.....</b>	<b>79</b>
<b>5.2. The assessment of the effects of the mesh-to-mesh value comparison method on fragmentary remains. ....</b>	<b>82</b>
<b>5.3. The real-world application of the mesh-to-mesh value comparison on a small scaled commingled forensic collection. ....</b>	<b>84</b>
<b>5.4. LCV mesh-to-mesh comparison method analysis vs ROC curve statistical analysis.....</b>	<b>85</b>
<b>5.5. The potential use of 3D editing softwares: Viewbox 4.1 and Meshlab 2022.12.....</b>	<b>86</b>
<b>6 Conclusion .....</b>	<b>88</b>
<b>7. References.....</b>	<b>90</b>
<b>Appendix A: Agisoft Metashape Photogrammetry Process.....</b>	<b>97</b>
<b>Appendix B: Viewbox Femora ROC curve graphs.....</b>	<b>116</b>
<b>Appendix C: Meshlab Femora ROC curve graphs.....</b>	<b>120</b>
<b>Appendix D: Viewbox Humeri ROC curve graphs .....</b>	<b>124</b>
<b>Appendix E: Meshlab Humeri ROC curve graphs.....</b>	<b>128</b>

## List of Figures

Figure 3.1. Examples of the four different surface viewpoints of the femur captured for generating the mesh model (left-right: A - medial, B - posterior, C - lateral, D - anterior). .....	15
Figure 3.2. Examples of the four different surface viewpoints of the humerus captured for generating the mesh model (left-right: A - medial, B - anterior, C - lateral, D - posterior).....	16
Figure 3.3. Model rendering of a sparse point cloud indicating camera alignment and positioning in Agisoft Metashape. ....	17
Figure 3.4. Model rendering of a sparse point cloud in Agisoft Metashape. ....	17
Figure 3.5. Model rendering of a mesh model in Agisoft Metashape.....	20
Figure 3.6. Model rendering of a dense point cloud in Agisoft Metashape. ....	19
Figure 3.7. A completed 3D model with texture added using Agisoft Metashape. ....	20
Figure 3.8. Examples of the fragmented femora sample from each group were used for the study. ....	22
Figure 3.9. Examples of the fragmented humeri sample from each group used for the study.....	23
Figure 3.10. Flowchart describing the process of creating a mirrored model rendering in Meshlab....	25
Figure 3.11. Alignment and selection of points on Meshlab 2022.2 software.....	26
Figure 3.12. The set criteria were used for determining the root mean square differences between the two meshes.....	27
Figure 3.13. Determining the Hausdorff distance (average error) using Meshlab.....	28
Figure 3.14. Set parameters used for comparison for Viewbox 4.1. Beta Version software. ....	29
Figure 3.15. Statistical equations to test the sensitivity and specificity of the mesh-to-mesh value comparison method (Loong, 2003; Karell et al., 2019). ....	32
Figure 4.1. Viewbox femora intra-observer (IA) bilateral analysis, bilateral and unilateral mesh-to-mesh value ROC curves analysis comparison .....	38
Figure 4.2. Viewbox interobserver (IE) femora bilateral analysis and bilateral and unilateral mesh-to-mesh value ROC analysis comparison. ....	39
Figure 4.3. Meshlab femora intra-observer (IA) bilateral, bilateral and unilateral mesh-to-mesh analysis ROC curve analysis comparison. ....	39
Figure 4.4. Meshlab interobserver femora bilateral analysis and bilateral and unilateral mesh-to-mesh value ROC analysis comparison. ....	40
Figure 4.5. Viewbox humeri intra-observer (IA) bilateral and bilateral and unilateral mesh-to-mesh value ROC analysis comparison. ....	43
Figure 4.6. Viewbox humeri inter-observer (IE) bilateral and bilateral and unilateral mesh-to-mesh value ROC analysis comparison. ....	44
Figure 4.7. Meshlab humeri intra-observer (IA) bilateral and bilateral and unilateral mesh-to-mesh value ROC analysis comparison. ....	45
Figure 4.8. Meshlab humeri inter-observer (IE) bilateral and bilateral and unilateral mesh-to-mesh value ROC analysis comparison. ....	46
Figure 4.9. Viewbox Cadaveric femora bilateral and bilateral and unilateral mesh-to-mesh value ROC analysis comparison. ....	49
Figure 4.10. Meshlab Cadaveric femora bilateral and bilateral and unilateral mesh-to-mesh value ROC analysis comparison.....	50
Figure 4.11. Viewbox humeri bilateral and bilateral and unilateral mesh-to-mesh value ROC analysis comparison.....	57
Figure 4.12. Meshlab humeri bilateral and bilateral and unilateral mesh-to-mesh value ROC analysis comparison.....	57
Figure 4.13. Viewbox and Meshlab femora proximal fragment mesh-to-mesh value ROC analysis comparison.....	64

Figure 4.14. Viewbox and Meshlab femora distal fragment mesh-to-mesh value ROC analysis comparison.....	66
Figure 4.15. Viewbox and Meshlab femora shaft fragment mesh-to-mesh value ROC analysis comparison.....	69
Figure 4.16. Viewbox and Meshlab humeri proximal fragment mesh-to-mesh value ROC analysis comparison.....	71
Figure 4.17. Viewbox and Meshlab humeri distal fragment mesh-to-mesh value ROC analysis comparison.....	73
Figure 4.18. Viewbox and Meshlab humeri shaft fragment mesh-to-mesh value ROC analysis comparison.....	75

## List of Tables

Table 3.1. Demographic distribution of the skeletal cadaveric sample used for the study .....	12
Table 3.2. Image specifications for Structure-from-Motion .....	14
Table 3.3. Contains all the anatomical landmarks and feature points that were removed to illustrate a fragmented femora bone. ....	22
Table 3.4. Contains all the anatomical landmarks and feature points that were removed to illustrate a fragmented humeri bone. ....	23
Table 4.1. Intra and inter-observer femora results using the LCV mesh-to-mesh comparison with Viewbox and Meshlab.....	36
Table 4.2. Intra and inter-observer femora sensitivity, specificity, PPV and NPV values using the LCV mesh-to-mesh comparison with Viewbox and Meshlab. ....	37
Table 4.3. Intra and inter-observer humeri results using the LCV mesh-to-mesh comparison with Viewbox and Meshlab.....	41
Table 4.4. Intra and inter-observer humeri sensitivity, specificity, PPV and NPV values using the LCV mesh-to-mesh comparison with Viewbox and Meshlab. ....	42
Table 4.5. Femora complete cadaver mesh results using the LCV mesh-to-mesh comparison with Viewbox and Meshlab.....	47
Table 4.6. Femora complete cadaver mesh sensitivity, specificity, PPV and NPV values using the LCV mesh-to-mesh comparison with Viewbox and Meshlab.....	48
Table 4.7. Femora complete cadaver mesh LCV demographical sensitivity and specificity for the bilateral sample and bilateral and unilateral sample using the Viewbox. ....	51
Table 4.8. Femora complete cadaver mesh LCV demographical sensitivity and specificity for the bilateral sample and bilateral and unilateral sample using the Meshlab. ....	52
Table 4.9. Femora complete cadaver mesh ROC demographical sensitivity and specificity for the bilateral sample and bilateral and unilateral sample using the Viewbox. ....	53
Table 4.10. Femora complete cadaver mesh ROC demographical sensitivity and specificity for the bilateral sample and bilateral and unilateral sample using the Meshlab. ....	54
Table 4.11. Humeri complete cadaver mesh results using the LCV mesh-to-mesh comparison with Viewbox and Meshlab.....	55
Table 4.12. Humeri complete cadaver mesh sensitivity, specificity, PPV and NPV values using the LCV mesh-to-mesh comparison with Viewbox and Meshlab.....	56
Table 4.13. Humeri complete cadaver mesh LCV demographical sensitivity and specificity for the bilateral sample and bilateral and unilateral sample using the Viewbox. ....	58
Table 4.14. Humeri complete cadaver mesh LCV demographical sensitivity and specificity for the bilateral sample and bilateral and unilateral sample using the Meshlab. ....	59
Table 4.15. Humeri complete cadaver mesh ROC demographical sensitivity and specificity for the bilateral sample and bilateral and unilateral sample using the Viewbox. ....	60
Table 4.16. Humeri complete cadaver mesh ROC demographical sensitivity and specificity for the bilateral sample and bilateral and unilateral sample using the Meshlab. ....	61
Table 4.17. Fragmented proximal femora mesh results using the LCV mesh-to-mesh comparison with Viewbox and Meshlab.....	63
Table 4.18. Fragmented proximal femora mesh sensitivity, specificity, PPV and NPV values using the LCV mesh-to-mesh comparison with Viewbox and Meshlab.....	64
Table 4.19. Fragmented distal femora mesh results using the LCV mesh-to-mesh comparison with Viewbox and Meshlab.....	65
Table 4.20. Fragmented distal femora mesh sensitivity, specificity, PPV and NPV values using the LCV mesh-to-mesh comparison with Viewbox and Meshlab.....	66

Table 4.21. Fragmented shaft femora mesh results using the LCV mesh-to-mesh comparison with Viewbox and Meshlab.....	67
Table 4.22. Fragmented shaft femora mesh sensitivity, specificity, PPV and NPV values using the LCV mesh-to-mesh comparison with Viewbox and Meshlab.....	68
Table 4.23. Fragmented proximal humeri mesh results using the LCV mesh-to-mesh comparison with Viewbox and Meshlab.....	70
Table 4.24. Fragmented proximal humeri mesh sensitivity, specificity, PPV and NPV values using the LCV mesh-to-mesh comparison with Viewbox and Meshlab.....	70
Table 4.25. Fragmented distal humeri mesh results using the LCV mesh-to-mesh comparison with Viewbox and Meshlab.....	72
Table 4.26. Fragmented distal humeri mesh sensitivity, specificity, PPV and NPV values using the LCV mesh-to-mesh comparison with Viewbox and Meshlab.....	72
Table 4.27. Fragmented shaft humeri mesh results using the LCV mesh-to-mesh comparison with Viewbox and Meshlab.....	74
Table 4.28. Fragmented shaft humeri mesh sensitivity, specificity, PPV and NPV values using the LCV mesh-to-mesh comparison with Viewbox and Meshlab.....	74
Table 4.29. The number of true and false positive and negative results obtained through Viewbox 4.1 and Meshlab 2022.12. ....	76
Table 4.30. Statistical sensitivity, specificity, PPV and NPV values obtained for the LCV method using Viewbox 4.1 and Meshlab 2022.12.....	77
Table 4.31. The number of true and false positive and negative results obtained through Viewbox 4.1 and Meshlab 2022.12 for the humeri commingled sample. ....	78
Table 4.32. Statistical sensitivity, specificity, PPV and NPV values obtained for the LCV method using Viewbox 4.1 and Meshlab 2022.12 for the humeri commingled sample.....	78

# 1 Introduction

Mass victim fatalities can be found in many unexpected and devastating situations, often resulting in the inadvertent commingling of human remains. Remains may be found in different stages of decomposition and may present with soft tissue (e.g., skin and muscle tissue) or as hard tissue (e.g., skeletal material) (Garrido Varas, 2013). In most cases, the use of mapping and systematic retrieval of commingled remains, followed by primary and secondary methods of identification greatly assist in sorting commingled remains (Garrido Varas, 2013; Keyes *et al.*, 2022). Primary methods of identification typically include fingerprint, dentition, and DNA (deoxyribonucleic acid) analyses and the estimation of the biological profile of skeletonised remains, while secondary methods of identification include tattoos, scars, possessions, and clothing items (Puerto *et al.*, 2021; Keyes *et al.*, 2022). These methods may be applied when working with soft tissue remains but may be problematic when working with completely ossified/skeletonised remains in which these identifiable markers or associated personal effects may not be found. Thus, the process of identification and matching of skeletonised remains to a single individual may become increasingly more difficult.

In forensic anthropology dealing with mass graves, natural disasters or mass fatalities are common occurrences (Garrido Varas, 2013; Karell, 2019; Orr, 2019). These environments may be very complex, particularly where this concerns commingled human remains which require unique methods to facilitate sorting, matching and eventual identification (L'Abbè, 2005; Adams and Byrd, 2006; Ruotsala, 2016; Fancourt *et al.*, 2021).

Commingled human remains refers to a deliberate or accidental mixing of more than one individual's remains in a single environment (Adams and Byrd, 2006; Lambacher *et al.*, 2016; Ruotsala, 2016). Commingling may occur in fleshed or skeletonised remains, with the latter often further hampered by fragmentation of skeletal elements. When dealing with commingled human remains, the main objective is to sort the remains to ultimately identify the minimum number of individuals (MNI) (L'Abbè, 2005; Adams and Byrd, 2006; Lambacher *et al.*, 2016). Following the main objective, depending on the sample size, preservation, and context of the remains in which it was found, the matching of individual skeletal elements (e.g., right, and left humeri bones) may be attempted.

The traditional sorting methods (visual-pair-matching, articulation, process of elimination and taphonomy) are well-documented and proven to be fairly accurate (L'Abbè, 2005; Adams and

Byrd, 2006; Thomas *et al.*, 2013; Lambacher *et al.*, 2016). However, they are highly subjective and rely substantially on the experience and knowledge of the forensic anthropologist (Fancourt *et al.*, 2021). Thus, developing new ways and strategies that are objective and scientifically testable is necessary while expanding the field of forensic anthropology (Karell *et al.*, 2016; Fancourt *et al.*, 2021; McWhirter *et al.*, 2021). Currently, the field of forensic anthropology is exploring the use of various types of digital platforms to more effectively record macro- and microscopic features of bone and to more objectively analyse these using computer-aided programs and machine learning (Mahfouz *et al.*, 2017; Fancourt *et al.*, 2021; Lucenti *et al.*, 2021; Lynch, 2021; McWhirter *et al.*, 2021). In line with the Daubert criteria, taking this step is essential for advancing precision and objectivity in forensic anthropology (Dirkmaat *et al.*, 2008; Ruotsala, 2016; Fancourt *et al.*, 2021). The Daubert criteria underlines the importance of a repeatable and testable scientific method to substantiate statements with statistical and quantitative assessments. This criterion expresses the importance of a clear scientific method and its use as admissible evidence in a court of law (Dirkmaat *et al.*, 2008).

The study aimed to evaluate the effectiveness of using three-dimensional surface renderings of bone, and the subsequent comparison of mesh-to-mesh values, as a more objective and repeatable method for pair-matching commingled human remains.

Specifically focusing on the following objectives:

1. Develop three-dimensional surface models of left and right humeri and femora of South African male and female skeletal remains, using Structure-from-Motion.
2. To compare the mesh-to-mesh values of left and right humeri and femora, respectively.
3. To test the accuracy, sensitivity, and specificity of the mesh-to-mesh value comparisons for humeri and femora.
4. To test the overall accuracy, reliability, and feasibility of mesh-to-mesh value comparisons on fragmentary remains.
5. To test whether taphonomy alterations affect the statistical validity and reliability of pair-matching by making use of a small forensic sample that presents with commingling.

## 2 Literature Review

### 2.1 Different approaches to sorting commingled remains.

Commingled human remains refer to a deliberate or accidental mixing of more than one individual's remains in a single environment (Adams and Byrd, 2006; Lambacher *et al.*, 2016; Ruotsala, 2016). "Commingled" remains is most commonly found during excavation of sites for development or accidental unearthing of remains (Meyer, 2013; De Bruyn and Meyer, 2018). The remains are generally found scattered, damaged, or fragmented by natural or man-made means (Meyer, 2013; De Bruyn and Meyer, 2018).

According to Lynch, (2021), there are two ways to classify commingled remains, a closed and open commingled assemblage which can further be divided by the scale of the remains found. A closed-commingled assemblage is when the minimum number of individuals in a given environment is known prior to the retrieval of the remains, for example, an aeroplane crash for which a manifest can be used to assist in identifying the number of individuals that should be found (Garrido Varas, 2013; Karell, 2019; Lynch, 2021). The other type is an open commingled assemblage where the minimum number of individuals is unknown and there is a level of uncertainty on how many people may be found, for example, the disinterment of grave sites with archaeological significance or in situations where explosives are involved such as mass terrorist attacks (Garrido Varas, 2013; Karell, 2019; Lynch, 2021).

These two types can further be divided by their scale, a large-scaled commingled assemblage, and a small-scaled commingled assemblage. The scale of the assemblage is categorised by the number of commingled elements present within the environment (Garrido Varas, 2013; Karell, 2019; Lynch, 2021). A small-scaled assemblage is when one or more different bony elements within the sample are commingled (the humerus of five individuals), while a large-scale commingled assemblage occurs when all the elements within the sample are commingled (e.g., the entire skeleton of 20 individuals) (Garrido Varas, 2013; Karell, 2019; Lynch, 2021). In such cases, where there is a large-scale commingled assemblage present, manual and traditional sorting methods become time-consuming and laborious (Garrido Varas, 2013; Karell, 2019; Lynch, 2021). Therefore, the development of digital sorting techniques was created to circumvent these problems and establish new techniques that incorporate knowledge and information from the traditional methods and combines them with different types of programming softwares and equipment.

At present, the general methods used to sort commingled remains involve manual organisation through visual observations, osteometric statistical analyses and in some cases deoxyribonucleic acid (DNA) sequencing analysis (Dirkmaat *et al.*, 2008; Garrido Varas, 2013; Karell, 2019; Lynch, 2021). Each of these techniques has its strengths and limitations. Conventional methods used include visual pair-matching (L'Abbé, 2005; Adams and Byrd, 2006), landmark analysis (Lambacher *et al.*, 2016) and osteometric sorting. Newer methods have explored the use of geometric morphometrics in assessing shape differences and similarities (López-Lázaro *et al.*, 2020; Rohmani *et al.*, 2022), mesh-to-mesh value comparison technique (Karell *et al.*, 2016) and Elliptical Fourier Analysis (Fancourt *et al.*, 2021).

### **2.1.1 Visual pair-matching**

Pair-matching of osteological elements is one of the primary and most common methods currently used to sort commingled human remains. Various techniques have been created to ensure that this method is effectively used (Karell *et al.*, 2016; Fancourt *et al.*, 2021). Pair-matching comprises the relationship between homologous elements (left-right) based on morphological similarities (Adams and Byrd, 2006; Thomas *et al.*, 2013; Fancourt *et al.*, 2021). These similarities between homologous elements provide specific characteristics to each pair.

Visual pair-matching involves the process of manually pair-matching homologous elements based on the observation and experience of the anthropological practitioner analysing/sorting the remains. Landmark analysis focuses on well-known landmarks or osteological features such as articular surfaces and bony processes, which are evident on bone (Lambacher *et al.*, 2016). Visual pair-matching and landmark analysis have a high accuracy rate but can be arduous and subjective and needs a highly experienced qualified practitioner to pair-match the remains (Thomas *et al.*, 2013; Lambacher *et al.*, 2016; Fancourt *et al.*, 2021).

As part of visual pair matching and landmark analysis, articulation of skeletal elements is based upon the approximation of the best fit between congruent skeletal joints e.g., acetabulum of the pelvis and the head of the femur (L'Abbé, 2005; Adams and Byrd, 2006). This method has proven to be effective, however, articulation does have a high degree of variation depending on the skeletal elements associated (Adams and Konigsberg, 2004; L'Abbé, 2005; Adams and Byrd, 2006). For instance, the articular facets like those of the ribs and the body of the sternum may become increasingly problematic with highly fragmented or partial skeletal elements recovered from the site (L'Abbé, 2005; Adams and Byrd, 2006). Inter-individual variation may

further complicate the use of this method, even in cases where close-fitting joints such as the elbow and hip are used. This method is limited in that it can only include bony elements that form a joint (e.g., the humerus and femur cannot be matched/excluded using this method).

The process of elimination generally takes place after the pair-matching and articulation methods have already been conducted, thus any duplication of skeletal elements on the right or left side would indicate another individual and assist with the determination of the MNI (L'Abbè, 2005; Adams and Byrd, 2006). This method becomes very beneficial in small cases of commingling but challenging as the number of potential MNI increases (L'Abbè, 2005; Adams and Byrd, 2006).

Additional visual assessors that can be used to aid in sorting and pair-matching of commingled remains is taphonomy. Taphonomy refers to the factors that may affect the condition of skeletal remains after death, such as depositional factors (fluvial, floral, subaerial activity) and depositional manipulators (faunal and human activity) (Dirkmaat *et al.*, 2008). Taphonomy-based sorting techniques are particularly useful and may be highly individualized in some cases, however this technique is not recommended to be used as a primary sorting technique when working with commingled remains. (L'Abbè, 2005; Adams and Byrd, 2006).

Geometric morphometrics is a statistical analytical method that involves the two-dimensional or three-dimensional comparison and transformation of the surface morphology of objects based on their shape and specific landmark co-ordinates on the object (Garrido Varas, 2013; Karell, 2019; Lynch, 2021). The method uses defined landmarks to extrapolate information about the shape and size of the object while incorporating the Procrustes distance analysis method (Garrido Varas, 2013; Karell, 2019; López-Lázaro *et al.*, 2020; Lynch, 2021; Rohmani *et al.*, 2022). This method has been used to assess estimation of sex (Rohmani *et al.*, 2022) and the sexual dimorphism (López-Lázaro *et al.*, 2020) present in skeletal remains.

### **2.1.2 Osteometric analysis**

The osteometric sorting technique involves metrically comparing osteological measurements through statistical analyses (Garrido Varas, 2013; McCormick, 2016; Byrd and LeGarde, 2018; Lynch, 2021). Osteometric sorting is generally performed by taking precise anatomical measurements such as the length, height, breadth, width, and diameter of the bone by using calibrated measuring tools. Using this method allows for the positive determination in pair-matching and articulating remains while using a quantifiable scientific method that can be

repeated. This method has however been critiqued as it often has a low success rate in excluding bones that do not match because the results are dependent on the reference data set and do not account for the secular changes found within bone growth and development (Adams and Konigsberg, 2004; Adams and Byrd, 2006; Thomas *et al.*, 2013; Bertsatos and Chovalopoulou, 2019; Fancourt *et al.*, 2021).

### **2.1.3 Mesh-to-mesh value comparison method**

The mesh-to-mesh value comparison (MVC) method has become an intriguing new topic of interest in the world of anthropology. The method involves the process of creating a three-dimensional mirror image of the left or right side of a skeletal element model and aligning the model over the opposite respective side of the element using common reference points and identifiable markers (Karell *et al.*, 2016). The method compares the digital geometry of the models and produces an error value which indicates the difference between the two mesh models when aligned, this error value is also considered the mesh-to-mesh value (Karell *et al.*, 2016). The lowest mesh-to-mesh value between both left and right models is considered a positive pair-match between two of the same skeletal elements also known as the Lowest Common Value (LCV) mesh-to-mesh value comparison method (Karell *et al.*, 2016; Karell, 2019).

The superimposing of 3D right and left meshes to generate a root mean square value to produce a difference index has been applied to pair-matching bilateral bones in a commingled assemblage (Karell *et al.*, 2016; Karell *et al.*, 2017; Tsiminikaki *et al.*, 2019; Fancourt *et al.*, 2021; Palamenghi *et al.*, 2023), in pair-matching fragmentary remains (Acuff *et al.*, 2021; McWhirter *et al.*, 2021), in testing against remains at different levels of preservation (Palamenghi *et al.*, 2023), in re-associating articular surfaces (Acuff *et al.*, 2021; Cappella *et al.*, 2022) and in the difference between antemortem and post mortem CT scanned models for identification (Palamenghi *et al.*, 2021). The MVC has produced substantial results in sensitivity and specificity when it comes to pair-matching bilateral bones such as the humerus, temporal, clavicle, calcaneus, phalanges, mandibular fossae, and condyles as well pelvic bones.

The mesh-to-mesh value comparison method has proven to produce positive sensitivity and specificity results in pair-matching similar elements such as the humerus (sensitivity: 95 %; 60 %) (Karell *et al.*, 2016; Karell *et al.*, 2017; Tsiminikaki *et al.*, 2019; Acuff *et al.*, 2021; Fancourt

*et al.*, 2021; McWhirter *et al.*, 2021; Palamenghi *et al.*, 2023). In the study performed by Karell (2019), the humerus, clavicle, temporal and calcaneus bones were compared and analysed using the Lowest Common Value (LCV) mesh-to-mesh value comparison method and Receiver Operator Characteristic (ROC) curve analysis using a Structured Light and Computer Tomography scanner. ROC curve analysis presents a more visual representation of the connection between sensitivity and specificity rates within a sample (Fawcett, 2006; Watson and Petrie, 2010). The results were positive for all bones except the clavicle (sensitivity: 37.74 %; specificity: 43.48 %) (Karell, 2019).

The next-generation osteometric sorting function method which includes Elliptical Fourier Analysis and Hausdorff distance is an improved version of the mesh-to-mesh value comparison method (Fancourt *et al.*, 2021). The method creates a three-dimensional longitudinal outline that curves around the perimeter of the bone using a three-dimensional Elliptical Fourier Analysis (Fancourt *et al.*, 2021). This version reduces the overall size of the model by capturing and comparing the outline of the object only, thus removing any internal matrix data and simplifying the model data used for analysis (Fancourt *et al.*, 2021). The implications of this small change substantially shorten the computational processing time for the model generation and the comparison of the models (Fancourt *et al.*, 2021).

Although this method simplifies the computational processing time and comparison, it still maintains a high accuracy and sensitivity (femur: 100 %; tibia: 91,7 %; humerus: 100 %) rate in anatomically identifying positive pair-matches among commingled situations instead of focusing on excluding bones such as traditional methods. These factors make this method highly advantageous and applicable for field usage (Fancourt *et al.*, 2021). However, may be problematic when working with severely fragmented remains with different levels of preservation since the method relies on extracting the entire outline of the bone for matching which would not be possible for fragmented remains.

In the McWhirter *et al.* (2021) study the three-dimensional surface rendered models were created with a Multi-Slice Computer Tomography (MSCT) scanner from complete cadaveric clavicle bones and sliced into different sections to simulate a fragmented bone. The sensitivity and specificity rates using the LCV method for the acromial fragments (54 %; 40 %), midshaft fragments (31,3 %; 37,3 %) and sternal fragments (65,4 %; 52,6 %) performed moderately. The result may be related to the amount of variation present, and the few bony landmarks present in the shape to assist in the comparison. This technique has proven to be quite valuable,

however, there are limitations to its use in the field. The method involves the use of expensive equipment (Computer tomography and Structured Light scanners) and generally is time-consuming, specifically for the generation of the mesh models (Fancourt *et al.*, 2021).

The effects of the different states of preservation on the superimposition of 3D meshes have been assessed by pair-matching iliac bones by Palamenghi *et al.* (2023). In their study, the authors introduced a small sample of bones at what was considered optimal and suboptimal preservation of remains. For each match, a root mean square value was generated. According to their study, they found that the root mean square values of the less/poorly preserved models were considerably higher compared to the better- and well-preserved models, which may result in a high number of false positives being generated and a decrease in sensitivity rates.

## **2.2 Different types of three-dimensional (3D) modalities**

Incorporating three-dimensional technology and forensic anthropology has become an increasingly fascinating topic of interest among anthropologists. These techniques have been used to establish differences between sex, population groups and age among skeletal remains. In recent years, there have been many advances in introducing three-dimensional technology to assist in the sorting and identification of commingling among skeletal human remains.

### **2.2.1. Photogrammetry and Structure-from-Motion (SfM)**

Photogrammetry incorporates information about the surface morphology of an object or structure using a set of photographs, creating a model that contains in-depth information about the object or structure's visual and spatial characteristics (Schenk, 2005; Urbanova *et al.*, 2015; Ruotsala, 2016; Lussu and Marini, 2020). Photogrammetry has been around since 1839, alongside the invention of photography (Schenk, 2005; Lussu and Marini, 2020). Over the years, photogrammetry has advanced with the advancement of technology thus enabling this technique to be more associated with various disciplines. Photogrammetry has evolved into four generations: first, analogue, analytical, and digital - with the latest being the digital generation (Schenk, 2005; Lussu and Marini, 2020). Each phase has a historical significance and impact on how we use photogrammetry today. The analogue phase introduced the concept of stereophotogrammetry, and the digital phase allowed the use of digital images instead of aerial photographs (Schenk, 2005). While photogrammetry has made many improvements over the years, the most recent is Structure-from-Motion. Structure-from-Motion (SfM) is a

photogrammetric technique that differs from conventional photogrammetry in the sense that it does not require prior position information of an object (Westoby *et al.*, 2012; Fonstad *et al.*, 2013; Ruotsala, 2016).

For instance, a study explored different approaches to using SfM and Structured Light techniques to analyse the accuracy, efficiency, and time consumption of the different approaches (Adamopoulos *et al.*, 2021). The study was conducted by using different types of three-dimensional structured light scanners and cameras (android phones and DSLR cameras), the time taken for each surface renderings to build the mesh and texture model was observed and recorded (Adamopoulos *et al.*, 2021). Adamopoulos *et al.*, (2021), demonstrated the potential of using affordable photogrammetry and scanning techniques to obtain a good quality model.

Another study examined the accuracy of using SfM to pair-match lower limb bones in a large, commingled assemblage using CSG (Cross-Sectional Geometric) properties (Bertsatos and Chovalopoulou., 2020). In the study, the sample included 396 femora and 422 tibias (pathological conditions included) obtained from the Athens Collection housed at the National and Kapodistrian University of Athens (Bertsatos and Chovalopoulou., 2020). Each bone in the sample is processed by using the long bone diaphyseal CSG-Toolkit which demonstrates and extracts the anatomical orientation and descriptive statistical information of the bone. The variable descriptive statistics used extracts geometric information along the shaft of the bone at percentages along the entire length of the bones.

The differences between the descriptive statistical information provided for the right and left were compared to establish possible pair matches. Once possible pair matches have been established, they are subdivided and given an accumulative z-score value (similarity-dissimilarity measure) (Bertsatos and Chovalopoulou., 2020). A true pair match is finally determined when the lowest z-score value among the possible pair-matches between any two right and left sides of the bone is found (Bertsatos and Chovalopoulou., 2020). The study evaluated bilateral and unilateral elements as well as the variability in the size of the commingled assemblage. The analysis of the sensitivity of the femora was found to be 1 while the tibias were 0.997. The study produced successful results and demonstrated the effectiveness of the method on complete bones. The size of the commingled assemblage did not affect the sensitivity (Bertsatos and Chovalopoulou., 2020).

### **2.2.2. Structured Light**

The structured light method uses an image-based scanner that projects a series of light patterns onto the object of focus with an array of cameras. This method captures the three-dimensional geometry of the object by using the information from how the patterns are presented after being distorted by the location to obtain a three-dimensional model with shape, size, and colour information (Bell *et al.*, 1999; Chan *et al.*, 2016; Reichert *et al.*, 2016; Chan *et al.*, 2020). Structured light scanners have been used in archaeology to document and reconstruct digital models of excavation sites and archaeological human remains recovered from the sites (McPherron *et al.*, 2009; Randolph-Quinney *et al.*, 2018; Siebke *et al.*, 2018). In forensic anthropology, the technique has been used to reconstruct three-dimensional models of cadaveric remains to assist in building a biological profile, such as age estimation (e.g., Kotěrová *et al.*, 2019; Joubert *et al.*, 2020), sex estimation (e.g., Kotěrová *et al.*, 2019; Cae *et al.*, 2021) There have been a few studies that have tested the effectiveness of structured light techniques in sorting commingled remains through pair-matching of bilateral elements in a limited sample (Karell *et al.*, 2016; Karell *et al.*, 2019; Fancourt *et al.*, 2020).

### **2.2.3. Laser scanning**

Laser scanners function on the principle of laser triangulation systems that consists of two parts: the positioning laser and the detector. The laser is projected onto an object and reflected at an angle that is able to capture the surface morphology of the object accurately through a set of point clouds (Carew and Errickson, 2019). Laser scanners are employed in a variety of industries and are frequently compared to various forms of photogrammetry (Nuttens *et al.*, 2011). Archaeologists use laser scanners to document and model information at archaeological excavation sites in a non-invasive manner (Nuttens *et al.*, 2011; Siebke *et al.*, 2018). In forensic anthropology, the technique has been used to create three-dimensional models of human skeletal elements to aid in the development of a biological profile (e.g., Lee and Gerdau-Radonic, 2020), capturing taphonomically alterations on bones (e.g., Randolph-Quinney *et al.*, 2018), trauma damage, and re-associating fragmented remains (e.g., Jani *et al.*, 2020).

### **2.2.4. Lodox scan**

Lodox scanners is a low dose X-ray machine that produces minimal distortion along the y-axis to generate highly detailed full body scans. The machine has an X-ray tube situated on one end of the arm and an image receptor at the other end. A beam is produced by the machine's C-arm

which is perpendicular to its movement along the horizontal direction of the object (Stull *et al.*, 2013; Mamabolo, 2020). The Lodox machine, a South African creation, is used to examine human remains in forensic pathology and anthropology, particularly for identification in forensic mortuaries (Keyes *et al.*, 2022). At present, there are no studies assessing the efficacy of Lodox equipment in matching bilateral elements when sorting mixed human remains.

### **2.2.5. Computer Tomography (CT) Scan**

Computer Tomography combines a mixture of multidirectional radiographic scans that are processed through a computer to construct cross-sectional images of the bone (Franklin *et al.*, 2016; Carew and Errickson, 2019; Mamabolo *et al.*, 2020). In the beginning, CT imaging mainly focused on deriving 2D images to obtain morphological information, however over time, the development of Multi-Slice Computer Tomography (MSCT) has allowed obtaining shape and size information from 3D images (Franklin *et al.*, 2016; Carew and Errickson, 2019). One of the first applications of CT imaging in anthropology was conducted to investigate the structure and biomechanical properties of fossilised hominid skeletal remains (Franklin *et al.*, 2016; Carew and Errickson, 2019). Computer Tomography has become a widely popular and common technique used in a majority of applications in forensic anthropology. Numerous applications have been conducted in the study of age, ancestry, sex, and stature estimation of skeletonized remains and more recently, in the sorting and identifying commingled remains (Karell *et al.*, 2016; Karell *et al.*, 2019; Tsiminikaki *et al.*, 2020; Acuff *et al.*, 2021; McWhirter *et al.*, 2021; Palamenghi *et al.*, 2023a).

The most popular and acceptable types of acquisition techniques spoken in literature for sorting commingled remains are computed tomography (Karell *et al.*, 2016; Karell *et al.*, 2019; Tsiminikaki *et al.*, 2020; Acuff *et al.*, 2021; McWhirter *et al.*, 2021; Palamenghi *et al.*, 2023a) and structured light (Karell *et al.*, 2016; Karell *et al.*, 2019; Fancourt *et al.*, 2020) scanners. These techniques have proven to be quite effective and successful in generating positive sensitivity and specificity rates in pair-matching bilateral bones as demonstrated by Karell *et al.* (2016), Karell *et al.* (2019), Fancourt *et al.* (2020), Tsiminikaki *et al.* (2020), Acuff *et al.* (2021), McWhirter *et al.* (2021) and Palamenghi *et al.* (2023a).

### 3 Materials and Methods

#### 3.1. Materials

The sample comprised the left and right humeri (n=80) and femora (n=80) of 40 adult individuals selected from the Raymond A. Dart Collection of Modern Human Skeletons housed at the School of Anatomical Sciences, Faculty of Health Sciences, University of the Witwatersrand. The Raymond A. Dart Collection of Modern Human Skeletons began as early as the 1920s and houses over 2500 human cadaveric skeletons (Dayal *et al.*, 2009). The collection consists of bequeathed and unclaimed remains (Dayal *et al.*, 2009). The sample included male and female individuals aged between 19 to 70 years of southern African black and white population affinity. The sample demographics were chosen to ensure inter-and intra-sex and population variability across the adult lifespan. An equal distribution of male and female individuals from each population group was obtained to maintain the consistency of results (Table 3.1).

**Table 3.1. Demographic distribution of the skeletal cadaveric sample used for the study.**

	Population groups (Southern Africans)		Sex		Age (Years)				
					18 - 30	31- 40	41- 50	51- 60	61- 70
<b>Humerus</b>	Black	20	Male	10	1	2	5	2	0
			Female	10	3	5	2	0	0
	White	20	Male	10	0	0	2	5	3
			Female	10	2	0	3	4	1
<b>Total</b>		<b>40</b>		<b>40</b>	<b>6</b>	<b>7</b>	<b>12</b>	<b>11</b>	<b>4</b>
<b>Femur</b>	Black	20	Male	10	1	2	5	2	0
			Female	10	4	4	2	0	0
	White	20	Male	10	0	1	2	4	3
			Female	10	2	0	3	4	1
<b>Total</b>		<b>40</b>		<b>40</b>	<b>7</b>	<b>7</b>	<b>12</b>	<b>10</b>	<b>4</b>

The criteria for selection included individuals with 100 % completeness of bilateral humeri and femora. Skeletal elements that presented with pathological conditions (e.g., severe osteoarthritis, dislocations, misalignment, congenital deformities, osteomalacia, residual rickets, cancer), ante-mortem trauma and/or curatorial damage were excluded. Bones that were large and textured with distinct features were included to simplify the modelling process. The study sample was divided into two subsamples; one representing complete skeletal elements (complete surface meshes for humeri and femora) and a simulated fragmentary sample (representing meshes that excluded the proximal and/or distal ends of the humeri and femora).

In addition to the study sample, a small commingled forensic sample consisting of a minimum number of 11 individuals was also examined to test the effectiveness of the method in a sample that presented with some taphonomic alterations and incompleteness/fragmentation of the proximal and distal ends of the femora and/or humeri. The skeletonized remains of various individuals were discovered in Johannesburg (DR 2026/14) and analysed by the Human Variation and Identification Research Unit (HVIRU) at the University of the Witwatersrand. Only the humeri and femora of these individuals were examined to enable comparison. The sample consisted of 6 (3 left; 3 right) femora and 5 (2 left; 3 right) humeri. The minimum number of individuals (MNI) was originally estimated using the number of crania present, as these were the most frequently occurring skeletal elements, followed by the femur and humerus (Meyer, 2016). Results from the original pair-matching, utilising the methods as outlined by Snow, (1948); Ubelaker, (2002); Byrd and Adams, (2003); L'Abbé, (2005); İşcan and Steyn, (2013), were not able to pair match any of the humeri or femora, suggesting an MNI of 5 for the humeri and 6 for the femora. No pathological conditions and/or trauma were present.

All cadaveric skeletons have been collected under the South African Human Tissue Act No. 65 of 1983 (Dayal *et al.*, 2009). An ethics clearance waiver had been granted to access the Raymond A. Dart Collection of Modern Human Skeletons at the School of Anatomical Sciences. Ethical clearances was obtained from The Human Research Ethics Committee (Medical) have granted ethics approval to access the forensic case needed for the study. Ethics Certificate number: M210715.

## 3.2. Methods

### 3.2.1. Structure-from-Motion (SfM) surface modelling

Structure-from-Motion (SfM) is a photogrammetric technique that works on the fundamentals of stereophotogrammetry. SfM incorporates information about the surface morphology of an object or structure by capturing patterns through the use of photographs. Creating a three-dimensional model that contains in-depth information about the object or structure's visual and spatial characteristics without the use of prior position information of an object (Westoby *et al.*, 2012; Fonstad *et al.*, 2013; Ruotsala, 2016).

All 160 cadaveric and 11 forensic humeri and femora were photographed with a Nikon D5600 DSLR with AF-P 18-55mm DX VR Lens 24-megapixel camera (Table 3.2). A tripod was used to ensure consistency in photograph angles and distances. Each image captured the bone within the full frame. The camera was positioned at an angle ( $20^{\circ}/70^{\circ}$ ) perpendicular to the bone. To ensure that all surfaces of each individual's humeri and femora were captured, there was a 50-70% overlap between each photo. Additionally, the skeletal elements were placed onto a rotating table to get  $360^{\circ}$  images for all four bone surfaces (anterior, posterior, medial, and lateral). A black cloth was used as a backdrop to conceal any unnecessary objects. The backdrop also provides a contrast between the background and the bone which assists in adding the masks (described below) to each individual image.

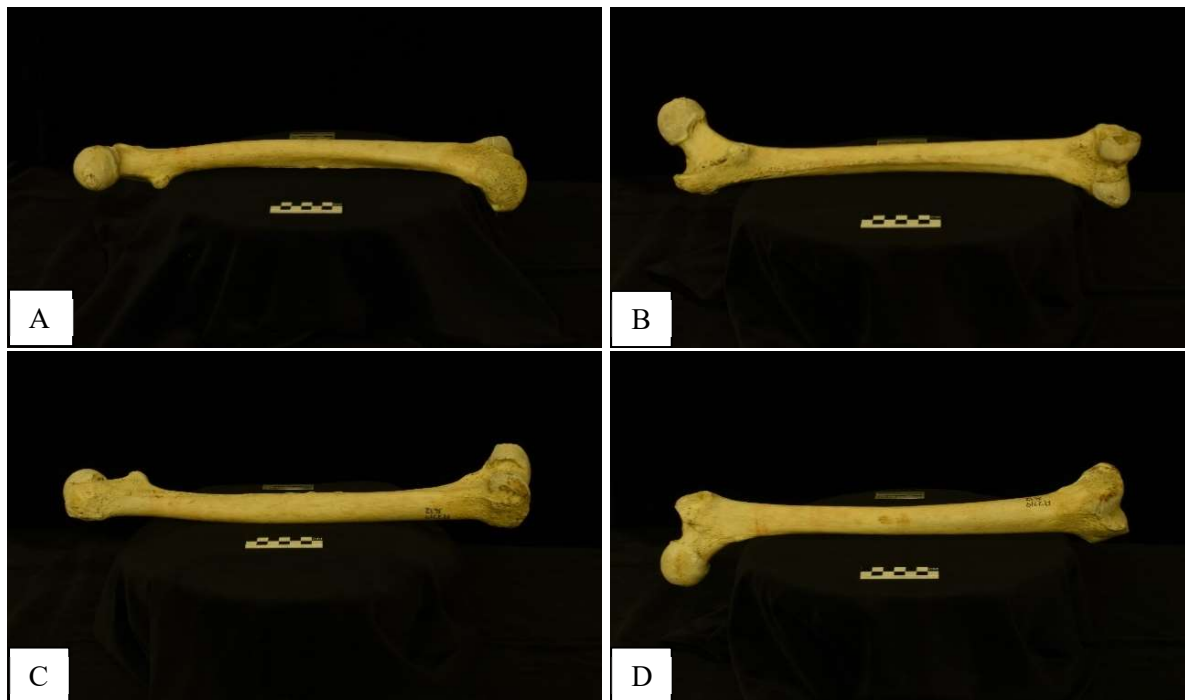
**Table 3.2. Image specifications for Structure-from-Motion**

Image Specifications	
ISO	200
Shutter speed	1.3 – 2
Aperture	f/29
Megapixels	24
Lens focal length	34 - 35 mm
Image resolution	6000 x 4000
Exposure meter	1.5 – 2

Once the photographs were taken, they were sorted according to the surface viewpoints (medial, posterior, lateral, anterior) taken and uploaded into the modelling software as four different chunks (Figure 3.1 and Figure 3.2). The software used to generate the three-dimensional model was Agisoft Metashape Professional 1.7.3 software. The desktop

specifications containing the software were an Intel Core I5-2400 CPU with 4 cores and a clock speed of 3.10GHz. The graphics card was an AMD Radeon HD 6700 Series (Juniper) and the RAM size of a dual 32GB DDR3 aligned in series. An estimated image quality check was performed on each chunk. A chunk within the software refers to a project that contains a set of photos.

The estimated image quality check is a function on Agisoft Metashape that automatically provides an estimated value on the quality of the images. Images below 0.5 units are considered poorly focused and thus should be removed from the photogrammetric process. All images with a quality check greater than 0.5 were used. Masks were applied to each photo using Adobe Photoshop CS version 8.0 software.



**Figure 3.1. Examples of the four different surface viewpoints of the femur captured for generating the mesh model (left-right: A - medial, B - posterior, C - lateral, D - anterior).**

A mask was used to specify and conceal the area on the image that the software might consider as confusing or interfere with the photo alignment. The application of masks to images improves the quality and speed of image processing as the various algorithms of the software are only applied to unmasked areas.

Once the masks had been applied to each image in a chunk, the photos were aligned according to a generic preselection alignment mode (Figure 3.3). Generic preselection mode automatically aligns a pair of images based on matched overlapping feature points across the

images, which helps in shortening the overall time needed to process the photos. The alignment settings were set to medium accuracy with a key point limit of 80 000 and a tie point limit of 40 000 excluding the stationary tie points. The key point limit indicates the number of feature points to be considered in every image for alignment processing.

The tie point limit indicates the number of matching points and the 40 000 points that are most clearly aligned from the 80 000 points, among the feature points on every image to be considered for alignment (Agisoft, LCC). Stationary points are points that do not change in situations where a turntable and a constant background were being used (Agisoft, LCC).

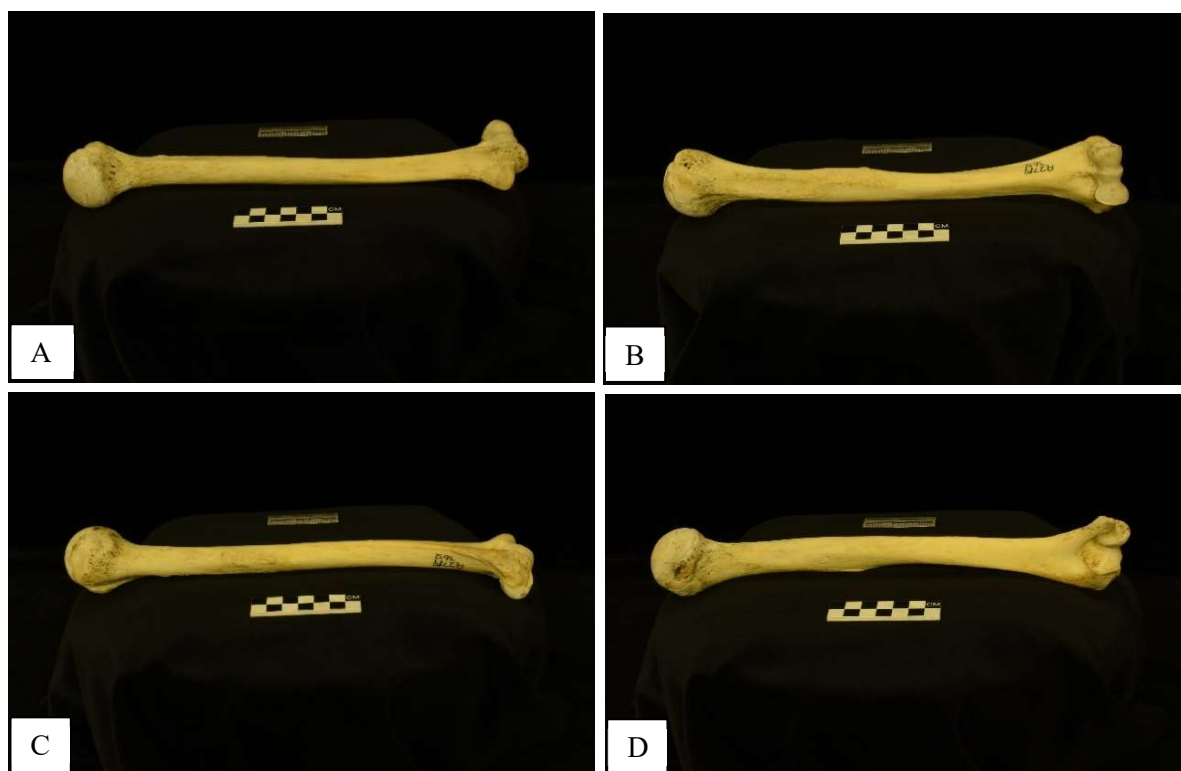


**Figure 3.2. Examples of the four different surface viewpoints of the humerus captured for generating the mesh model (left-right: A - medial, B - anterior, C - lateral, D -**

Excluding the stationary points from the alignment assists in removing false tie points that can occur due to the camera sensor and the lens. The image alignment process generates a sparse point cloud (Figure 3.4). A sparse point cloud is a rough surface reconstruction of the image alignment process.

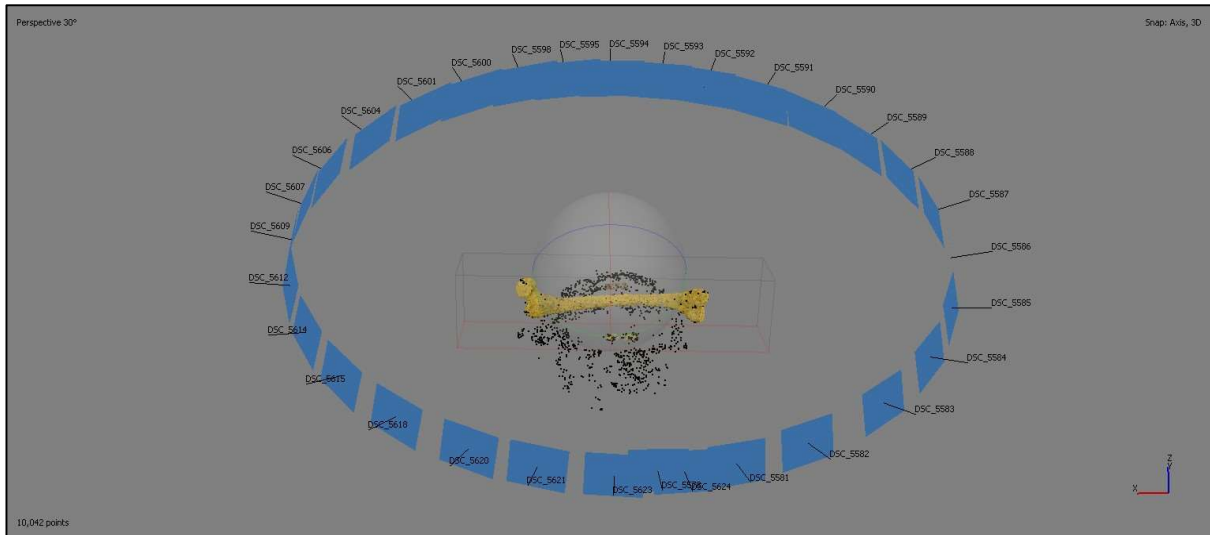


**Figure 3.3. Model rendering of a sparse point cloud indicating camera alignment and positioning in Agisoft Metashape.**

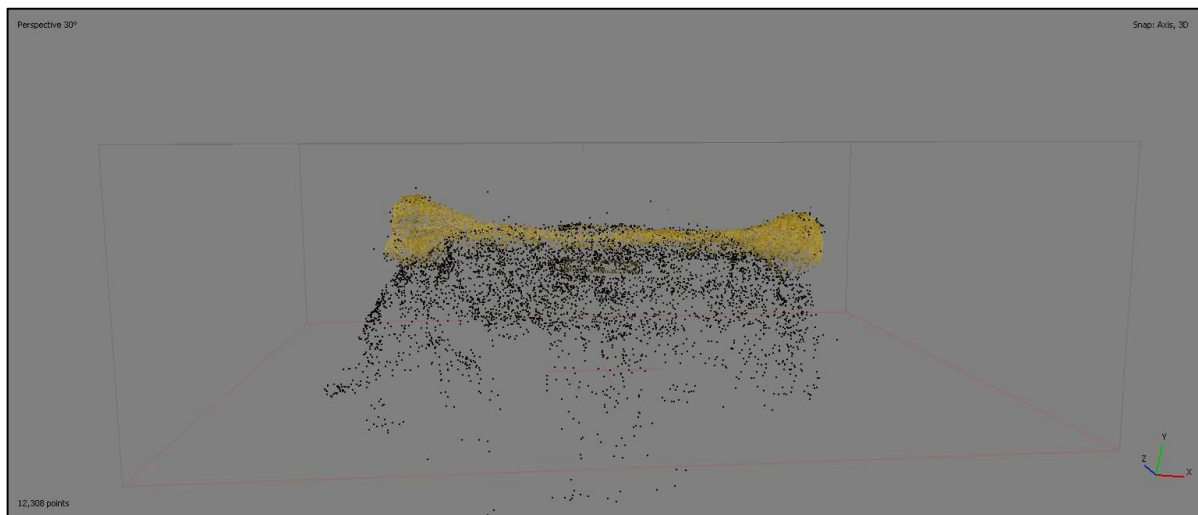


**Figure 3.4. Model rendering of a sparse point cloud in Agisoft Metashape.**

The “align chunks” feature was used to align two or more chunks at once. A point-based matching method with medium accuracy and a key point limit of 40 000 was used for chunk alignment. The lower the accuracy settings, the shorter the time was to align a group of chunks. The chunks were aligned and merged into one 360-degree model (Figure 3.5). If no misalignments were visible, a dense point cloud was built on medium quality with aggressive depth filtering activated. In case of misalignments, manual alignment is necessary for aligning sparse point clouds. The sparse point cloud was manually aligned by marking the same points on multiple photos.

Once the markers have been placed, a marker-based alignment method was chosen. A dense point cloud generates a cloud based on depth maps which are calculated using dense stereo matching of points, this is needed to determine the relative exterior and interior orientation of the bones among the overlapping image pairs (Figure 3.6) (Agisoft, LCC). The depth filtering options were mild, moderate, and aggressive filtering modes. Aggressive depth filtering was used to remove as much of the noise as possible and outlier points from the dense cloud (Agisoft LCC).

This filter removes any noise that may affect the surface mesh morphology and reduces the amount of time needed to clean and edit the dense cloud. The depth filtering method depends on the quality of the sparse point cloud. If the quality is low, the aggressive filtering option may display holes in the dense point cloud that were not previously noticeable through the sparse point cloud. Dense point cloud took an average of 20 minutes for each rendering and was the most time-consuming step of the overall process. After the dense point cloud was built, the rendering had to be cleaned and edited. The rendering was examined and all features such as black dots appearing over the rendering that could affect the mesh comparison analysis were removed. Black dots that appeared around the model was residual points caused by the black background used for the photos. Each dot was selected and deleted to provide a cleaner model.

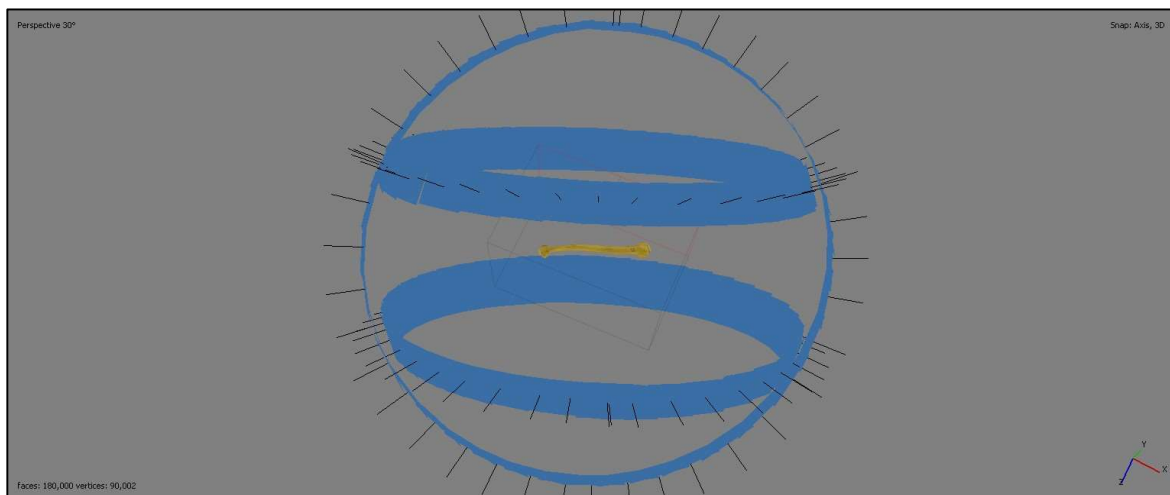


**Figure 3.5. Model rendering of a merged dense point cloud in Agisoft Metashape.**

After editing, a representation of a dense point cloud can be seen in Figure 3.6. After the dense cloud was built, the generated model was scaled. Agisoft does scale each model it generates automatically; however, this scale is an artificial one created during the alignment of the process of the photos thus the scaling of the model will not reflect the object being scanned. To negate this problem, four markers were placed on the scaling bars that were captured in more than two separate photos. Each black and white block on the scaling bar tool represented 1cm. The points were selected on the images and not on the rendering itself to obtain a higher scaling accuracy Agisoft allows the user to place markers in two ways, the markers may be placed on the photos or the dense cloud model. Two marker points at a time were selected to create a scale bar and the distance between the two points was entered as 0.01 m (Agisoft Metashape's default value is in meters and thus all measurements need to be converted to meters.).

Thereafter the mesh was built by using the source data from the dense cloud, arbitrary (3D) surface type information with a high face count, and calculated vertex colours. Arbitrary surface type information was applied since this surface type may be used for any object being modelled without making any assumptions about the type of object being modelled. The interpolation of data was set to default parameters. A representation of the solid mesh structure is illustrated in Figure 3.7.



**Figure 3.6. Model rendering of a dense point cloud in Agisoft Metashape.**

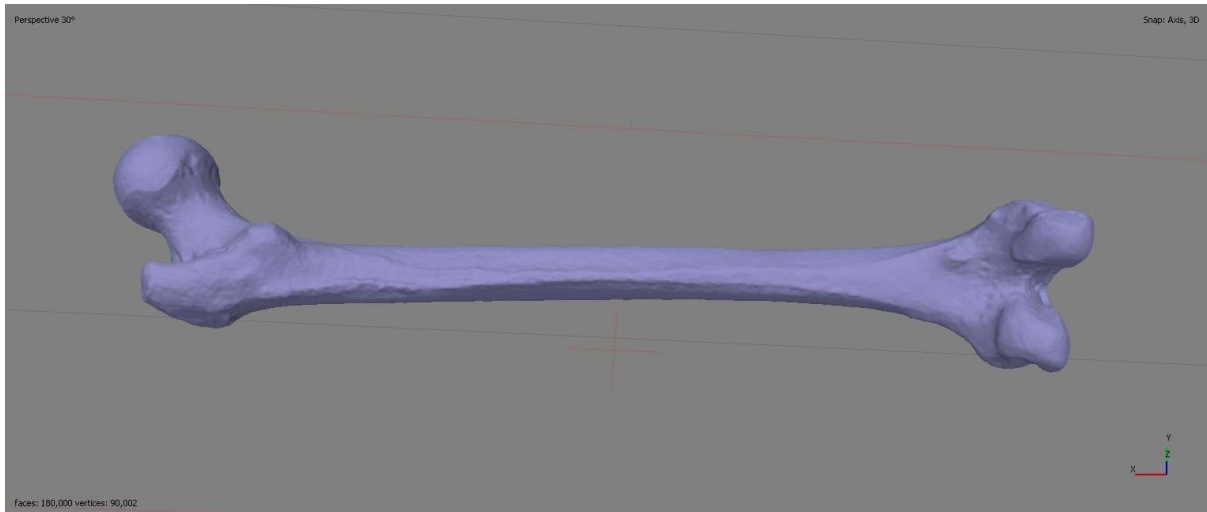


**Figure 3.7. Model rendering of a mesh model in Agisoft Metashape.**

The texture was added to provide a more realistically accurate texture appearance to the rendering. The texture parameters were set to obtain the source data from the images while using a diffuse texture type map, a basic texture map that stores the colours of the surface model. The mapping and blending modes were set to generic and mosaic with a texture size of  $4096 \times 1$ . Default texture size was applied since using higher texture sizes would have used more RAM and was not necessary for this specific study. The hole-filling and ghosting filters were enabled to complete the texturing process. Hole filling was enabled to ensure the mesh model was complete and to avoid any unwanted noise that may affect the mesh comparison. The final result of the rendering process is shown in Figure 3.8.



**Figure 3.8. A completed 3D model with texture added using Agisoft Metashape.**

The files were saved, and each rendering was exported as an alias wavefront object (obj.) format for further mesh comparison on MeshLab. Alias wavefront object (obj.) contains information about the coordinates of the vertices of the triangles and the direction of the normals. The obj file format was exported because the software that is being used only detects obj file formats. For a more illustrative approach to the methodology used in Agisoft Metashape software refer to Appendix A.

### **3.2.2. Simulated ‘sliced’ fragmented remains.**

The three-dimensional surface renderings of the original 40 individuals of each femora and humeri bone sampled (20 males and 20 females) were used to test the overall feasibility of the Structure-from-Motion and mesh-to-mesh value comparison method in pair-matching simulated fragmented humeri and femora. The 160 3D reconstructed surface renderings of the skeletal elements were imported into Agisoft Metashape software and sliced at specific anatomical points (Table 3.3 and Table 3.4) along the proximal and distal ends of the bone to simulate a case of fragmented remains in a commingled assemblage. The humeri and femora samples were divided into three subsample groups: distal part removed, proximal part removed, distal and proximal parts removed (Figure 3.9 and Figure 3.10).

The original projects for each bone model were saved and used for slicing. Each project was imported into Agisoft Metashape. The 3D view settings were set to display the dense point cloud model. The dense point cloud model was sliced at the proximal and distal ends by using the rectangular selection tool to capture the area and removed by using the delete selection tool.

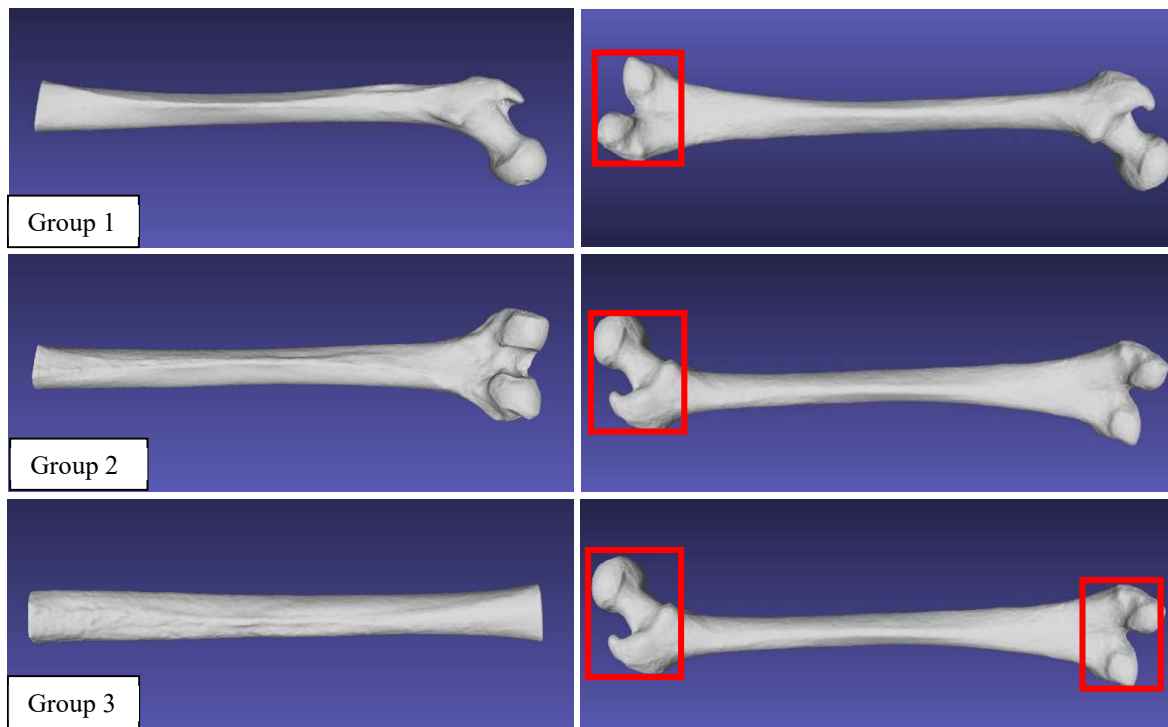


**Figure 3.9. Examples of the fragmented femora sample from each group were used for the study (The red square blocks are the areas that were removed).**

**Table 3.3. The anatomical landmarks and feature points that were removed to illustrate a fragmented femora bone.**

Group 1	Removed the lateral and medial condyles, intercondylar fossa, popliteal groove, lateral and medial epicondyles, adductor tubercle, and popliteal surface. The model was sliced at the origin of the femur's lateral and medial supracondylar lines.
Group 2	Removed the fovea capitis, head, neck, intertrochanteric line, intertrochanteric crest, trochanteric fossa, quadrate tubercle, and greater and lesser trochanter of the femur. The model was sliced at the inferior end of the lesser trochanter of the femur.
Group 3	The model was sliced at the inferior end of the lesser trochanter and the origin of the femur's lateral and medial epicondylar lines. The model consisted only of the shaft of the femur.



**Figure 3.10. Examples of the fragmented humeri sample from each group used for the study (The red square blocks are the areas that were removed).**

**Table 3.4. The anatomical landmarks and feature points that were removed to illustrate a fragmented humeri bone.**

Group 1	Removed the humerus's capitulum, trochlea, coronoid fossa, radial, olecranon fossa, and medial and lateral epicondyles. The model was sliced at the origin of the humerus's medial and lateral supracondylar crests.
Group 2	Removed the head, anatomical neck, and greater and lesser tubercles of the humerus. The model was sliced at the surgical neck of the humerus.
Group 3	The model was sliced at the surgical neck of the humerus and the origin of the humerus's medial and lateral supracondylar crests. The model consisted only of the shaft of the humerus.

Thereafter, the mesh model was built using the default settings. The default settings were an arbitrary (3D) surface type, the source data was obtained from the dense cloud with a high face count and the vertex colours were calculated. Next, the mesh model built was exported as an alias wavefront object (obj) file format for mesh-to-mesh value comparison.

All complete cadaveric skeletons simulated fragmented skeletons and forensic commingled skeletons were compared using the mesh-to-mesh comparison method. To correctly evaluate the effectiveness of the mesh-to-mesh comparison, two different software were used, Meshlab 2022.2 and Viewbox 4.1. beta software. Viewbox 4.1 beta software was used and tested in the original study by Karell *et al.* (2016). Meshlab 2022.2 software was another free open-source software that is compatible with most devices and easy to find. Viewbox uses a trimmed Iterative Closest Point (ICP) algorithm while Meshlab uses a basic ICP algorithm for alignment and similarity testing. The two different software were used to test whether different types of software and algorithms affect the number of true positive matches, sensitivity, and specificity rates.

### **3.2.3. Mirrored image mesh models using Meshlab 2022.2**

Meshlab is an open-source software used for processing and editing three-dimensional meshes. Mesh-to-mesh value comparison method involves the process of creating a three-dimensional mirror image of the left or right side of a skeletal element model and aligning the model over the opposite respective side of the element using common reference points and identifiable markers (Karell *et al.*, 2016). The method compares the digital geometry of the models and produces an error value that indicates the difference between the two mesh models when aligned, this error value is also considered the mesh-to-mesh value (Karell *et al.*, 2016). The lowest mesh-to-mesh value between both left and right models is considered a positive pair-match between two of the same skeletal elements (Karell *et al.*, 2016). Therefore, to overlap the right and left meshes to determine a match, one side of the meshes is mirrored. The right side was chosen per the study performed by Karell *et al.* (2016) and McWhirter *et al.* (2021), with the left meshes used as references meshes.

All right humerus and femur meshes were imported into Meshlab. Once imported, the filter tab was selected and the options “Normals”, “orientation” and “curvature” were chosen. The transformation filters chosen were “Transform: Flip and/or swap axis”, and the “Flip Y axis and freeze matrix” for the mesh (Figure 3.11).

The “freeze matrix” option ensures that the filter option chosen was applied. After this, “Normals” was once again selected, and the invert face orientation and a forced flip of the matrix function was performed. This step was required due to the flipping of the Y axis, whilst also flipping the internal and external surfaces of the matrix. To correct the matrix, the “invert face orientation transformation” filter was chosen (Figure 3.11). After all the transformations have been applied, the mesh was exported as an object file format. Each mesh model name was entered on a Microsoft Excel 2016 spreadsheet, randomised, and renamed. Randomisation was performed by selecting the random function [rand ()], random numbers were generated next to the column with the designated mesh model name and sorted into descending order. The randomised list of mesh models was renamed in order.

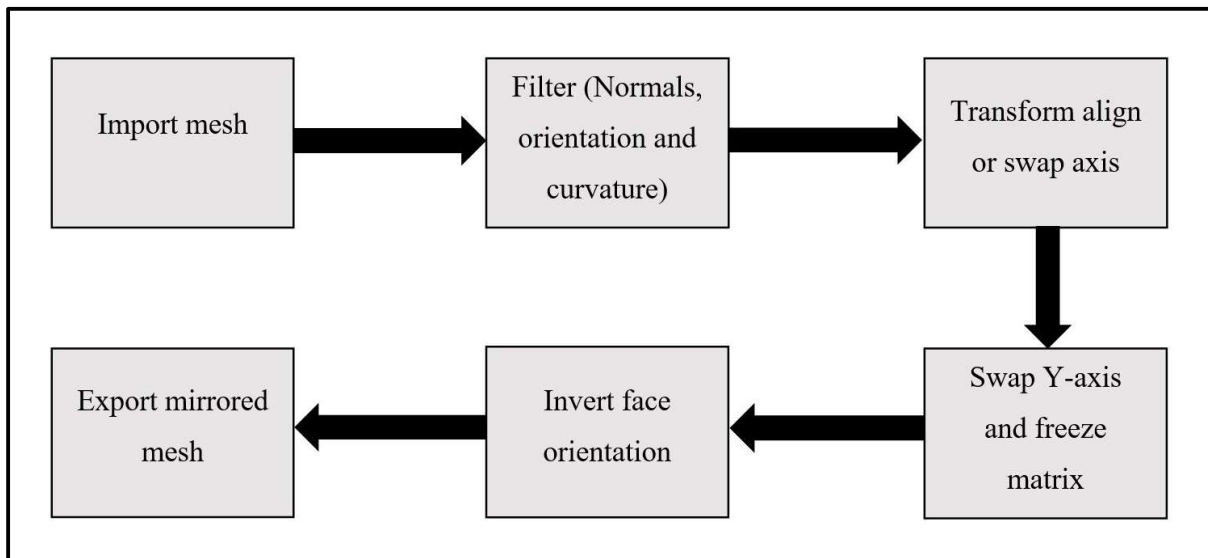


**Figure 3.11. Flowchart describing the process of creating a mirrored model rendering in Meshlab.**

### 3.2.4. Mesh-to-mesh value comparison using Meshlab

The process of alignment and determining the mesh-to-mesh value on Meshlab was followed by Cignoni *et al.* (2008). To obtain a value for each comparison between the right mirrored mesh and left mesh, one set of mesh (right mirrored and left) was imported at a time into Meshlab (Figure 3.11). The alignment tool was used to assist in automatically positioning one mesh that is unfixed over another mesh that is fixed. The mirrored right mesh was then selected as the “glued mesh” (fixed). The left mesh was used for point-based gluing.

The point-based gluing function aligns two meshes based on corresponding common fixed points on the mesh. Once point-based gluing was selected, another pop-up window would appear with the two meshes side by side as depicted in Figure 3.12.

Common anatomical landmarks that were distinct and present on both meshes were selected (Figure 3.12). There were eight points chosen for the femur such as the greater and lesser trochanter and the lateral and medial epicondyles of the femur. Five points were chosen for the humerus and were selected on the greater and lesser tubercles and the trochlea of the humerus. The options of false colouring and fixed scaling were used for alignment. False colouring was applied to the mesh to assist with identifying and distinguishing the differences between the two meshes, which assists in identifying points. Fixed scaling uses the scale from the mesh, instead of the software. After the points have been selected and applied, the process button was selected to apply the transformation to the model.

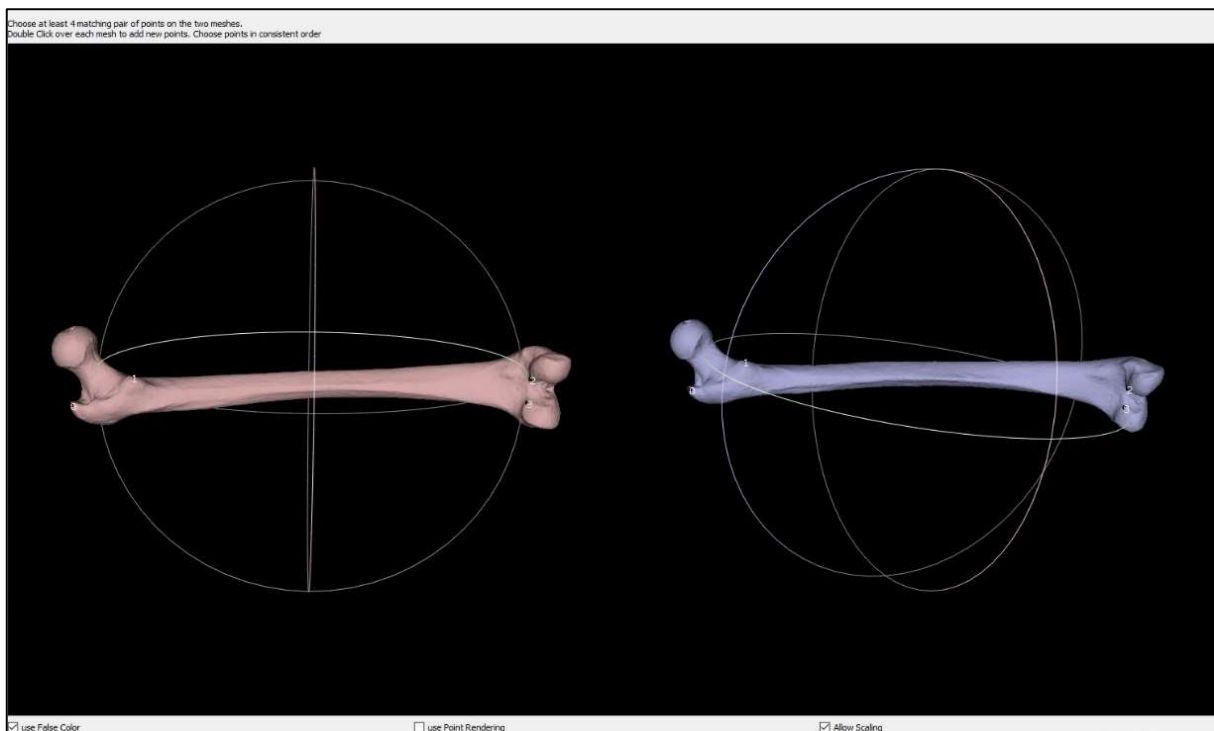


**Figure 3.12. Alignment and selection of points on Meshlab 2022.2 software.**

The “Normals”, “orientation” and “curvatures” options were chosen from the filters tab and the “transformation freeze matrix filter” with the transformation applied to all visible layers was selected (Figure 3.14). Next, the Sampling option within the filters tab was selected and the option Hausdorff distance was chosen (Figure 3.14).

The Hausdorff distance function calculates the distance of one point in a mesh to the closest point in the other mesh (measured in millimetres). The parameters used for this function are set to the default settings except the mirrored mesh was selected as the target mesh and the left mesh was selected as the sampled mesh with the sample vertices checked. When the Hausdorff distance function was applied, the output result was displayed on the right bottom corner of the screen and the Hausdorff distance computed root mean square (RMS) value (Figure 3.13) was recorded on a Microsoft Excel spreadsheet and stored for analysis.

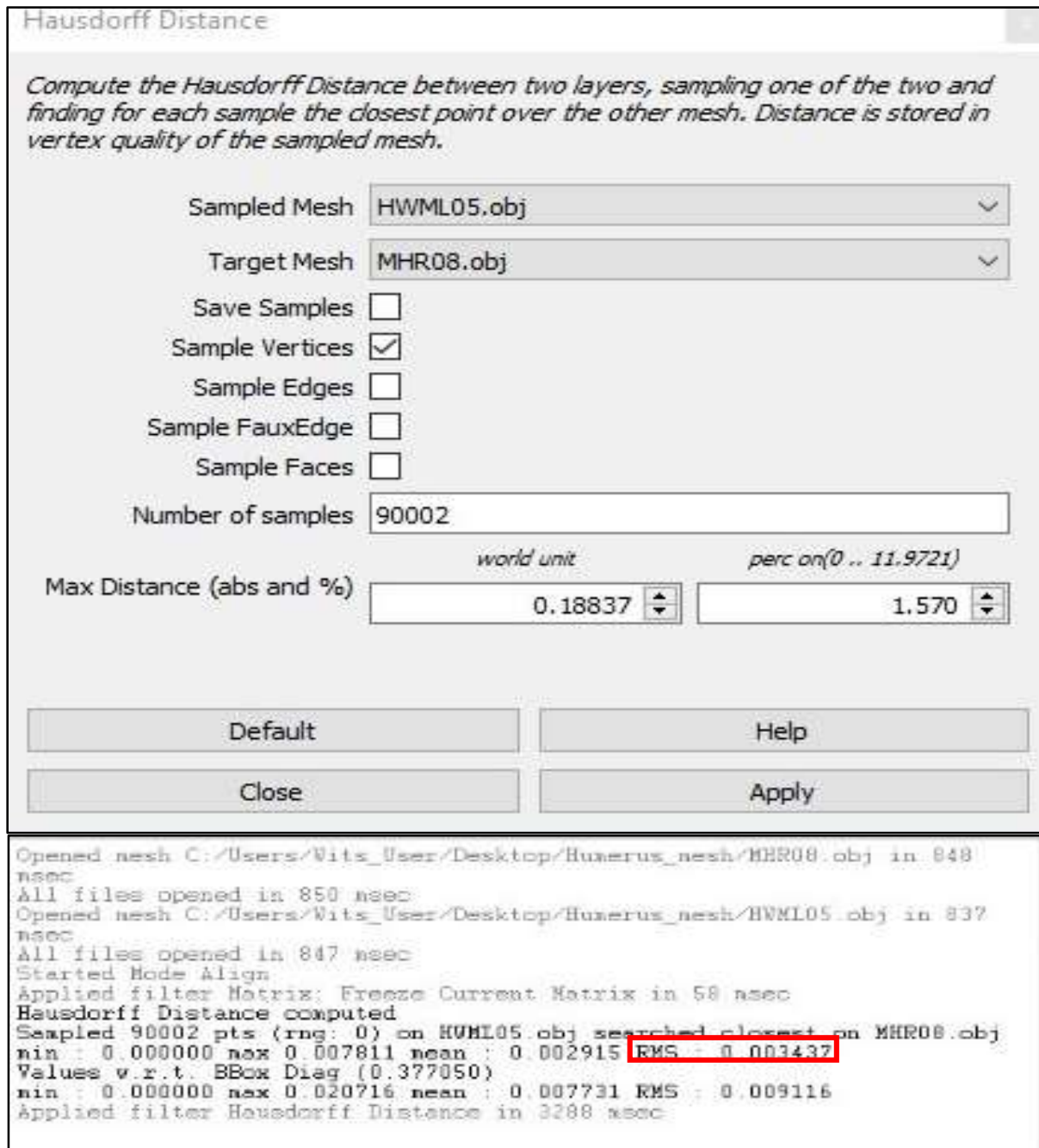


**Figure 3.13.** The set criteria were used for determining the root mean square differences between the two meshes.

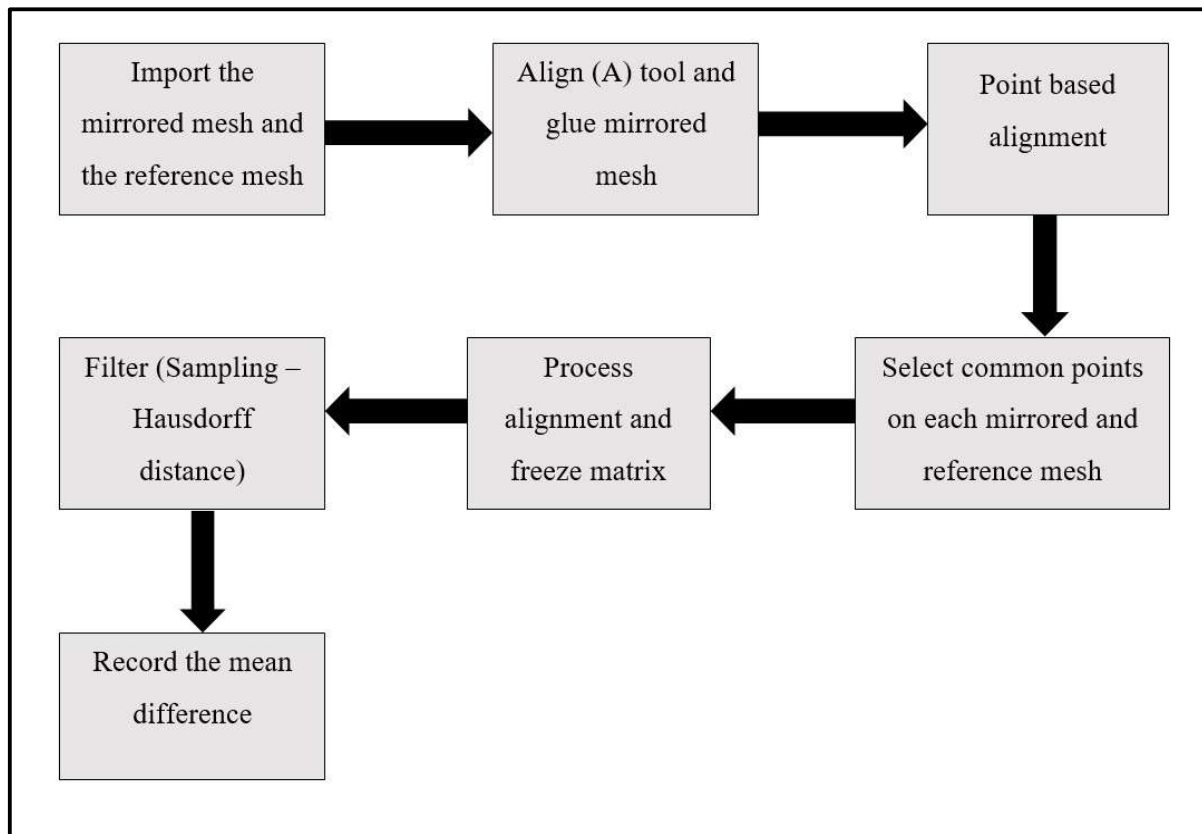


**Figure 3.14. Determining the Hausdorff distance (average error) using Meshlab.**

### 3.2.5. Mesh-to-mesh value comparison and Viewbox 4.1. Beta

Agisoft Metashape only recreates the surface morphology of an object and thus hollowing was not needed. Hollowing is performed when 3D models contain internal and external data but only the external data is needed for analysis thus the internal data is removed (generally performed in cases where full 3D scans are performed such as with computer tomography and Lodox). The obj models were imported into Viewbox 4.1. for comparison. The mirror image of the right models was compared to all the left ones. The selection criteria used within this study were based on the criteria used and developed by Karell *et al.*, (2016), Karell, (2019) and McWhirter *et al.*, (2021).

To determine whether different types of software affect the mesh-to-mesh value comparison method, the data was run on two different software, Meshlab and Viewbox software. Viewbox software was used in the original study that involved mesh-to-mesh value comparison and Multi-Slice Computer Tomography (MSCT) scans to create the rendered 3D models (Karell *et al.*, 2016., Karell, 2019., McWhirter *et al.*, 2021). Viewbox 4.1 includes a tool called “Mesh Similarity” which automatically compares several meshes to each other (Figure 3.15).

Viewbox uses a trimmed ICP algorithm, a variant of the general ICP algorithm. Trimmed ICP sorts out the distances between paired points and rejects the largest of points, the overall percentage of rejected points is identified by the user (dHAL Software, 2020). The matching setting allows the user to match each target mesh to each source mesh from point to point which means matching each vertex identified in the mesh to its corresponding vertex projection in the next mesh (dHAL Software, 2020). Point-to-plane allows the program to match each vertex of the source mesh to the vertex on the plane (x, y, z-axis plane) that is tangent at the position of the point closest to the target mesh (dHAL Software, 2020). The estimated overlap of meshes refers to the percentage of expected points overlapping the meshes. The number of iterations for rough and final alignment indicates the number of times the algorithm will run until there is no improvement in the alignment process (Figure 3.15).

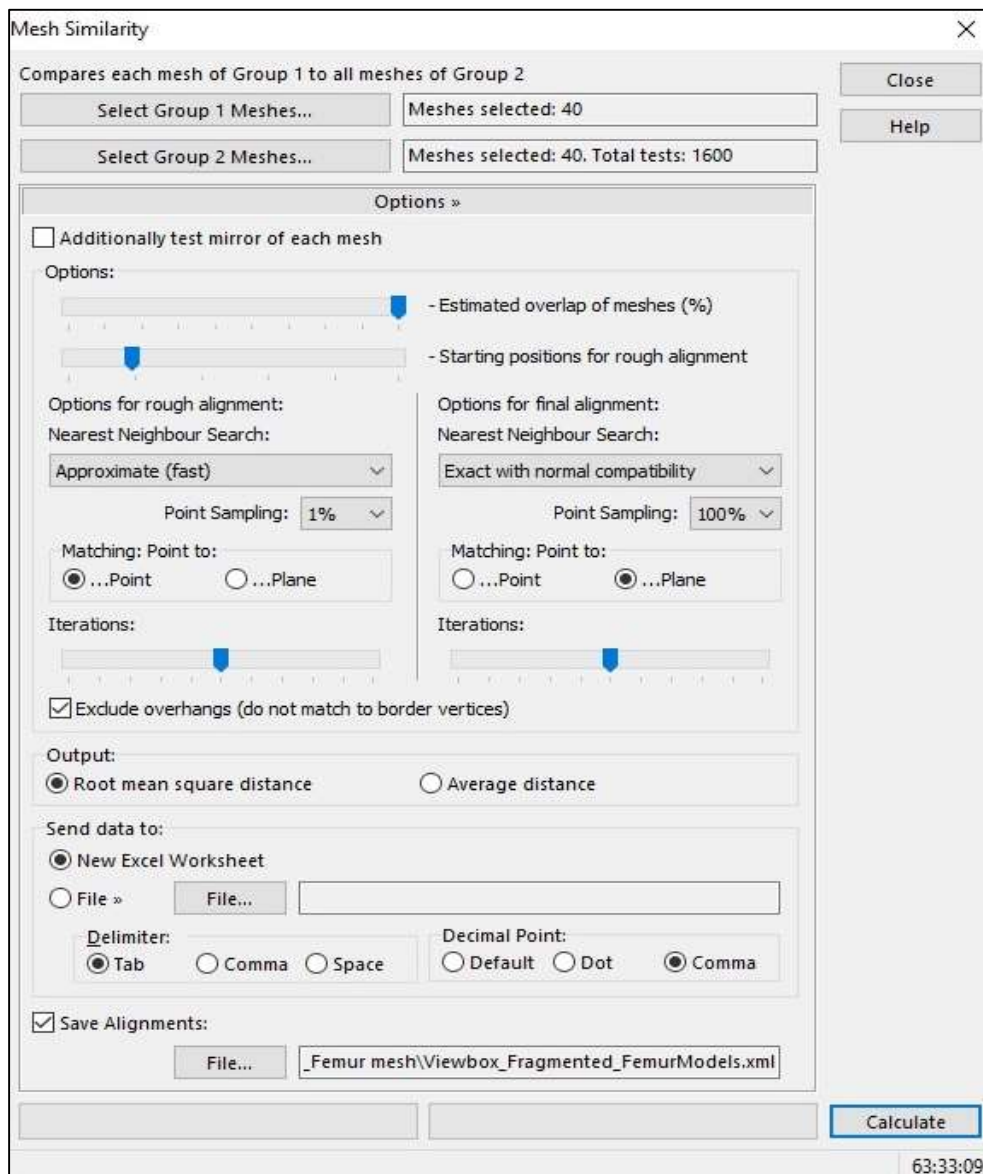


Figure 3.15. Set parameters used for comparison for Viewbox 4.1. beta

Point sampling refers to the number of vertices to be sampled for testing. The nearest neighbour search comprises a kd-tree (which involves point clouds and a multidimensional search key) for fast searching throughout large datasets (dHAL Software, 2020). The approximate fast option increases the overall computational greatly, unfortunately, it does not ensure that the closest point will be identified each time. The “exact with normal compatibility” locates points between the meshes with compatible normals ensuring that surfaces that are orientated differently do not match (dHAL Software, 2020). However, this option takes a lot more computational processing time (Figure 3.15). The parameters used were: Estimated overlap of Meshes (100%), Starting positions for rough alignment (20) and Iterations for rough and final alignment (100). Once completed, the comparison data was automatically uploaded as an Excel spreadsheet and used to determine the lowest mesh-to-mesh values for a true positive pair match.

### **3.2.6. Mesh-to-mesh value comparison analysis**

All rendered humeri and femora were compared, respectively. Distance values obtained for each were analysed and cross-compared to determine the three lowest distance values (reflecting three different individuals showing the closest match) (Karell *et al.*, 2016). The alignment was run again for those three humeri or femora and a true match was considered when the left and right sides both presented with the lowest mesh-to-mesh values (Karell *et al.*, 2016).

The root means square values obtained from Viewbox and Meshlab were entered in a Microsoft Excel spreadsheet to determine the lowest mesh-to-mesh value match. The spreadsheet was formatted with all the left mesh models listed within each row and the mirrored mesh models listed within each column. All true pair matches were highlighted within the Excel sheets to allow for verification during the pair-matching process.

Two main alignment comparison tests were performed: complete bilateral mesh comparison analysis, and bilateral and unilateral mesh comparison analysis. A complete bilateral mesh comparison indicates that for every true positive left mesh model, there is a corresponding true positive right mesh model. A unilateral and bilateral mesh comparison indicates that for every left mesh model, there may or may not be a corresponding right mesh model.

Therefore, every bone within the sample would not have a true positive match. This step was performed to accurately identify true negative and positive results and false negative and

positive results within the sample. For the unilateral and bilateral comparison, 8 left humeri and femora bones were excluded from the original sample. These bones were excluded to ensure that there would be a true negative match which was needed to determine the overall specificity of the sample.

A separate set of analyses were conducted similarly, to compare mesh-to-mesh values of humeri and femora of male individuals and humeri and femora of female individuals separately, then a separate test of humeri and femora for all South African black males and white males, respectively and South Africa black females and white females, respectively to account and observe any differences among the mesh-to-mesh values.

### **3.3. Data Analysis**

#### **3.3.1. Intra-observer and Inter-observer error**

For an inter-observer error analysis test, Lowest Common Value (LCV) mesh-to-mesh comparison analysis and Receiver Operating Characteristics (ROC) curve analysis was performed to evaluate the accuracy of the results. For the intra-observer error analysis test, a small randomly selected sub-sample of skeletons was reassessed. The individual skeletons were randomised by using the random function on Microsoft Excel 2016 spreadsheet. Random numbers were generated next to the column with the designated bone labels and sorted into descending order. A total of 5 individuals with 10 humeri and 10 femora bones were cross-compared to the original sample result of mesh-to-mesh values of true pair matches created from the three-dimensional surface renderings. To test for unilateral and bilateral pairs, 2 left humeri and femora were excluded from the intra/inter-observer sample. For the intra and inter-observer, the same sample of bones were used.

#### **3.3.2. Normality and Descriptive Statistic Analysis**

A normality test was conducted by using a Kolmogorov-Smirnov test. A Kolmogorov-Smirnov test is a non-parametric test to determine whether a sample follows a normal distribution. Analysis was performed to determine the specificity and sensitivity of the SfM technique on complete cadaveric skeletons, simulated fragmented cadaveric skeletons and the forensic commingled skeletons.

To statistically evaluate the reliability and validity of the information that was recorded, sensitivity and specificity were tested according to Loong (2003) and Karell *et al.* (2016) methods. According to Loong (2003), sensitivity refers to how proficient a test is at accurately pair-matching a bone with its counterpart by calculating the percentage of correct matches over the number of actual matches present in the sample. Specificity refers to how proficient a test is at accurately identifying incorrect matches (true negatives) by calculating the percentage of the number of true positives over the number of true positives and false negatives found within the sample (Figure 3.16).

$$\text{Sensitivity} = \frac{\text{number of true positives}}{\text{number of true positives} + \text{number of false negatives}}$$

$$\text{Specificity} = \frac{\text{number of true negatives}}{\text{number of true negatives} + \text{false positives}}$$

$$\text{Positive Predictive Value} = \frac{\text{number of true positives}}{\text{number of true positives} + \text{number of false positives}}$$

$$\text{Negative Predictive Value} = \frac{\text{number of true negatives}}{\text{number of true negatives} + \text{number of false negatives}}$$

**Figure 3.16. Statistical equations to test the sensitivity and specificity of the mesh-to-mesh value comparison method (Loong, 2003; Karell *et al.*, 2019).**

Receiver Operating Characteristics (ROC) curve analysis was performed to evaluate the sensitivity and specificity values for each complete and fragmented comparison of the humeri and femora models (Fawcett, 2006; Watson and Petrie, 2010). ROC analysis provides a more visual representation of the relationship between sensitivity and specificity among the femora and humeri bones respectively (Fawcett, 2006; Watson and Petrie, 2010). The standard deviation of the mesh-to-mesh true pair values was calculated to determine whether a possible threshold value can be obtained to assist in efficiently and correctly identifying all true pair matches within a large dataset.

To generate the mesh-to-mesh values to different softwares were used: Viewbox 4.1 which is a proprietary software that requires a license and uses a Trimmed Iterative Closest Point (ICP) algorithm to run the program and Meshlab 2022.12 which is an open-source software that does not require a license and uses a general ICP algorithm to run the program. Each software was programmed to generate a root mean square value; the root mean square value in this study was used to be the mesh-to-mesh value required for comparison.

To assess the effectiveness of the sorting method between the two softwares, analysis was performed using two different techniques: LCV (Lowest Common Value) mesh-to-mesh comparison which was performed using Microsoft Excel and ROC (Receiver Operating Characteristic) curve analysis performed using MedCalc. The LCV mesh-to-mesh comparison requires the user to filter, sort and eliminate values based on observation using specific commands on Microsoft Excel until the lowest agreed upon value is found across left-right and right-left (Karell *et al.*, 2019). The method provides sensitivity, specificity, positive predictive value (PPV) and a negative predictive value (NPV).

The ROC curve analysis that was performed on MedCalc follows the principle stated by Delong *et al.* (1988). The method works with a scoring system. The root mean square outputs were gathered, each value was given a score (0;1) to indicate a positive result and a negative result. From the root mean square values, the program was able to plot a curve of sensitivity against specificity with a threshold/criterion value (Fawcett, 2006; Watson and Petrie, 2010). The threshold value is a numerical cut-off value generated to achieve the optimum sensitivity and specificity values within a given sample. The values above the threshold would be considered negatives or non-matches while values below the threshold would be considered a positive result or a pair-match.

The closer the threshold value is to the top-left corner of the graph, the higher the accuracy of the test being performed. The program produces several different threshold values, each with its own specificity and sensitivity rates, allowing the output to be adjusted according to the user's preferences (e.g., high sensitivity and low specificity or low sensitivity and high specificity rates). The graph also provides an AUC and a p-value. The area under the curve (AUC) indicates the ability of the curve to accurately identify and distinguish between positive and negative results (Fawcett, 2006; Watson and Petrie, 2010). While p-value indicates the relationship between the observed AUC and the true population AUC of the ROC curve. If the

value is less than 0,5, it can be concluded that the AUC of the ROC curve is significantly different (Fawcett, 2006; Watson and Petrie, 2010).

All statistical analysis was performed using MedCalc version 20.215. An alpha of 0.05 (95 % confidence interval) was used to determine a threshold for accuracy and specificity.

## **4 Results**

The Structure-from-Motion (SfM) technique was used to create and render 171 three-dimensional mesh model samples using a photogrammetric software, Agisoft Metashape. These models were used to test the effectiveness of a new digital pair-matching method, the mesh-to-mesh value comparison (MVC) method against a South African populated sample. The 171 models were used to create three different types of samples: cadaveric complete femora and humeri samples to assess the sensitivity and specificity rates of the mesh-to-mesh value comparison, a simulated fragmented sample (proximal, distal and shaft) to assess the feasibility and reliability of the method and a forensic commingled sample to assess the effects of taphonomy on the method.

### **4.1. Intra and Inter-observer error analysis**

A total of 10 femora and humeri were reassessed to test the repeatability and reliability of the Structure-from-Motion technique and the mesh-to-mesh value comparison method for analysis.

#### **4.1.1. LCV mesh-to-mesh comparison femora**

Analysis introduced an increased amount of false positive outputs for the intra-observer compared to the inter-observer which produced 0 false positives but a high number of false negative and true positive results. With regards to the software, Meshlab was able to identify a higher number of false negatives and low false positives while Viewbox was able to identify a high number of false positives and low number of false negatives (Table 4.1).

**Table 4.1. Intra and inter-observer femora results using the LCV mesh-to-mesh comparison with Viewbox and Meshlab.**

<b>Samples</b>	<b>False Negative</b>	<b>False Positive</b>	<b>True Negative</b>	<b>True Positive</b>	<b>Total</b>
<b>Intra-observer Viewbox</b>					
<b>Bilateral</b>	0	4	0	6	10
<b>Unilateral and Bilateral</b>	0	4	2	2	8
<b>Inter-observer Viewbox</b>					
<b>Bilateral</b>	2	0	0	8	10
<b>Unilateral and Bilateral</b>	2	0	2	4	8
<b>Intra-observer Meshlab</b>					
<b>Bilateral</b>	2	2	0	6	10
<b>Bilateral and Unilateral</b>	2	2	2	2	8
<b>Inter-observer Meshlab</b>					
<b>Bilateral</b>	2	0	0	8	10
<b>Bilateral and Unilateral</b>	2	0	2	4	8

The results obtained for the Viewbox intra-observer error produced sensitivity and negative predictive values considerably higher when compared to the inter-observer results. While inter-observer performed better at producing higher specificity and positive predictive values. The results for the intra- and inter-observer error for Meshlab were the same while the intra-observer results between Viewbox and Meshlab produced a substantial difference between the sensitivity and specificity rates (Table 4.2).

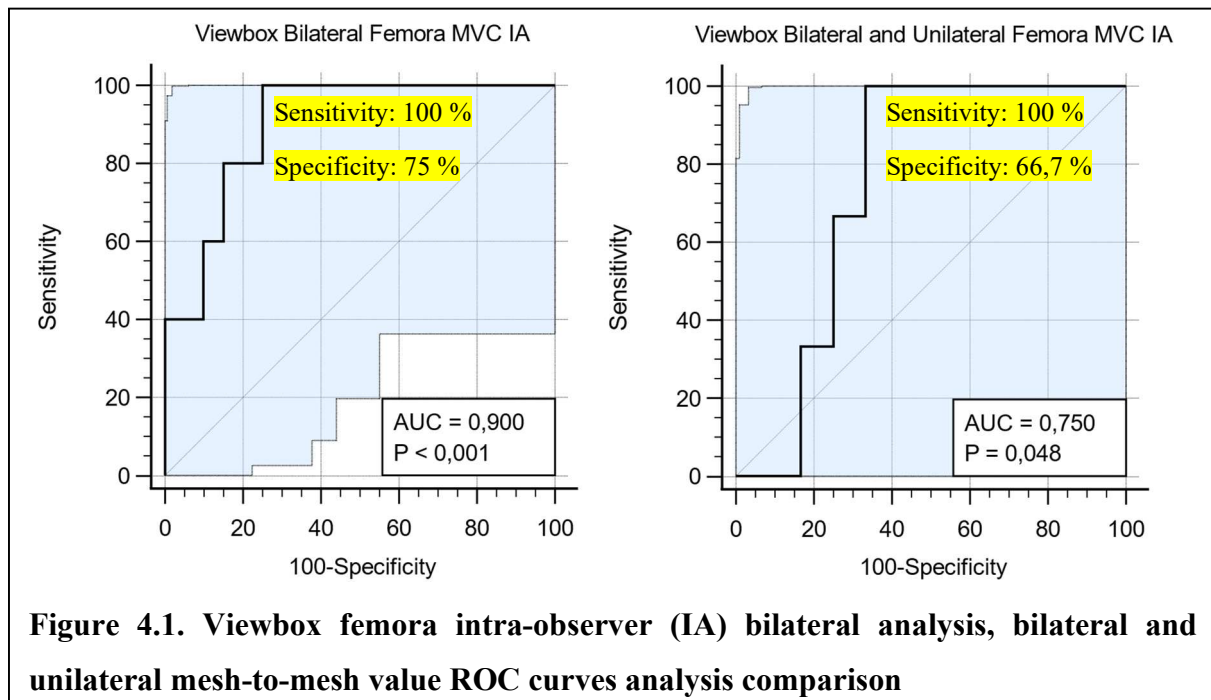
**Table 4.2. Intra and inter-observer femora sensitivity, specificity, PPV and NPV values using the LCV mesh-to-mesh comparison with Viewbox and Meshlab.**

<b>Samples</b>	<b>Sensitivity</b>	<b>Specificity</b>	<b>Positive Predictive value</b>	<b>Negative Predictive value</b>
<b>Intra-observer Viewbox</b>				
<b>Bilateral</b>	100 %	0	60 %	0
<b>Unilateral and Bilateral</b>	100 %	33,33 %	33,33 %	100 %
<b>Inter-observer Viewbox</b>				
<b>Bilateral</b>	80 %	0	100 %	0
<b>Unilateral and Bilateral</b>	66,67 %	100 %	100 %	50 %
<b>Intra-observer Meshlab</b>				
<b>Bilateral</b>	75 %	0	75 %	0
<b>Unilateral and Bilateral</b>	50 %	50 %	50 %	50 %
<b>Inter-observer Meshlab</b>				
<b>Bilateral</b>	80 %	0	100 %	0
<b>Unilateral and Bilateral</b>	66,67 %	100 %	100 %	50 %

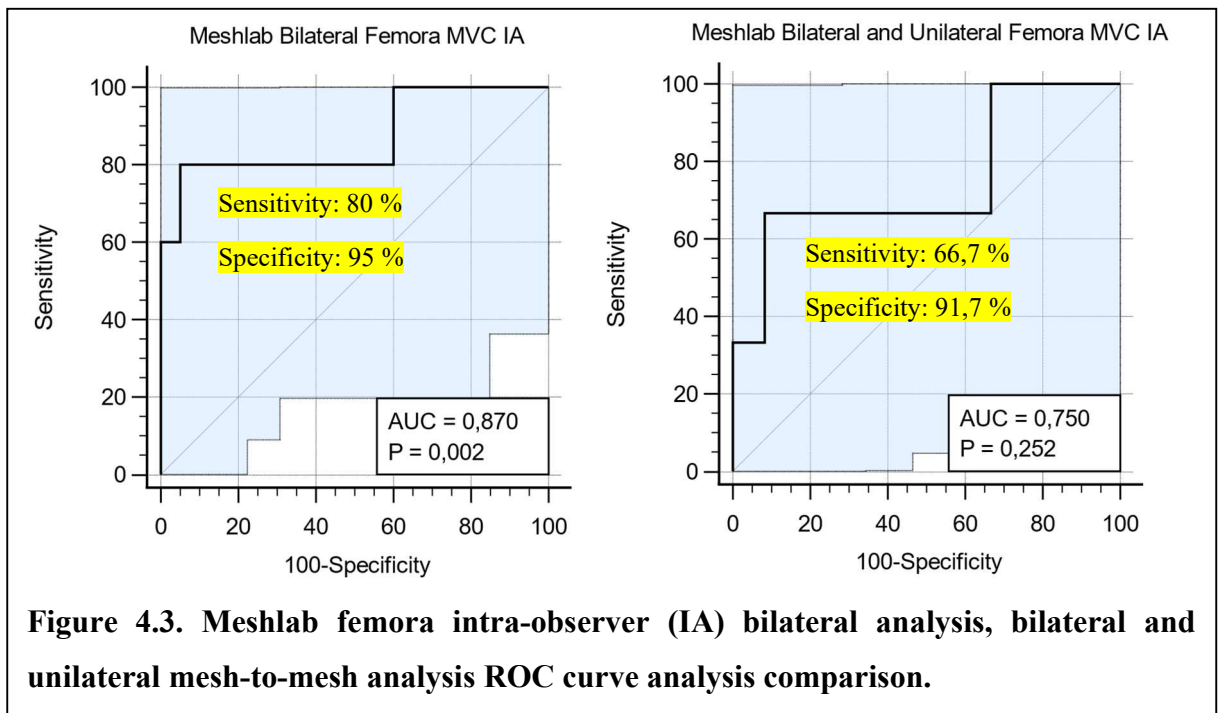
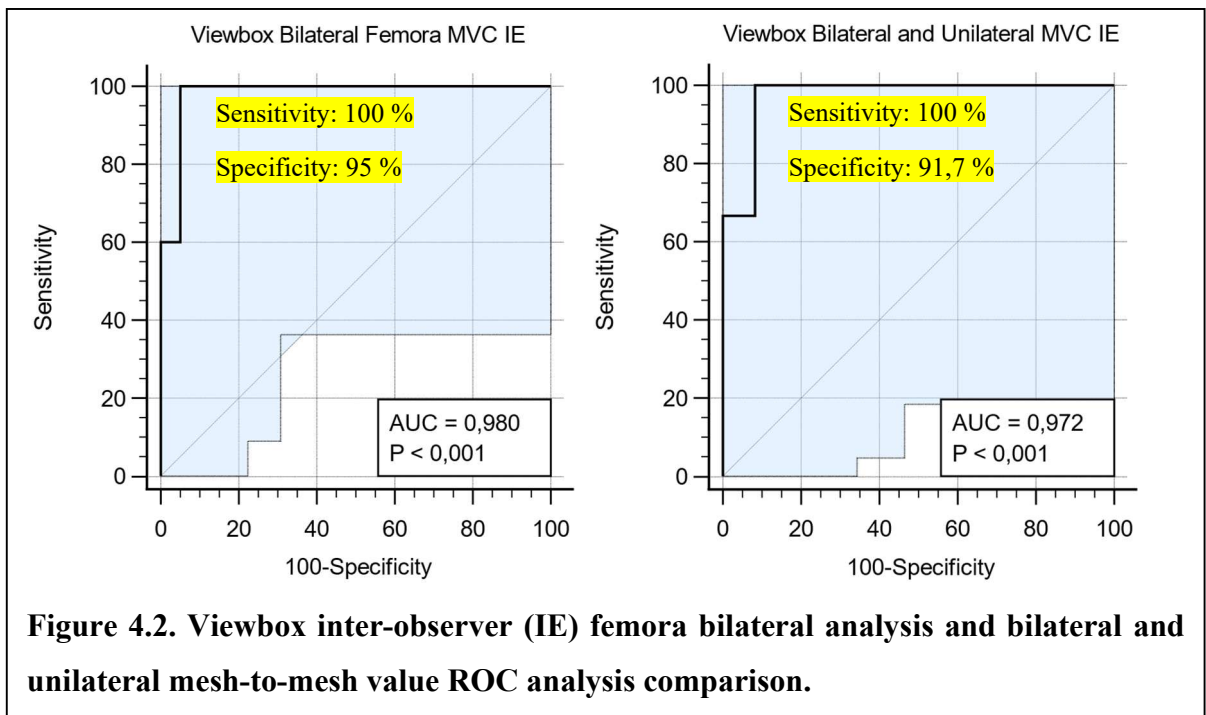
**4.1.2. Femora ROC curve intra and inter-observer error analysis.**

The ROC curve analysis for the Viewbox intra-observer results generated excellent sensitivity (100 %) values. The high AUC (0,90; 0,75) values indicate that the method was able to accurately distribute and discriminate strongly between the positive and negative groups contained within the sample (Figure 4.1). The Viewbox bilateral femora intra-observer and the bilateral and unilateral sample threshold value is (0,000364867). The standard error of the area under the curve for the bilateral sample is (0,0652).

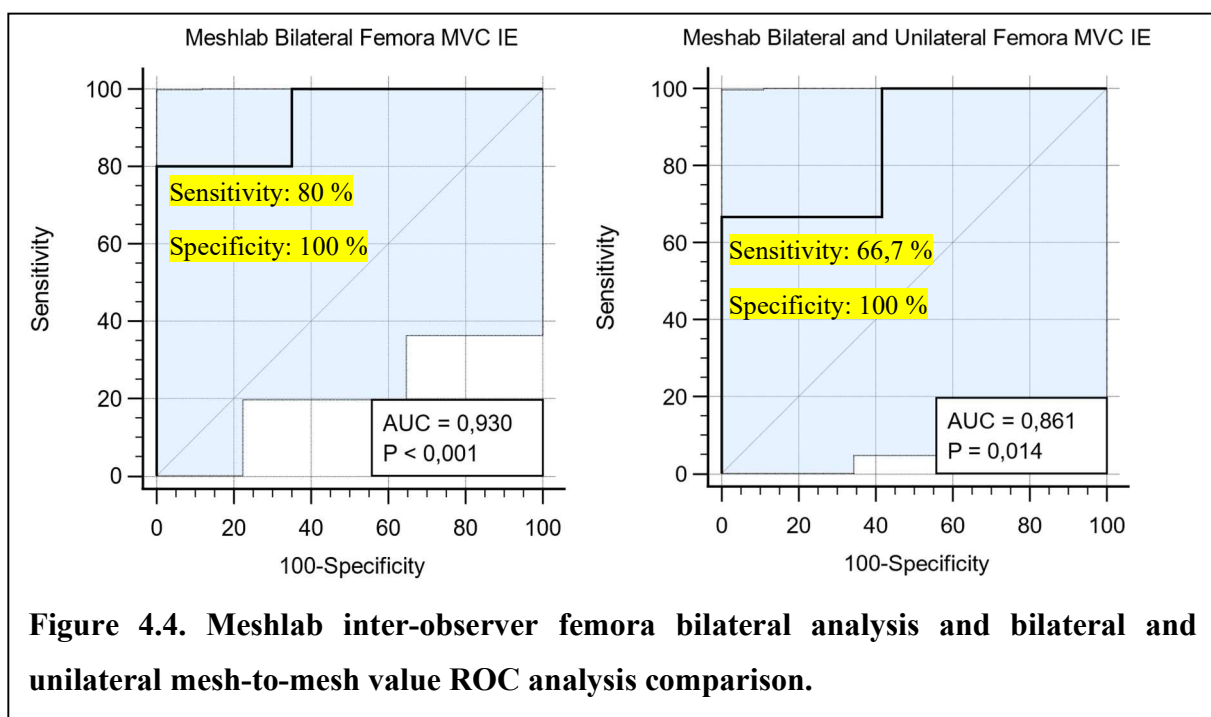
While the bilateral and unilateral sample has a standard error of (0,126) but p-value (0,048) considerably close to 0,05 which suggests that this sample does not perform very well at discriminating between the negative and positive results. The result states that the values below the threshold are classified as a positive pair match result and values above this threshold are considered negative non-matches.



The ROC curve analysis performed for the Viewbox interobserver results indicated a low p-value ( $< 0,001$ ) and a high AUC value (0,98; 0,97), which suggests that the method was able to accurately discriminate between the positive matched pairs and the negative non-matches within the sample. Both samples produced considerably high sensitivity (100 %) and specificity (95 %; 91,7 %) values. The threshold value generated for both graphs is (0,0002414) with a standard error of (0,0235) for the bilateral sample and a standard error of (0,0393) for the bilateral and unilateral sample. For this threshold, results generated below this value are considered a positive pair match and values above indicates a negative result (Figure 4.2).



The ROC curve analysis for the Meshlab intra-observer results produced low sensitivity (66,7 %) levels for the bilateral and unilateral sample which could be related to the p-value (0,252) being greater than 0,05. The p-value indicates that for this sample the observed area under the curve is not significantly different and does not have the ability to distinguish between the positive and negative results. However, the bilateral sample serves as a better indicator of the suitability of the method for the intra-observer sample. The threshold value for the sample is (0,002885), smaller values will indicate a positive pair match while the larger values will be considered negative matches (Figure 4.3).



The inter-observer error results for the Meshlab generated outputs produced excellent specificity (100 %) values for both samples with high AUC values (0,93; 0,86) and low p-values (< 0,001; 0,014) which indicates that the sample is good at accurately discriminating between the positive and negative matched values within the sample. The threshold value for both graphs were (0,001911), values within the sample that are lower would indicate a positive match while value samples higher than the threshold indicates a negative match (Figure 4.4).

### 4.1.3. LCV Humeri

All results for the intra and inter-observer error produced were equal and showed no difference except for the Viewbox intra-observer results which was the only sample that produced false positives and negatives (Table 4.3).

**Table 4.3. Intra and inter-observer humeri results using the LCV mesh-to-mesh comparison with Viewbox and Meshlab.**

<b>Samples</b>	<b>False Negative</b>	<b>False Positive</b>	<b>True Negative</b>	<b>True Positive</b>	<b>Total</b>
<b>Intra-observer Viewbox</b>					
<b>Bilateral</b>	2	0	0	8	10
<b>Unilateral and Bilateral</b>	1	2	1	4	8
<b>Inter-observer Viewbox</b>					
<b>Bilateral</b>	0	0	0	10	10
<b>Unilateral and Bilateral</b>	0	0	2	6	8
<b>Intra-observer Meshlab</b>					
<b>Bilateral</b>	0	0	0	10	10
<b>Bilateral and Unilateral</b>	0	0	2	6	8
<b>Inter-observer Meshlab</b>					
<b>Bilateral</b>	0	0	0	10	10
<b>Bilateral and Unilateral</b>	0	0	2	6	8

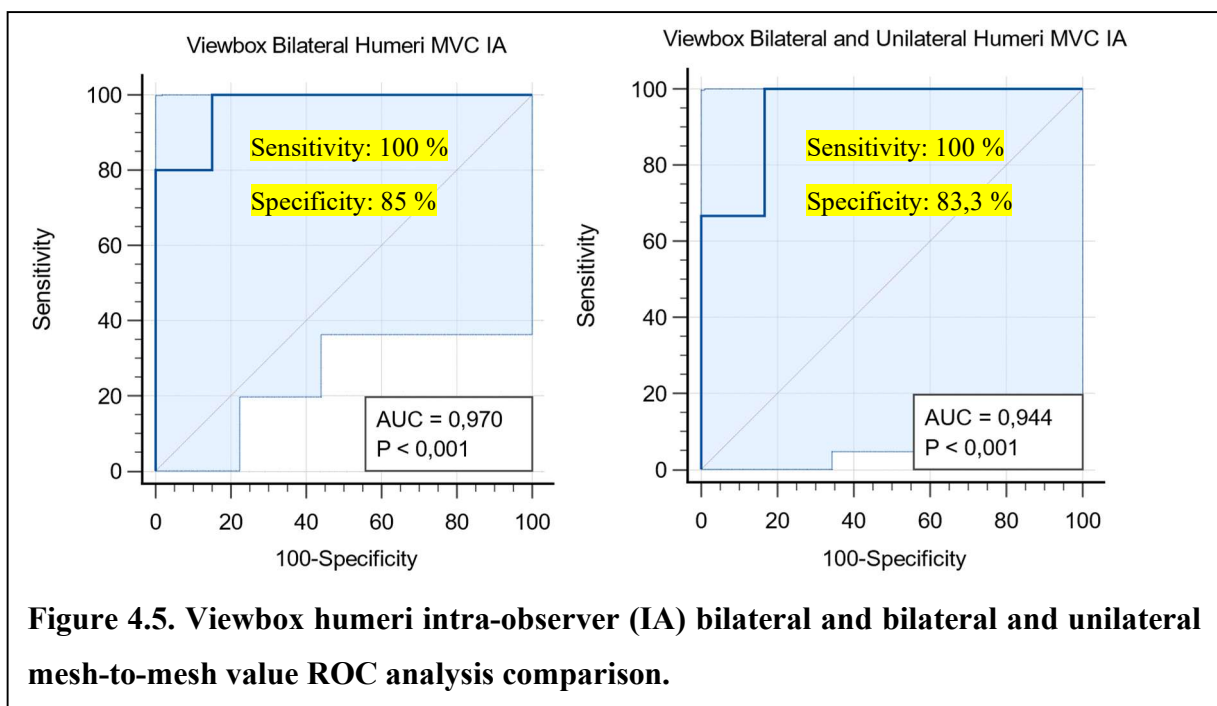
Humeri results generated excellent sensitivity and specificity values for the intra and inter observer results showcasing that the method is well adapted to identifying matches and non-matches within a small-scaled sample consisting of humeri bones (Table 4.4).

**Table 4.4. Intra and inter-observer humeri sensitivity, specificity, PPV and NPV values using the LCV mesh-to-mesh comparison with Viewbox and Meshlab.**

<b>Samples</b>	<b>Sensitivity</b>	<b>Specificity</b>	<b>Positive Predictive value</b>	<b>Negative Predictive value</b>
<b>Intra-observer Viewbox</b>				
<b>Bilateral</b>	80 %	0	100 %	0
<b>Unilateral and Bilateral</b>	80 %	33,33 %	66,67 %	50 %
<b>Inter-observer Viewbox</b>				
<b>Bilateral</b>	100 %	0	100 %	0
<b>Unilateral and Bilateral</b>	100 %	100 %	100 %	100 %
<b>Intra-observer Meshlab</b>				
<b>Bilateral</b>	100 %	0	100 %	0
<b>Unilateral and Bilateral</b>	100 %	100 %	100 %	100 %
<b>Inter-observer Meshlab</b>				
<b>Bilateral</b>	100 %	0	100 %	0
<b>Unilateral and Bilateral</b>	100 %	100 %	100 %	100 %

#### 4.1.4. ROC Humeri

ROC analysis for the humeri intra-observer models produced high sensitivity (100 %) and specificity (85 %; 83,3 %) values for the bilateral sample and the bilateral and unilateral sample. The high AUC value (0,97; 0,94) with the low p-value ( $< 0,001$ ) indicates that there is a significant difference between the positive and negative results and the method is able to accurately discriminate between the two results. The threshold value for both graphs is (0,000228) with all the values higher than the threshold value are considered negative matches while values lower than the threshold are positive paired matches (Figure 4.5).



The interobserver ROC curve analysis performed considerably well at producing excellent sensitivity (100 %) and specificity (100 %) values. The AUC (1,0) and the p-value ( $< 0,001$ ) produced perfect results which means that the sample is able to perfectly discriminate between positive and negative results. The threshold value for the graphs is (0,0001139), smaller values would indicate a positive match while larger values would indicate a negative match (Figure 4.6).

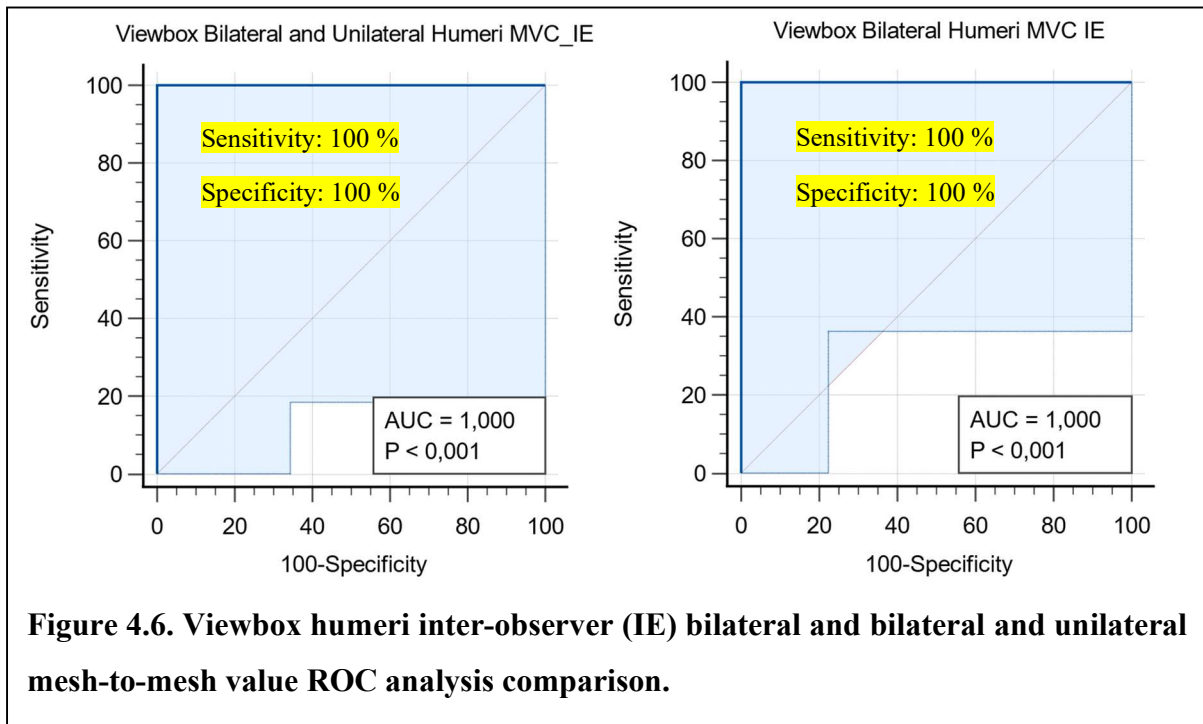
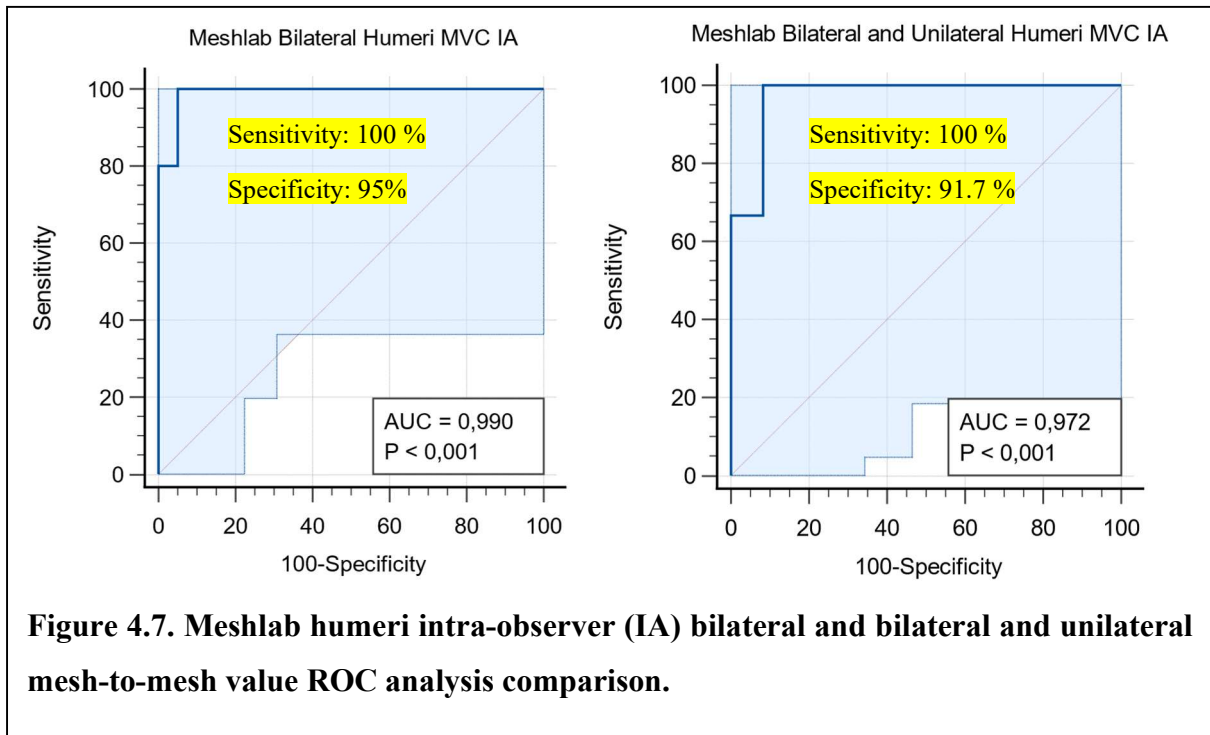


**Figure 4.6. Viewbox humeri inter-observer (IE) bilateral and bilateral and unilateral mesh-to-mesh value ROC analysis comparison.**

The Meshlab intra-observer results produced high AUC values (0,99; 0,97) and p-values (< 0,001) below 0,05 which indicates that the results are significantly different, and the method is able to accurately discriminate between the positive and negative groups within the sample. The threshold value for both graphs is (0,001708) with a standard error of (0,0141) for the bilateral sample and (0,0393) for the bilateral and unilateral sample. The threshold value is able to numerical differentiate between the two samples with lower values indicating a positive pair match while higher values indicating a negative match (Figure 4.7).



The inter-observer error results for Meshlab produced perfect sensitivity (100 %), specificity (100 %), AUC value (1,0) and p-value (< 0,001) for both graphs indicating that the results is significantly different and is able to differentiate between the two groups. The threshold value is (0,001521) with lower values representing positive pair match and higher values a negative match (Figure 4.8).

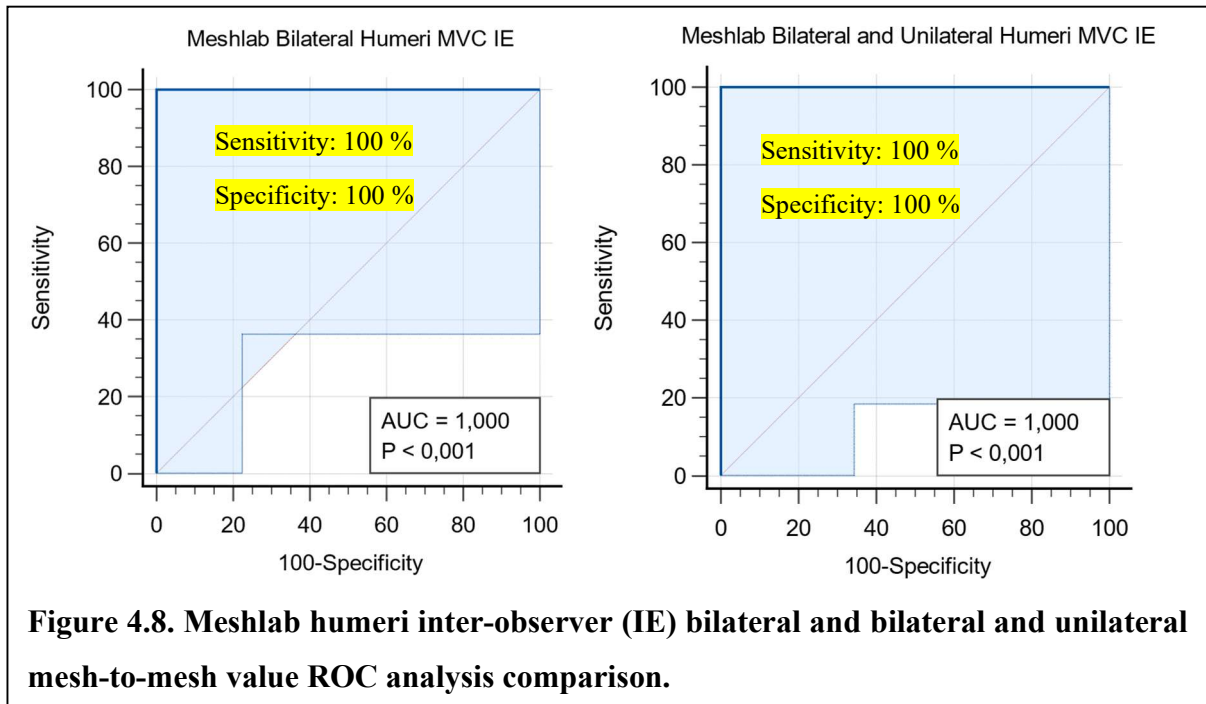


**Figure 4.8. Meshlab humeri inter-observer (IE) bilateral and bilateral and unilateral mesh-to-mesh value ROC analysis comparison.**

## 4.2. Cadaveric Femora Mesh Comparison Sample

A total of 80 humeri and femora were photographed and rendered to create photogrammetric 3D models. It was observed that female femora were slightly more difficult to model compared to the males. Female left bones proved to be more difficult than their right counterparts and contributed significantly to misalignments during the rendering process. For the bilateral comparison a total of 1600 tests were performed and for the bilateral and unilateral comparison, there were 1280 tests performed.

### 4.2.1. Normality test

A non-parametric normality test for the femora data was performed using the Kolmogorov-Smirnov test to determine whether the sample follows the normal distribution. The normality test p-value obtained was  $< 0,0001$  therefore the sample rejects the normality of distributed data.

#### 4.2.2. LCV Analysis

For the LCV mesh-to-mesh analysis results were obtained through Viewbox and Meshlab. Viewbox presented with a considerably higher number of false results (false positives and false negatives) but a higher number of true negatives within the sample when compared to Meshlab. Contrary, the number of true positives or matched bilateral pairs that was found within the sample doubled when the results generated by Meshlab was assessed (Table 4.5).

**Table 4.5. Femora complete cadaver mesh results using the LCV mesh-to-mesh comparison with Viewbox and Meshlab.**

Samples	False Negative	False Positive	True Negative	True Positive	Total
<b>Viewbox</b>					
Bilateral	34	16	0	30	80
Unilateral and Bilateral	22	16	8	26	72
<b>Meshlab</b>					
Bilateral	14	2	0	64	80
Bilateral and Unilateral	9	4	7	52	72

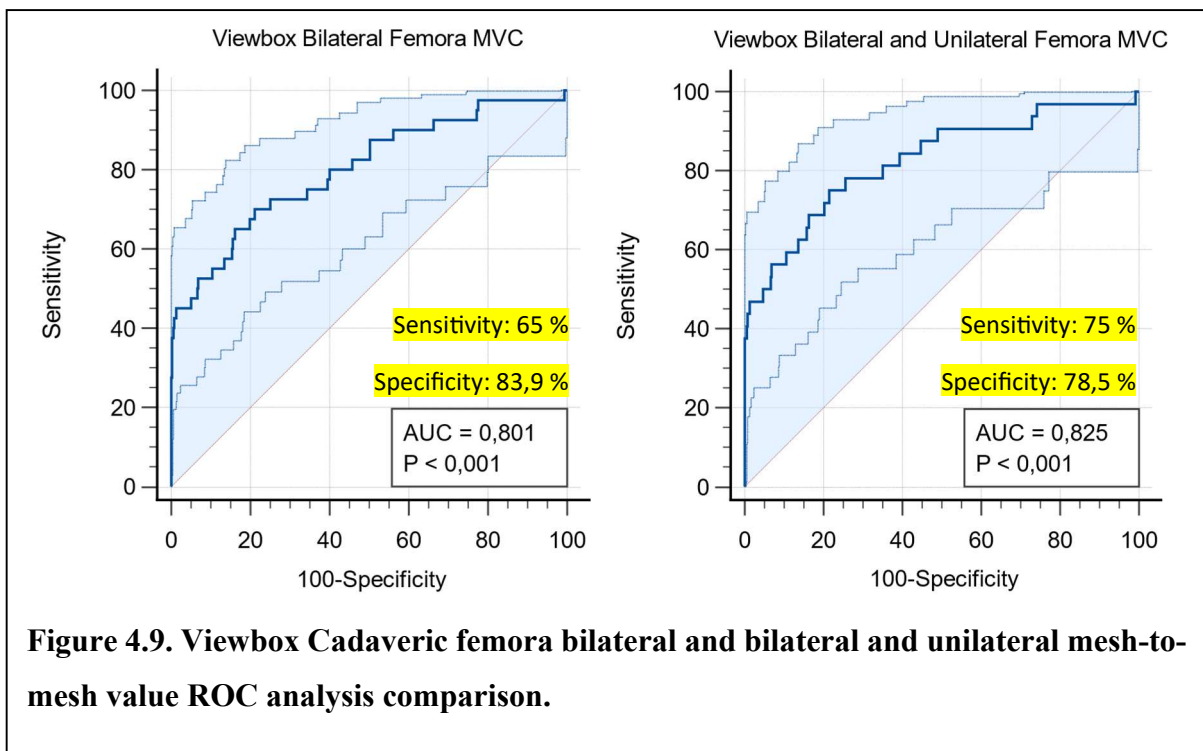
The sensitivity rates for the Viewbox and Meshlab bilateral and unilateral sample produced higher sensitivity rates (54,17 % and 85,25 %) when compared to the bilateral sample (46,88 % and 82,05 %), while lower positive predictive values (61,90 % and 92,86 %) were observed for same group compared to the just the bilateral group (65.22 % and 96.97 %). This implies that there is a higher probability of finding a mesh-to-mesh value within a bilateral and unilateral but a low probability of finding a positive result among the mesh-to-mesh values. Meshlab produces an increasingly higher result in accurately identifying true positives and true negatives within a sample (Table 4.6).

**Table 4.6. Femora complete cadaver mesh sensitivity, specificity, PPV and NPV values using the LCV mesh-to-mesh comparison with Viewbox and Meshlab.**

Samples	Sensitivity	Specificity	Positive Predictive value	Negative Predictive value
<b>Viewbox</b>				
Bilateral	46,88 %	0	65,22 %	0
Unilateral and Bilateral	54,17 %	33,33 %	61,90 %	26,67 %
<b>Meshlab</b>				
Bilateral	82,05 %	0	96,97 %	0
Unilateral and Bilateral	85,25 %	63,64 %	92,86 %	43,75 %

#### **4.2.3. ROC Analysis**

For the ROC curve analysis, Viewbox generated higher specificity values and slightly lower sensitivity values for both bilateral sample (83,9 %; 65 %) and the bilateral and unilateral sample (78,5 %; 75 %). The AUC values (0,80; 0,825) and the p-values (< 0,001) for both graphs are high and significant, respectively. The result implies that the method is able to accurately discriminate between the two positive and negative groups within the sample. The threshold value for the bilateral sample is (0,000398) and the threshold value for bilateral and unilateral sample is (0,000439). Mesh values obtained that is lower than the threshold value is considered positive pair match and values higher are considered negative non-matches (Figure 4.9).



The ROC curve analysis for the Meshlab results demonstrates higher sensitivity (87,5 %; 84,4 %) and specificity (94,6 %; 95,8 %) values compared to Viewbox (sensitivity: 65 %; 75 %) (specificity: 83,9 %; 78,5 %). The Meshlab AUC values (0,96; 0,95) for each graph are high while the p-values (< 0,001) produced represent significant differences between the two positive and negative groups found within the sample. The threshold value for the bilateral sample and the bilateral and unilateral sample is (0,002545). The standard error for the bilateral sample is (0,0202) and (0,0240) for the bilateral and unilateral sample. Mesh values that are higher than the threshold value is considered negative results while values that are lower are considered positive pair matches (Figure 4.10).

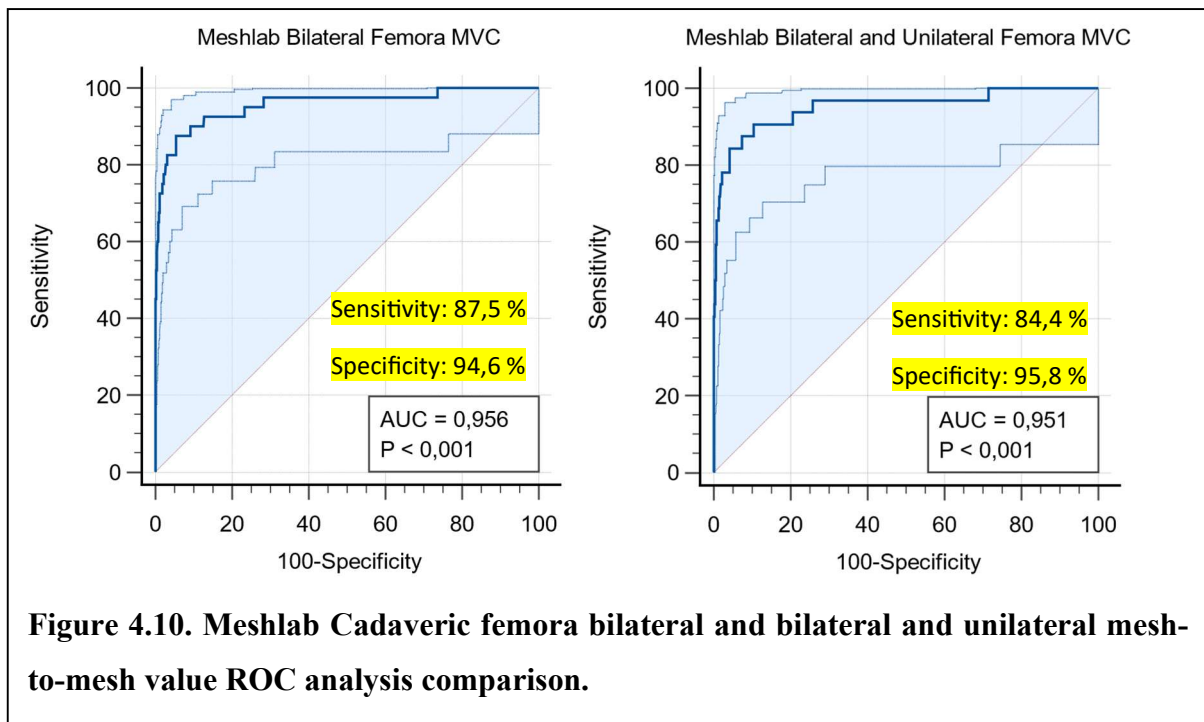


**Figure 4.10. Meshlab Cadaveric femora bilateral and bilateral and unilateral mesh-to-mesh value ROC analysis comparison.**

#### 4.2.4. LCV demographical analysis

The demographical information obtained through the LCV method using Viewbox demonstrates an increase in sensitivity levels in females (60 %; 70,59 %) when compared to males (53,33 %; 59,26 %) and South African Black individuals (56,25 %; 60,87 %) when compared to South African White individuals (43,75 %; 52,17 %). Among the population and sex differences between the two population groups, South African Black males (66,67 %; 80 %) and females (71,43 %; 66,67 %) generated a considerably higher sensitivity level compared to South African White male (37,5 %; 42,86 %) and female (50 %; 66,67 %) individuals. In terms of specificity, South African Black male (33,33 %) individuals outperformed South African Black female (11,11 %) individuals, with the opposite observed among all male (20 %) individuals when compared to all female (22,22 %) individuals (Table 4.7).

**Table 4.7. Femora complete cadaver mesh LCV demographical sensitivity and specificity for the bilateral sample and bilateral and unilateral sample using the Viewbox.**

	<b>Viewbox Femora LCV</b>		
	<b>Only Bilateral</b>	<b>Bilateral and Unilateral</b>	
	<b>Sensitivity</b>	<b>Specificity</b>	<b>Sensitivity</b>
<b>Sex</b>			
Male	53,33 %	20 %	59,26 %
Female	60 %	22,22 %	70,59 %
<b>Population groups</b>			
<b>SA Blacks</b>	<b>56,25 %</b>	<b>23,08 %</b>	<b>60,87 %</b>
SA Black males	66,67 %	33,33 %	80 %
SA Black females	71,43 %	11,11 %	66,67 %
<b>SA Whites</b>	<b>43,75 %</b>	<b>23,8 %</b>	<b>52,17 %</b>
SA White males	37,5 %	20 %	42,86 %
SA White females	50 %	25 %	66,67 %

For the LCV Meshlab sample, demographical information obtained provided higher sensitivity levels for male individuals compared to females for the bilateral (84,21 %; 80 %) sample but slightly lower for the bilateral and unilateral (81,25 %; 89,66 %) sample. South African Black individuals were more well adapted to the method and produced a substantially higher sensitivity (85 %; 87,50 %) and specificity (100 %) results particularly the South African male individuals with (100 %) sensitivity and specificity levels. On the other hand, among South African White individuals, females (90 %; 100 %; 100 %) were the best the performing group (Table 4.8).

**Table 4.8. Femora complete cadaver mesh LCV demographical sensitivity and specificity for the bilateral sample and bilateral and unilateral sample using the Meshlab.**

Samples	Meshlab Femora LCV		
	Only Bilateral	Bilateral and Unilateral	
	Sensitivity	Specificity	Sensitivity
<b>Sex</b>			
Male	84,21 %	60 %	81,25 %
Female	80 %	66,67 %	89,66 %
<b>Population groups</b>			
<b>SA Blacks</b>	<b>85 %</b>	<b>100 %</b>	<b>87,50 %</b>
SA Black males	100 %	100 %	100 %
SA Black females	80 %	100 %	87,50 %
<b>SA Whites</b>	<b>78,95 %</b>	<b>66,67 %</b>	<b>80 %</b>
SA White males	66,67 %	33,33 %	62,50 %
SA White females	90 %	100 %	100 %

#### **4.2.5. ROC demographical analysis**

The complete femora mesh sample was broken down and analysed with the ROC curve statistical method. The ROC method demonstrated a high sensitivity rate for males (65 %; 76,5 %) compared to females (50 %; 46,7 %) while specificity rates were higher for females (96,8 %; 96,5 %) than males (80,3 %; 78,3 %). The threshold values for females (< 0,0002396) were half the values than that for males (< 0,000429). The sensitivity levels for South African Black (55 %; 87,5 %) individuals were slightly lower compared to South African White individuals (65 %; 68,6 %). In terms of specificity among the sex-population groups, South African Black male (100 %; 100 %) individuals performed better compared to South African White male (85 %; 84,2 %) individuals (Table 4.9).

**Table 4.9. Femora complete cadaver mesh ROC demographical sensitivity and specificity for the bilateral sample and bilateral and unilateral sample using the Viewbox (Appendix B).**

<b>Viewbox Femora ROC curve analysis</b>						
<b>Samples</b>	<b>Bilateral</b>			<b>Bilateral and Unilateral</b>		
	<b>Sensitivity</b>	<b>Specificity</b>	<b>Threshold</b>	<b>Sensitivity</b>	<b>Specificity</b>	<b>Threshold</b>
<b>Sex</b>						
Male	65 %	80,3 %	<0,000429	76,5 %	78,3 %	<0,000429
Female	50 %	96,8 %	<0,0002396	46,7 %	96,5 %	<0,0002396
<b>Population groups</b>						
<b>SA Blacks</b>	<b>55 %</b>	<b>95 %</b>	<b>&lt;0,000295</b>	<b>87,5 %</b>	<b>70,4 %</b>	<b>&lt;0,00469</b>
SA Black males	50 %	100 %	<0,000224	62,5 %	100 %	<0,00224
SA Black females	70 %	83,3 %	<0,000346	62,5 %	84,7 %	<0,000346
<b>SA Whites</b>	<b>65 %</b>	<b>85 %</b>	<b>&lt;0,000395</b>	<b>68,6 %</b>	<b>84,2 %</b>	<b>&lt;0,000395</b>
SA White males	60 %	85,6 %	<0,000374	66,7 %	84 %	<0,000374
SA White females	50 %	97,8 %	<0,000218	57,1 %	96,8 %	<0,00218

The ROC method produced high sensitivity and specificity rates for sex, population, and sex-population groups in the Meshlab results. The bilateral and unilateral group of males (94,1 %; 94,7 %) individuals were slightly higher for sensitivity and specificity values compared to females (86,7 %; 94,4 %). The bilateral and unilateral group of South African Black (87,5 %; 97 %) individuals performed high sensitivity and specificity values compared to South African White (93,7 %; 84,5 %) individuals. Among population-sex specific groups, the South African Black male individuals performed better compared to South African White male individuals whereas the South African White female (100 %; 100 %) individuals had better sensitivity levels compared to South African Black female (80 %; 75 %) individuals for both groups (bilateral; bilateral and unilateral) (Table 4.10).

**Table 4.10. Femora complete cadaver mesh ROC demographical sensitivity and specificity for the bilateral sample and bilateral and unilateral sample using the Meshlab (Appendix C).**

<b>Meshlab Femora ROC curve analysis</b>						
<b>Samples</b>	<b>Bilateral</b>			<b>Bilateral and Unilateral</b>		
	<b>Sensitivity</b>	<b>Specificity</b>	<b>Threshold</b>	<b>Sensitivity</b>	<b>Specificity</b>	<b>Threshold</b>
<b>Sex</b>						
Male	95 %	93,4 %	<0,002968	94,1 %	94,7 %	<0,002968
Female	90 %	92,9	<0,002225	86,7 %	94,4 %	<0,002225
<b>Population groups</b>						
<b>SA Blacks</b>	<b>90 %</b>	<b>97,6 %</b>	<b>&lt;0,002545</b>	<b>87,5 %</b>	<b>97 %</b>	<b>&lt;0,002545</b>
SA Black males	100 %	97,8 %	<0,002545	100 %	97,2 %	<0,002545
SA Black females	80 %	97,8 %	<0,002198	75 %	97,2 %	<0,002198
<b>SA Whites</b>	<b>80 %</b>	<b>95,3 %</b>	<b>&lt;0,002265</b>	<b>93,7 %</b>	<b>84,5 %</b>	<b>&lt;0,002968</b>
SA White males	90 %	93,3 %	<0,002968	88,9 %	92,6 %	<0,002968
SA White females	100 %	86,7 %	<0,002225	100 %	90,5 %	<0,002225

### **4.3. Cadaveric Humeri Mesh Comparison Sample**

A total of 80 humeri models were photographed and rendered to create a 3D model. From the 80 humeri, some of the bones had to be replaced or captured more than once. A lot of the smaller, more gracile, and lighter textured bones could not be captured and had to be replaced. The majority of the replaced bones were females and associated with left-sided humeri.

Once the rendering process was complete for all 80 models, the models were imported into Viewbox and Meshlab to produce a mesh-to-mesh value for comparison. The Viewbox bilateral sample ran a total of 1600 tests while for the bilateral and unilateral sample, 1280 tests were performed.

### 4.3.1. Normality test

A non-parametric normality test for the humeri data was performed using the Kolmogorov-Smirnov test to determine whether the sample follows a normal distribution. The normality for the sample rejects the normality of the distributed data for the humeri and therefore the humeri sample was not distributed normally.

### 4.3.2. LCV Analysis

The results generated with Viewbox and analysed through the LCV method displayed a considerably higher number of false results particularly false positives among the humeri samples. Meshlab results performed better at identifying substantially higher number of true positives and negatives within the sample (Table 4.11).

**Table 4.11. Humeri complete cadaver mesh results using the LCV mesh-to-mesh comparison with Viewbox and Meshlab.**

Samples	False Negative	False Positive	True Negative	True Positive	Total
<b>Viewbox</b>					
Bilateral	24	20	0	36	80
Unilateral and Bilateral	17	22	5	28	72
<b>Meshlab</b>					
Bilateral	20	4	0	56	80
Bilateral and Unilateral	12	6	6	48	72

The humeri sensitivity, positive predictive value (PPV) and negative predictive value (NPV) rates for Viewbox were lower compared to the Meshlab values found. Viewbox (18,52 %) performed considerably poorer for specificity compared to Meshlab (50 %). The sensitivity and specificity levels indicate that Viewbox was able to identify the positive matches within

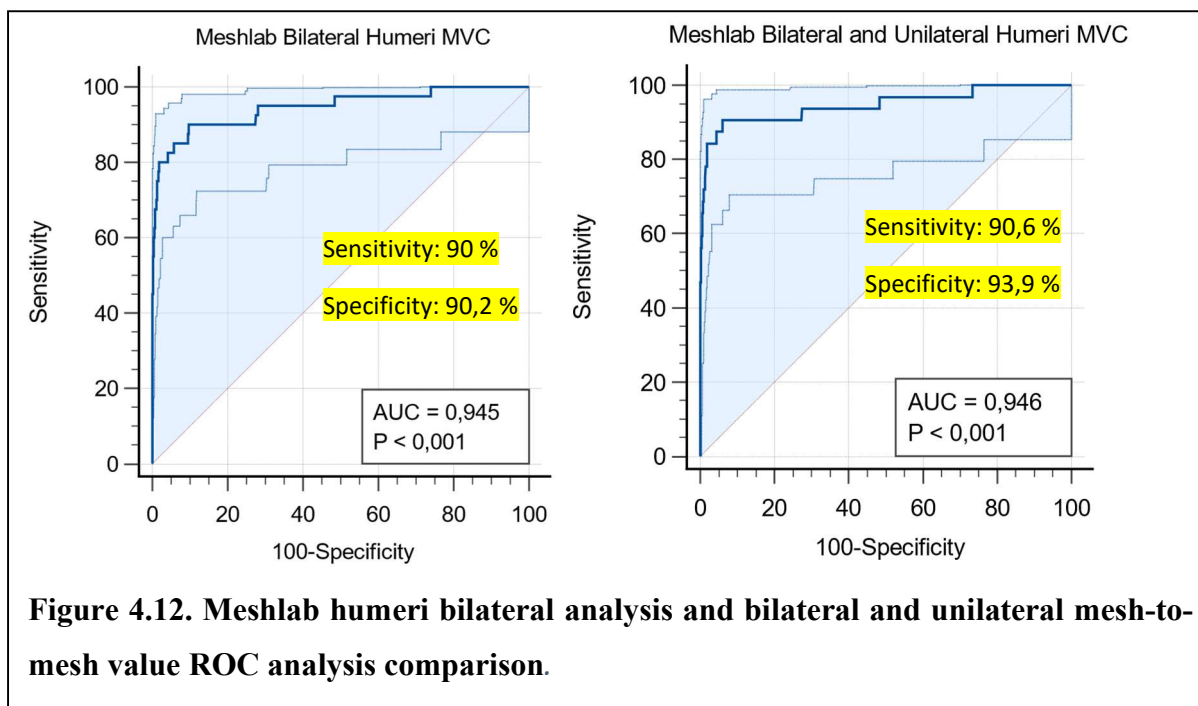
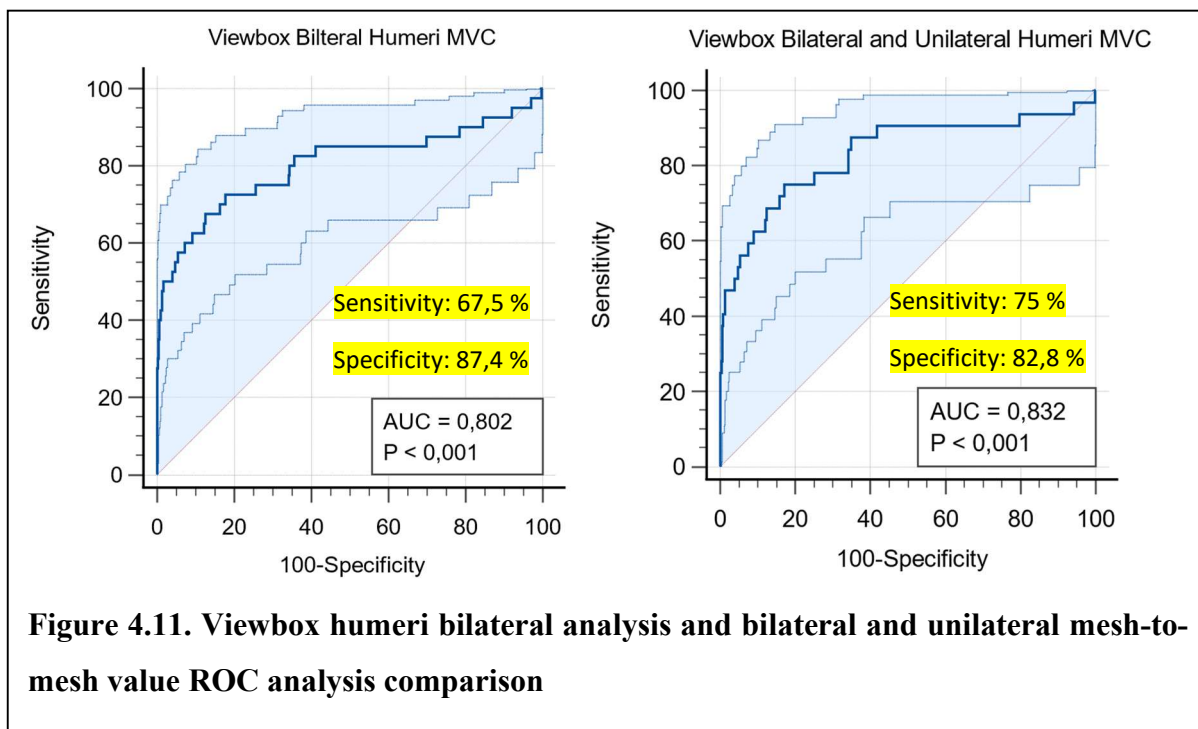
the sample but found it difficult to differentiate between matches and non-matches contained within the sample (Table 4.12).

**Table 4.12. Humeri complete cadaver mesh sensitivity, specificity, PPV and NPV values using the LCV mesh-to-mesh comparison with Viewbox and Meshlab.**

Samples	Sensitivity	Specificity	Positive Predictive value	Negative Predictive value
<b>Viewbox</b>				
Bilateral	60 %	0	64,29 %	0
Unilateral and Bilateral	62,22 %	18,52 %	56 %	22,73 %
<b>Meshlab</b>				
Bilateral	73,68 %	0	93,33 %	0
Unilateral and Bilateral	80 %	50 %	88,89 %	33,33 %

### 4.3.3. ROC Analysis

For the ROC curve analysis for the Viewbox humeri results, the method was able to produce higher specificity (87,4 %; 82,8 %) values compared to sensitivity (67,5 %; 75 %) values. The AUC values (0,80; 0,83) generated are high and closer to 1 while the p-values (< 0,001) are lower than 0,05, which suggests that the method is able to detect the significant differences between positive and negative groups and accurately discriminate between them. The standard error of the curve for the bilateral sample is (0,0491) and (0,0485) for the bilateral and unilateral samples. The threshold value for the bilateral sample is (0,000264) and the bilateral and unilateral sample is (0,000294). Values for each threshold assist in identifying positive (values smaller than the threshold) and negative matches (values higher than the threshold) (Figure 4.11).



The Meshlab values generated for the humeri samples presented with considerably high sensitivity (90 %; 90,6 %) and specificity (90,2 %; 93,9 %) values. The graphs display high AUC values (0,95; 0,95) with significant p-values (< 0,001) which indicates that the graphs are able to accurately discriminate between values for matched pairs and values for negative matches (Figure 4.12).

The threshold value for the bilateral sample is (0,002345) with a standard error of (0,0233) while the threshold value for the bilateral and unilateral sample is (0,002165) with a standard error of the curve of (0,0278). Values that are higher than the threshold are negative matches while values below the threshold are positive pair matches (Figure 4.12).

#### 4.3.4. LCV demographical analysis

Demographical breakdown of the humeri sample for Viewbox LCV analysis displayed higher sensitivity and specificity values for males compared to females and a higher value for South African White individuals compared to South African Black individuals. Elevated sensitivity values were observed for South African Black male (66,67 %; 72,73 %) individuals when compared to South African white male (57,14 %; 57,14 %) individuals and elevated sensitivity levels observed for South African White females (66,67 %; 62,50 %) when compared to South African Black female (57,14 %; 46,15 %) individuals. Specificity rates of all females (9,09 %) individuals and South African Black (9,09 %) individuals were found to be extremely low (Table 4.13).

**Table 4.13. Humeri complete cadaver mesh LCV demographical sensitivity and specificity for the bilateral sample and bilateral and unilateral sample using the Viewbox.**

Samples	Viewbox Humeri LCV		
	Only Bilateral	Bilateral and Unilateral	
	Sensitivity	Specificity	Sensitivity
<b>Sex</b>			
Male	62,50 %	33,33 %	66,67 %
Female	60 %	9,09 %	57,14 %
<b>Ancestry</b>			
<b>SA Black sample</b>	<b>56,25 %</b>	<b>9,09 %</b>	<b>61,54 %</b>
SA Black males	66,67 %	33,33 %	72,73 %
SA Black females	57,14 %	0	46,15 %
<b>SA White sample</b>	<b>62,50 %</b>	<b>23,08 %</b>	<b>63,64 %</b>
SA White males	57,14 %	33,33 %	57,14 %
SA White females	66,67 %	33,33 %	62,50 %

The specificity values observed for the Meshlab LCV analysis exhibited excellent results except for the South African Black (33,33 %) individuals. Males' sensitivity (77,78 %; 92,31 %) results were higher compared to the female (75 %; 77,78 %) results. South African White (85 %; 86,67 %) individuals produced better sensitivity levels compared to South African Black (66,67 %; 77,42 %) individuals for both groups (bilateral; bilateral and unilateral). South African White male (90 %; 100 %) individuals produced higher sensitivity values compared to South African Black male (62,50 %; 85,71 %) individuals while South African White and Black female (80 %; 77,78 %) individual results were equal (Table 4.14).

**Table 4.14. Humeri complete cadaver mesh LCV demographical sensitivity and specificity for the bilateral sample and bilateral and unilateral sample using the Meshlab.**

Samples	Meshlab Humeri LCV		
	Only Bilateral	Bilateral and Unilateral	
	Sensitivity	Specificity	Sensitivity
<b>Sex</b>			
Male	77,78 %	100 %	92,31 %
Female	75 %	100 %	77,78 %
<b>Ancestry</b>			
<b>SA Blacks</b>	<b>66,67 %</b>	<b>33,33 %</b>	<b>77,42 %</b>
SA Black males	62,50 %	100 %	85,71 %
SA Black females	80 %	100 %	77,78 %
<b>SA Whites</b>	<b>85 %</b>	<b>100 %</b>	<b>86,67 %</b>
SA White males	90 %	100 %	100 %
SA White females	80 %	100 %	77,78 %

#### 4.3.5. ROC demographical analysis

The ROC analysis for the humeri sample exhibited considerably lower sensitivity values for South African Black female (40 %; 33 %) individuals compared to all the other sample groups. Specificity levels obtained for all sample groups were notably high with a very small margin of difference between results. The sensitivity levels for males (60 %; 61,5 %) were higher compared to females (55 %; 52,6 %). The South African White (86,7 %) individual's sensitivity values were higher compared to South African Black (64,7 %) individuals for the bilateral and unilateral group (Table 4.15).

South African White females (70 %; 66,7 %) produced higher sensitivity values compared to South African Black female (40 %; 33 %) individuals while Black females (100 %; 100 %) produced higher specificity values compared to White female (94,4 %; 95,1 %) individuals (Table 4.15).

**Table 4.15. Humeri complete cadaver mesh ROC demographical sensitivity and specificity for the bilateral sample and bilateral and unilateral sample using the Viewbox (Appendix D).**

<b>Viewbox Humeri ROC curve analysis</b>						
<b>Samples</b>	<b>Bilateral</b>			<b>Bilateral and Unilateral</b>		
	<b>Sensitivity</b>	<b>Specificity</b>	<b>Threshold</b>	<b>Sensitivity</b>	<b>Specificity</b>	<b>Threshold</b>
<b>Sex</b>						
Male	60 %	92,4 %	<0,000243	61,5 %	94,3 %	<0,000243
Female	55 %	97,6 %	<0,000172	52,6 %	97,8 %	<0,000172
<b>Population groups</b>						
<b>SA Blacks</b>	<b>65 %</b>	<b>84,2 %</b>	<b>&lt;0,000264</b>	<b>64,7 %</b>	<b>83,6 %</b>	<b>&lt;0,000264</b>
SA Black males	60 %	95,6 %	<0,000205	57,1 %	96,8 %	<0,000205
SA Black females	40 %	100 %	<0,000166	33 %	100 %	<0,000162
<b>SA Whites</b>	<b>65 %</b>	<b>93,4 %</b>	<b>&lt;0,000215</b>	<b>86,7 %</b>	<b>76,5 %</b>	<b>&lt;0,000294</b>
SA White males	50 %	96,7 %	<0,000212	66,7 %	85,2 %	<0,000243
SA White females	70 %	94,4 %	<0,000172	66,7 %	95,1 %	<0,000172

The Meshlab ROC analysis yielded satisfactory results for all specificity values of each sample. The results obtained for the male and female individuals were over 90 % for sensitivity and specificity. The sensitivity levels obtained for South African White (90 %; 93,3 %) individuals were higher compared to South African Black (75 %; 82,4 %) individuals. South African White males (100 %; 100 %) and females (90 %; 88,9 %) performed better sensitivity levels compared to South African Black male (70 %; 85,7 %) and female (80 %; 77,8 %) individuals. With regards to specificity, all male (92,4 %; 99,6 %) individuals produced higher results compared to all female (91,6 %; 91,2 %) individuals. In comparison to South African White females (93,3

%; 93,8 %), South African Black females (97,8 %; 97,5 %) exhibited higher specificity rates (Table 4.16).

**Table 4.16. Humeri complete cadaver mesh ROC demographical sensitivity and specificity for the bilateral sample and bilateral and unilateral sample using the Meshlab (Appendix E).**

<b>Meshlab Humeri ROC curve analysis</b>						
<b>Samples</b>	<b>Bilateral</b>			<b>Bilateral and Unilateral</b>		
	<b>Sensitivity</b>	<b>Specificity</b>	<b>Threshold</b>	<b>Sensitivity</b>	<b>Specificity</b>	<b>Threshold</b>
<b>Sex</b>						
Male	90 %	92,4 %	<0,002345	92,3 %	99,6 %	<0,001852
Female	90 %	91,6 %	<0,002165	94,4 %	91,2 %	<0,002165
<b>Population groups</b>						
<b>SA Blacks</b>	<b>75 %</b>	<b>96,6 %</b>	<b>&lt;0,00177</b>	<b>82,4 %</b>	<b>96,3 %</b>	<b>&lt;0,00177</b>
SA Black males	70 %	97,8 %	<0,00177	85,7 %	98,4 %	<0,001696
SA Black females	80 %	97,8 %	<0,00177	77,8 %	97,5 %	<0,00177
<b>SA Whites</b>	<b>90 %</b>	<b>96,3 %</b>	<b>&lt;0,00206</b>	<b>93,3 %</b>	<b>96,1 %</b>	<b>&lt;0,00206</b>
SA White males	100 %	95,6 %	<0,002343	100 %	100 %	<0,001852
SA White females	90 %	93,3 %	<0,00206	88,9 %	93,8 %	<0,00206

#### **4.4. Comparative analysis between femora and humeri results**

The results obtained for the femora and the humeri were compared to assess the performance of the mesh-to-mesh value comparison method. The LCV comparison method described by Karell *et al.* (2019) yielded results showing a higher rate in specificity, PPV, and NPV for the humerus. The sensitivity rates, however, varied according to the software used. The humerus produced a higher sensitivity rate compared to the femur with Viewbox. While with Meshlab, the femur resulted in a higher sensitivity rate when compared to the humerus.

The ROC curve analysis performed as described by Delong *et al.* (1988) resulted in the humerus producing a higher sensitivity rate for Viewbox and Meshlab. The specificity rate, however, varied, with the femur producing a higher specificity rate and AUC value with Meshlab when compared to the humerus, and the humerus producing a higher specificity rate and AUC value with Viewbox.

The outcome suggests that the LCV and the ROC analytical methods for the humerus were able to identify a higher number of true positive and low number of false negatives within the sample. While the femur performed better at identifying true negatives within the sample.

A comparative analysis was performed for the AUC values for the ROC curves between the humerus and the femur. It was found that the p-values obtained were higher than 0,05, which suggests there was no significant difference between AUC values obtained for the humerus and the femur. Although for the two different softwares used, the AUC values obtained through Viewbox and Meshlab for both the humerus and femur were significantly different with the p-values less than and equal to 0.05.

#### **4.5. Cadaveric Fragmented Femora Mesh Comparison Sample**

The complete femora 3D models were grouped, randomised, and separated into different groups for each model to be sliced. The models were sliced to provide the appearance of fragmented bones. After being sliced, the models were renamed to aid in distinguishing and identifying the differences between the simulated fragmented meshes and the complete 3D femora models. The right-sided sliced models were mirrored using Meshlab to assist in the superimposing of meshes to obtain the mesh-to-mesh value for comparison.

A total of 20 femora comprising right and left were grouped into three groups: proximal fragments, distal fragments, and shaft fragments. The three groups were formed to determine which part of the bones would perform best for analysis when working with fragmented remains. The samples were sliced based on the distinct anatomical markers that can be used to identify them. Each group was tested against the Viewbox and Meshlab softwares to obtain mesh-to-mesh values, which were then analysed independently using LCV mesh-to-mesh analysis and ROC curve analysis.

#### 4.5.1. Group 1 - Proximal Mesh Sample

According to Viewbox, the duration of the program was 2hrs30mins, and a total of 99 tests were performed. Meshlab program ran for a total of 3hrs1min for 99 tests.

- **LCV Analysis**

Between the two softwares, Meshlab produced a higher number of true negative results and lower true positive results. The number of false results (false positives and negatives) produced for both softwares were almost equal (10 false results for Viewbox and 9 for Meshlab). The results indicate that Meshlab is more adapt at identifying negative results (non-matches) and Viewbox is better suited to identify positive results (matches) (Table 4.17).

**Table 4.17. Fragmented proximal femora mesh results using the LCV mesh-to-mesh comparison with Viewbox and Meshlab.**

<b>Samples</b>	<b>False Negative</b>	<b>False Positive</b>	<b>True Negative</b>	<b>True Positive</b>	<b>Total</b>
<b>Viewbox</b>					
Unilateral and Bilateral	2	8	6	4	20
<b>Meshlab</b>					
Bilateral and Unilateral	3	6	9	2	20

Viewbox (66,67 %) produced a higher sensitivity value when compared to Meshlab (40 %) while Meshlab (60 %) produced higher specificity value when compared to Viewbox (42,86 %). Both softwares produced considerably lower PPV (33,33 %; 25 %) values and high NPV (75 %; 75 %) rates (Table 4.18).

**Table 4.18. Fragmented proximal femora mesh sensitivity, specificity, PPV and NPV values using the LCV mesh-to-mesh comparison with Viewbox and Meshlab.**

Samples	Sensitivity	Specificity	Positive Predictive value	Negative Predictive value
<b>Viewbox</b>				
Unilateral and Bilateral	66,67 %	42,86 %	33,33 %	75 %
<b>Meshlab</b>				
Unilateral and Bilateral	40 %	60 %	25 %	75 %

▪ **ROC Analysis**

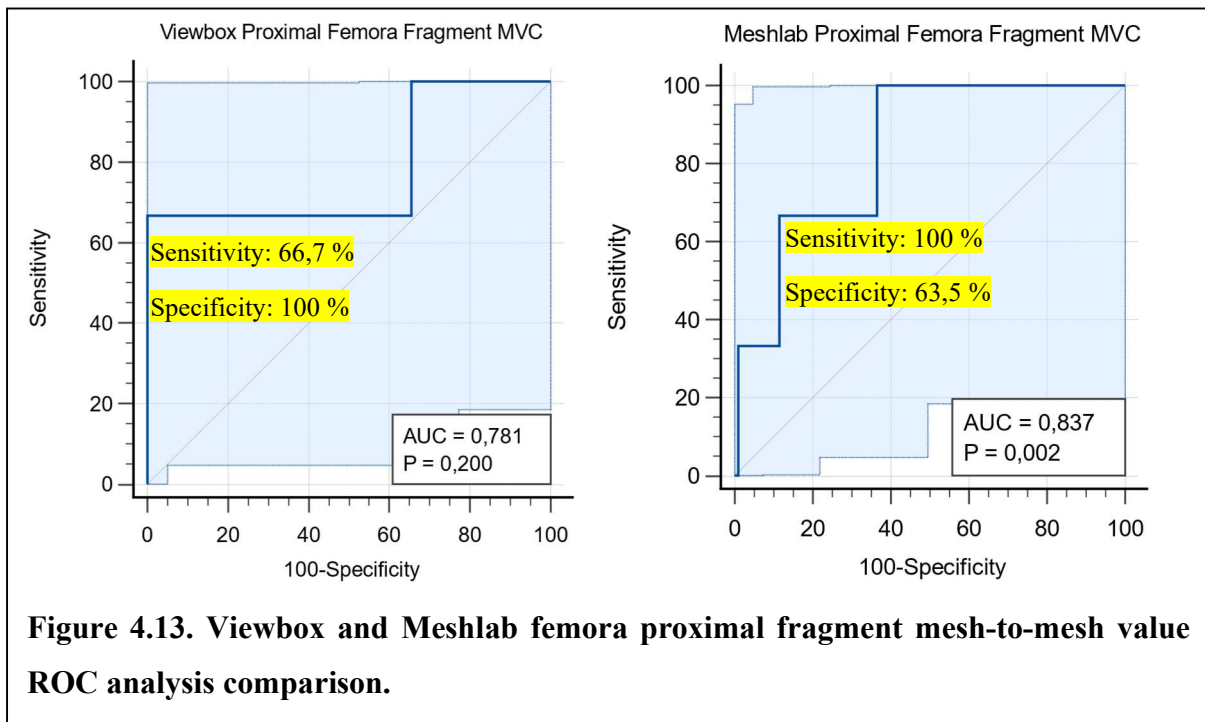


**Figure 4.13. Viewbox and Meshlab femora proximal fragment mesh-to-mesh value ROC analysis comparison.**

The ROC analysis for proximal fragment femora mesh exhibited higher specificity values for Viewbox (100 %) when compared to Meshlab (63,5 %) and higher sensitivity values for Meshlab (100 %) compared to Viewbox (66,7 %). The AUC value for Meshlab (0,84) is much better compared to Viewbox (0,78). The p-value for Meshlab (0,002) showed a significant difference between positive and negative results, whereas the p-value for Viewbox (0,2) showed no significant differences, and the statistical method found it difficult to differentiate between the two groups. The threshold value for Viewbox was (0,000137) while the threshold value for Meshlab was (0,003121). Values below the threshold for each software is considered

a positive match while values above the threshold are considered negative matches (Figure 4.13).

#### 4.5.2. Group 2 - Distal Mesh Sample

The distal mesh fragment models followed the same procedure as the proximal mesh fragment for slicing and mirroring of right models.

- **LCV Analysis**

For the distal fragment mesh, Viewbox was able to correctly identify the true positives and negatives within the sample and produced no false negative results.

While Meshlab was unable to identify the true positives within the sample but able to identify most of the true negatives (Table 4.19).

**Table 4.19. Fragmented distal femora mesh results using the LCV mesh-to-mesh comparison with Viewbox and Meshlab.**

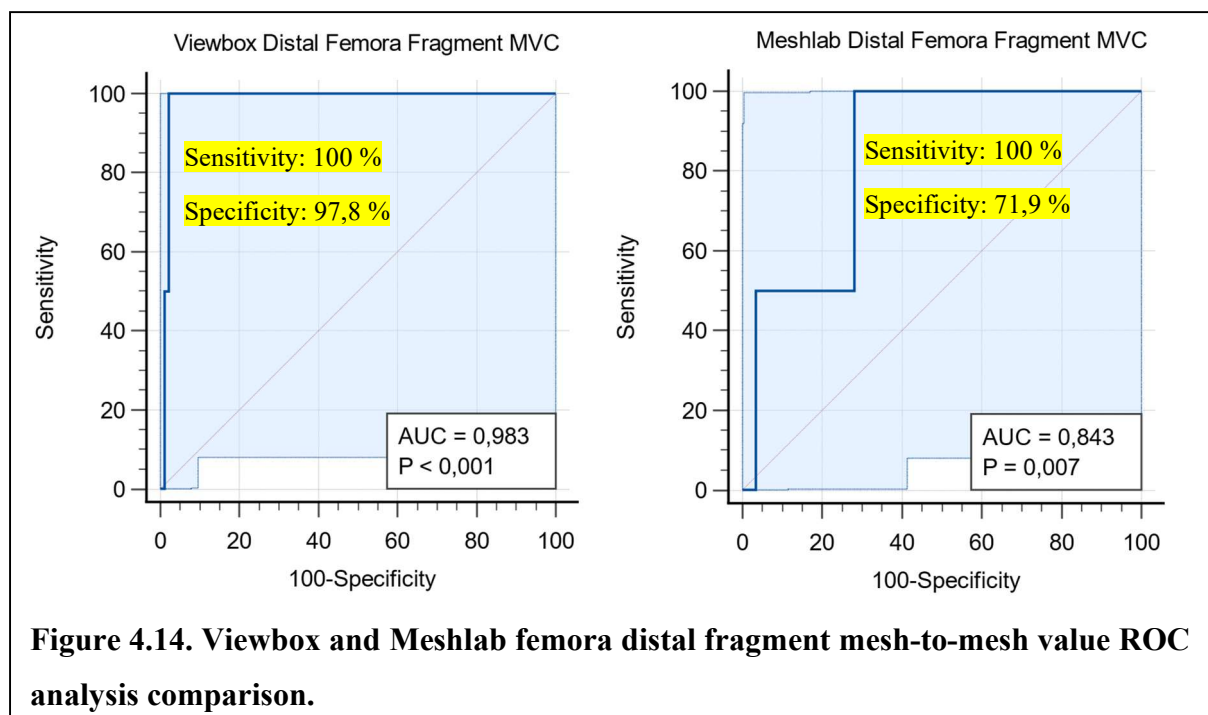
<b>Samples</b>	<b>False Negative</b>	<b>False Positive</b>	<b>True Negative</b>	<b>True Positive</b>	<b>Total</b>
<b>Viewbox</b>					
Unilateral and Bilateral	0	8	8	4	20
<b>Meshlab</b>					
Bilateral and Unilateral	3	6	11	0	20

Sensitivity (100 %) and NPV (100 %) levels for the distal femora fragment using Viewbox were excellent which suggests that software was able to correctly identify paired matches. For Meshlab (64,71 %), the software was able to produce higher specificity values when compared to Viewbox (50 %) however, was unable to identify any of the positive matches within the sample (Table 4.20).

Table 4.20. Fragmented distal femora mesh sensitivity, specificity, PPV and NPV values using the LCV mesh-to-mesh comparison with Viewbox and Meshlab.

Samples	Sensitivity	Specificity	Positive Predictive value	Negative Predictive value
<b>Viewbox</b>				
Unilateral and Bilateral	100 %	50 %	33,33 %	100 %
<b>Meshlab</b>				
Unilateral and Bilateral	0	64,71 %	0	78,57 %

▪ **ROC Analysis**



Between Meshlab and Viewbox (100 %), sensitivity levels were found to be equal while the specificity values were higher for Viewbox (97,8 %) compared to Meshlab (71,9 %). The AUC values (0,98; 0,84) for both softwares were high whereas the p-value for Meshlab (0,007) was slightly higher compared to Viewbox (< 0,001). The p-value suggests that Viewbox results produced slightly more significant results compared to Meshlab. The threshold value for Viewbox was (0,0001998) and for Meshlab was (0,003182). For all values below the threshold are positive matches and values above the threshold indicate negative matches (Figure 4.14).

### 4.5.3. Group 3 - Shaft only Mesh Sample

The fragmented shaft mesh models were renamed and sliced according to both the proximal and distal mesh slicing methods. After rendering the models, the models were imported into Viewbox, the Viewbox and Meshlab programs performed 99 tests for each software.

- **LCV Analysis**

When comparing the results obtained for fragmented shaft mesh in both softwares, Viewbox had a higher number of false positives and a lower number of true negatives than Meshlab. While the number of true positives and false negatives were equal for Viewbox and Meshlab (Table 4.21).

**Table 4.21. Fragmented shaft femora mesh results using the LCV mesh-to-mesh comparison with Viewbox and Meshlab.**

<b>Samples</b>	<b>False Negative</b>	<b>False Positive</b>	<b>True Negative</b>	<b>True Positive</b>	<b>Total</b>
<b>Viewbox</b>					
Unilateral and Bilateral	1	10	5	4	20
<b>Meshlab</b>					
Bilateral and Unilateral	1	6	9	4	20

The sensitivity values for both softwares were equal while for specificity, PPV and NPV values, Meshlab produced considerably higher results compared to Viewbox. Both softwares work well at accurately identifying paired matches within a sample but have difficulty in separating false results with true negative (non-matches) results (Table 4.22).

**Table 4.22. Fragmented shaft femora mesh sensitivity, specificity, PPV and NPV values using the LCV mesh-to-mesh comparison with Viewbox and Meshlab.**

Samples	Sensitivity	Specificity	Positive Predictive value	Negative Predictive value
<b>Viewbox</b>				
Unilateral and Bilateral	80 %	33,33 %	28,57 %	83,33 %
<b>Meshlab</b>				
Unilateral and Bilateral	80 %	60 %	40 %	90 %

- **ROC curve analysis**

The ROC curve analysis for the shaft femora fragment demonstrated higher specificity values for Viewbox (100 %) and higher sensitivity values for Meshlab (100 %). Between the AUC values displayed, Meshlab (0,95) produced a higher result, implying that Meshlab works better at differentiating and discriminating between positive and negative results. While the p-values suggests for both graphs that Meshlab (< 0,001) is able to identify significant differences between the groups while Viewbox (0,19) found it difficult. The threshold value for Viewbox is (0,00009445) and for Meshlab it is (0,001892). Values above the threshold would be used to identify positive matches while values above the threshold will indicate negative matches (Figure 4.15).

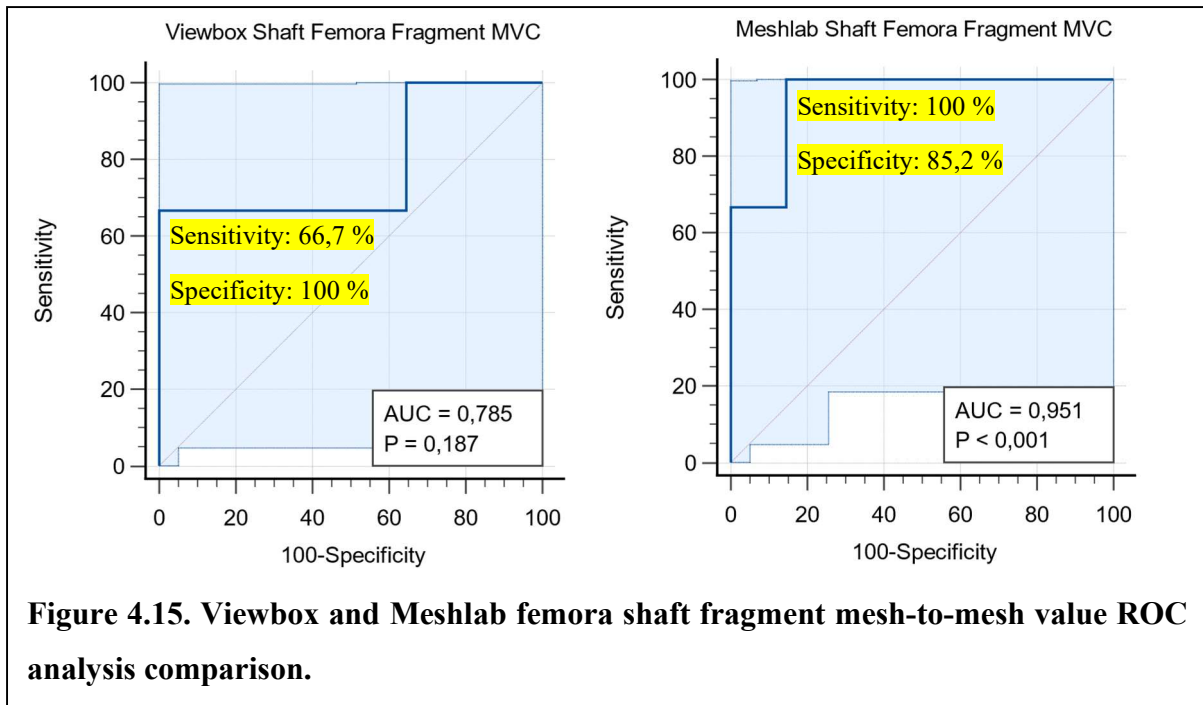


**Figure 4.15. Viewbox and Meshlab femora shaft fragment mesh-to-mesh value ROC analysis comparison.**

#### 4.6. Cadaveric Fragmented Humeri Mesh Comparison Sample

A total of 20 humeri bones consisting of right sided and left sided bones were grouped into three sub-groups: proximal fragments, distal fragments, and shaft fragments. Each group was tested against Viewbox and Meshlab softwares to obtain mesh-to-mesh values and analysed separately using LCV mesh-to-mesh analysis and ROC curve analysis.

##### 4.6.1. Group 1 – Proximal Mesh Sample

The proximal mesh fragment was sliced and renamed for randomisation and identification. The proximal mesh fragment on Viewbox and Meshlab performed 100 tests.

- **LCV Analysis**

The results obtained through Viewbox produced a higher number of true negatives and positives compared to Meshlab. Whereas the Meshlab results produced a higher number of false negatives and positives within the humeri samples when compared to Viewbox. The results obtained suggests that Viewbox is more adapt at identifying matches and non-matches among fragmented humeri bones compared to Meshlab (Table 4.23).

**Table 4.23. Fragmented proximal humeri mesh results using the LCV mesh-to-mesh comparison with Viewbox and Meshlab.**

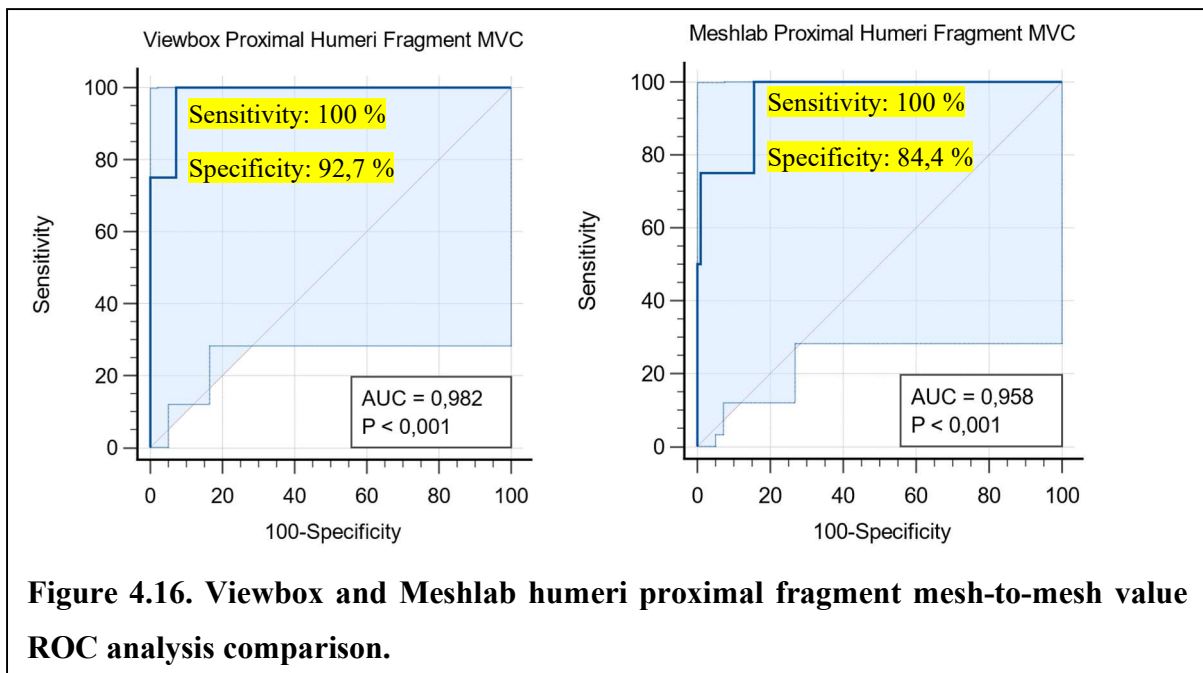
<b>Samples</b>	<b>False Negative</b>	<b>False Positive</b>	<b>True Negative</b>	<b>True Positive</b>	<b>Total</b>
<b>Viewbox</b>					
Unilateral and Bilateral	0	4	8	8	20
<b>Meshlab</b>					
Bilateral and Unilateral	1	8	5	6	20

Viewbox analytical results produced considerably higher sensitivity (100 %), specificity (66,67 %), PPV (66,67 %) and NPV (100 %) values when compared to the results obtained through Meshlab. In comparison to Viewbox, the results suggests that Meshlab was poorly suited to generate accurate results with the LCV method (Table 4.24).

**Table 4.24. Fragmented proximal humeri mesh sensitivity, specificity, PPV and NPV values using the LCV mesh-to-mesh comparison with Viewbox and Meshlab.**

<b>Samples</b>	<b>Sensitivity</b>	<b>Specificity</b>	<b>Positive Predictive value</b>	<b>Negative Predictive value</b>
<b>Viewbox</b>				
Unilateral and Bilateral	100 %	66,67 %	66,67 %	100 %
<b>Meshlab</b>				
Unilateral and Bilateral	85,71 %	38,46 %	42,86 %	83,33 %

- **ROC Analysis**



Analysis for the humeri proximal fragments display equal sensitivity values for Viewbox and Meshlab (100 %) while specificity values were higher for Viewbox (92,7 %) compared to Meshlab (84,4 %). The AUC values (0,98; 0,96) and p-values (< 0,001) for both softwares are quite similar. The threshold value for Viewbox was (0,000159) and for Meshlab it is (0,002437). Higher values than the threshold are negative results while values below the threshold are positive pair matches results (Figure 4.16).

#### 4.6.2. Group 2 – Distal Mesh Sample

For the distal mesh fragment, the models were sliced and renamed for randomisation and identification. The Viewbox and Meshlab software ran the program for 100 tests.

- **LCV Analysis**

For the distal mesh fragments for the humerus, Viewbox produced a higher number of true negatives and positives compared to Meshlab. Whereas Meshlab produced a high number of false results such as false positives and negatives within the sample compared to Viewbox and was unable to identify any true positive matches contained within the sample (Table 4.25).

**Table 4.25. Fragmented distal humeri mesh results using the LCV mesh-to-mesh comparison with Viewbox and Meshlab.**

<b>Samples</b>	<b>False Negative</b>	<b>False Positive</b>	<b>True Negative</b>	<b>True Positive</b>	<b>Total</b>
<b>Viewbox</b>					
Unilateral and Bilateral	0	8	8	4	20
<b>Meshlab</b>					
Bilateral and Unilateral	1	12	7	0	20

The sensitivity, specificity, PPV and NPV values for Viewbox were substantially higher compared to the results obtained through the Meshlab software. The results are a good indication that Meshlab is not well suited at matching fragmented distal remains (Table 4.26).

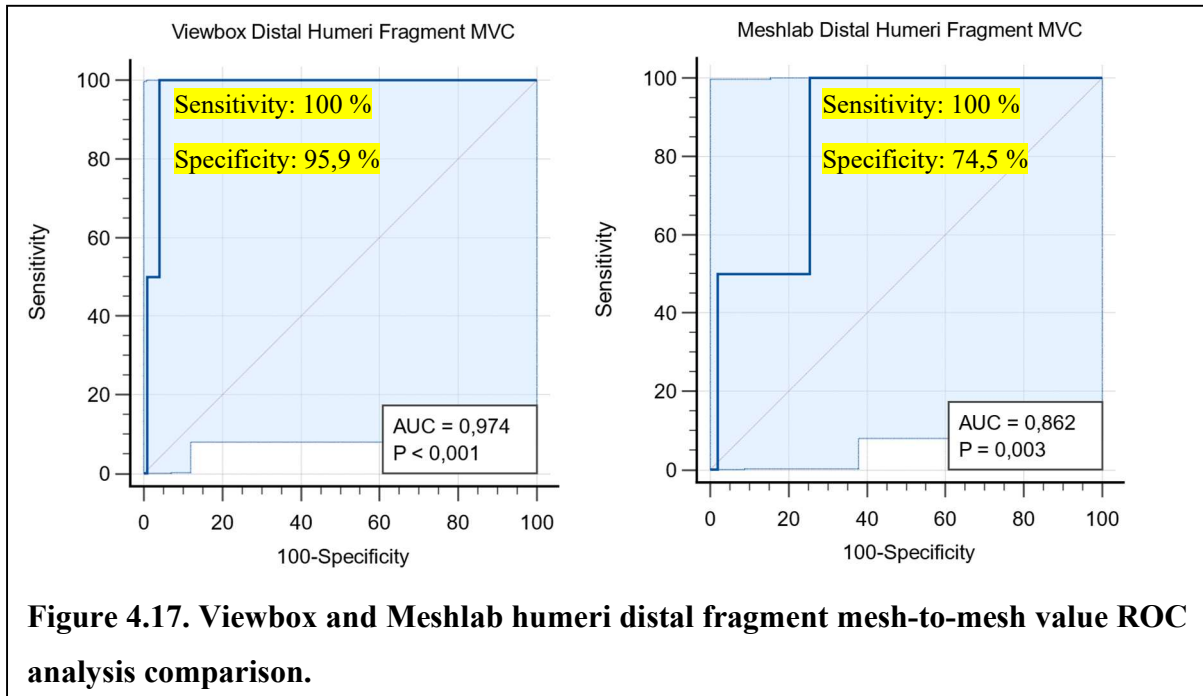
**Table 4.26. Fragmented distal humeri mesh sensitivity, specificity, PPV and NPV values using the LCV mesh-to-mesh comparison with Viewbox and Meshlab.**

<b>Samples</b>	<b>Sensitivity</b>	<b>Specificity</b>	<b>Positive Predictive value</b>	<b>Negative Predictive value</b>
<b>Viewbox</b>				
Unilateral and Bilateral	100 %	50 %	33,33 %	100 %
<b>Meshlab</b>				
Unilateral and Bilateral	0	36,84 %	0	87,50 %

- **ROC Analysis**

For ROC curve analysis, the distal humerus displayed equal sensitivity values for Viewbox and Meshlab (100 %). The specificity values between the softwares were higher for Viewbox (95,9 %) compared to Meshlab (74,5 %) (Figure 4.17).

Meshlab (0,003) produced a slightly higher p-value suggesting that the results obtained through Meshlab are not as significantly accurate to distinguish between the positive and the negative results as compared to Viewbox (< 0,001). The threshold value for Viewbox was (0,000146) and for Meshlab it is (0,002554). Higher values than the threshold are negative results while values below the threshold are positive pair matches results (Figure 4.17).



#### 4.6.3. Group 3 – Shaft only Mesh Sample

After modelling was complete, each model was sliced and renamed. A number of 99 tests were performed for Viewbox and Meshlab.

- **LCV Analysis**

The number of true negatives produced through Viewbox were higher compared to Meshlab while the number of true positive results for both softwares were equal. However, the number of false results were higher for Meshlab compared to Viewbox (Table 4.27).

**Table 4.27. Fragmented shaft humeri mesh results using the LCV mesh-to-mesh comparison with Viewbox and Meshlab.**

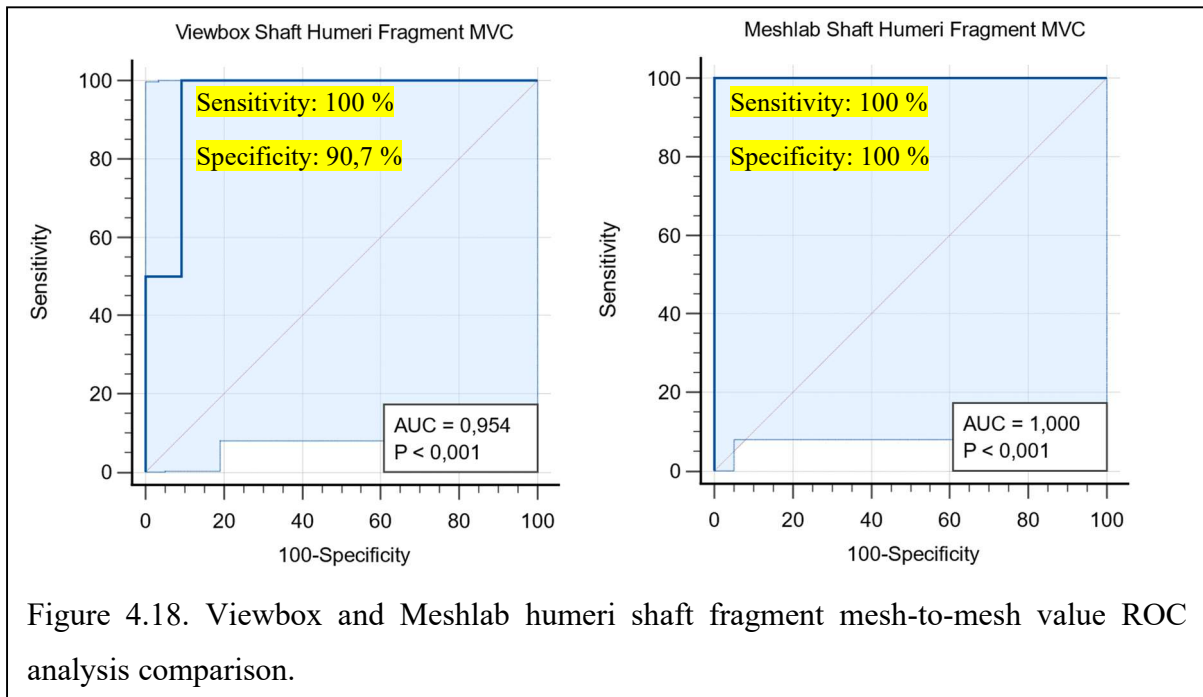
<b>Samples</b>	<b>False Negative</b>	<b>False Positive</b>	<b>True Negative</b>	<b>True Positive</b>	<b>Total</b>
<b>Viewbox</b>					
Unilateral and Bilateral	0	6	10	4	20
<b>Meshlab</b>					
Bilateral and Unilateral	0	8	8	4	20

The results obtained for the LCV method indicates that Viewbox was better adapted for fragmented results, producing higher specificity (62,50 %) and PPV (40 %) values. While the sensitivity and NPV values produced were equal for Viewbox and Meshlab (100 %) (Table 4.28).

**Table 4.28. Fragmented shaft humeri mesh sensitivity, specificity, PPV and NPV values using the LCV mesh-to-mesh comparison with Viewbox and Meshlab.**

<b>Samples</b>	<b>Sensitivity</b>	<b>Specificity</b>	<b>Positive Predictive value</b>	<b>Negative Predictive value</b>
<b>Viewbox</b>				
Unilateral and Bilateral	100 %	62,50 %	40 %	100 %
<b>Meshlab</b>				
Unilateral and Bilateral	100 %	50 %	33,33 %	100 %

- **ROC curve analysis**



The ROC curve analysis for the humeri shaft fragment produced excellent sensitivity (100 %) results for both softwares and slightly lower specificity (90,7 %) values for Viewbox. The AUC (0,95; 1,0) and p-values ( $< 0,001$ ) generated indicates that both softwares were able to significantly identify the differences between the positive and negative groups within the sample. The threshold value for Viewbox was 0,000157 and for Meshlab it is 0,001044. Higher values than the threshold are negative results while values below the threshold are positive pair matches results (Figure 4.18).

#### 4.7. Commingled Forensic Mesh Comparison

A total of 11 commingled femora and humeri were photographed and photogrammetrically 3D modelled using Agisoft Metashape software. ROC curve analysis could not be performed due to insufficient data. ROC curve requires positive and negative results within a sample to determine a threshold, however, within the commingled forensic sample, a positive result could not be obtained.

#### 4.7.1. Femora Mesh

There were six femora bones that were captured and rendered. The sample consisted of three right-sided bones and three left-sided bones. Evidence of fragmentation and taphonomy was present. The presence of taphonomy on the bones assisted in capturing distinct features that were used for alignment during the modelling process. There were no misalignments present during the modelling process.

- **LCV Analysis**

The minimum number of individuals (MNI) was first determined by Meyer (2016) through the frequency of crania, and then femurs and humeri. Pair-matching results for the case report were obtained using the methods described by Byrd and Adams, (2003); L'Abbé, (2005); Snow, (1948); Ubelaker, (2002); İşcan and Steyn, (2013), were not able to pair match any of the femora, suggesting an MNI of 6 for the femora. The LCV method yielded a high number of true negatives which is consistent with the results reported in the case report. The results obtained proves that the method is adapt at identifying non-matches within a real-world commingled case where prior knowledge of matches are unknown. Viewbox and Meshlab performed equally well and there was no difference in results observed between the two (Table 4.29).

**Table 4.29. The number of true and false positive and negative results obtained through Viewbox 4.1 and Meshlab 2022.12.**

<b>Samples</b>	<b>False Negative</b>	<b>False Positive</b>	<b>True Negative</b>	<b>True Positive</b>	<b>Total</b>
<b>Viewbox</b>					
Sample	0	2	4	0	6
<b>Meshlab</b>					
Sample	0	2	4	0	6

As the output results obtained for the LCV mesh-to-mesh comparison were the same for both softwares, the specificity (66,67 %) and NPV (100 %) values were equal. Sensitivity and PPV values could not be obtained since there were no true positive results obtained within the sample (Table 4.30).

**Table 4.30. Statistical sensitivity, specificity, PPV and NPV values obtained for the LCV method using Viewbox 4.1 and Meshlab 2022.12.**

Samples	Sensitivity	Specificity	Positive Predictive value	Negative Predictive value
<b>Viewbox</b>				
Sample	0	66,67 %	0	100 %
<b>Meshlab</b>				
Sample	0	66,67 %	0	100 %

#### 4.7.2. Humeri Mesh

A total of five commingled bones were captured and rendered for 3D modelling. The sample included three right-sided bones and two left-sided bones. The bones were highly fragmented which increased the overall modelling time and for one of the bones, the capturing method had to be slightly adjusted to accommodate its features. This bone had the proximal and distal ends missing, only the shaft was present.

- **LCV Analysis**

The minimum number of individuals (MNI) was first determined by Meyer (2016) through the frequency of crania, and then femurs and humeri. Pair-matching results for the case report were obtained using the methods described by Byrd and Adams, (2003); L'Abbé, (2005); Snow, (1948); Ubelaker, (2002); İşcan and Steyn, (2013), were not able to pair match any of the humeri, suggesting an MNI of 5 for the humeri. Meshlab performed better at identifying the true negatives within the sample compared to Viewbox. Viewbox's ability to identify negative matches was unsatisfactory, which led to a high number of false positives and inaccurate results (Table 4.31).

**Table 4.31. The number of true and false positive and negative results obtained through Viewbox 4.1 and Meshlab 2022.12 for the humeri commingled sample.**

Samples	False Negative	False Positive	True Negative	True Positive	Total
<b>Viewbox</b>					
Sample	0	4	1	0	5
<b>Meshlab</b>					
Sample	0	2	3	0	5

Viewbox (20 %) produced considerably lower specificity values compared to Meshlab (60 %) suggestive that Viewbox has a difficulty identifying true non-matches within a sample. The NPV (100 %) values for both softwares were equal which could mean that the method is able to detect the possibility of a negative matches among the samples (Table 4.32).

**Table 4.32. Statistical sensitivity, specificity, PPV and NPV values obtained for the LCV method using Viewbox 4.1 and Meshlab 2022.12 for the humeri commingled sample.**

Samples	Sensitivity	Specificity	Positive Predictive value	Negative Predictive value
<b>Viewbox</b>				
Sample	0	20 %	0	100 %
<b>Meshlab</b>				
Sample	0	60 %	0	100 %

## 5 Discussion

In recent years, there have been many advances in introducing three-dimensional technology to assist in the sorting and identification of commingled human remains. One of them is the superimposition of left and right 3D meshes or the mesh-to-mesh value comparison (MVC) method. The MVC method digitally compares two bilateral three-dimensional models by superimposing the two and producing a root-mean-square distance value based on the similarity between the models. The lowest value produced between all the right and left models would be considered a true positive pair match. Thus, to assess the overall effectiveness and accuracy of the method, the method was applied against three-dimensional models created using Structure-from-Motion. The method was further assessed through the application of a complete, fragmented, and small-scaled forensic archaeological sample of femora and humeri. The results were obtained through two different 3D editing softwares: Viewbox 4.1 and Meshlab 2022.12.

### 5.1. Comparative analysis of the three-dimensional femora and humeri models created using Structure-from-Motion.

The humerus and the femur are two of the largest bones in the upper and lower limb, respectively (White and Folkens, 2005). Both bones are long bones which consist of epiphyses and a dense cortical midshaft (White and Folkens, 2005). These bones are often discovered in archaeological, forensic, and paleontological environments due to their density, durability, and strength (White and Folkens, 2005; Winter *et al.*, 2021). In forensic situations, they can be used for sex and stature estimations of skeletal material due to their anatomical morphological attributes (White and Folkens, 2005; Karell, 2019; Winter *et al.*, 2021).

In the study performed by Karell *et al.* (2016) on mesh-to-mesh comparisons, the humerus was selected based on the bone's highly asymmetrical characteristics. Therefore, including the humerus in the current study makes it comparable to the previous study while taking into account asymmetrical variability among pair-matched long bones (Auerbach and Ruff, 2006; Karell *et al.*, 2016). The femur was selected since most often in commingled cases other than the cranium, this element is commonly recovered at the site because of the bone's morphology and structural integrity (Adams and Konigsberg, 2004; L'Abbè, 2005; Adams and Byrd, 2006). The upper limb bones have been known to be slightly more asymmetrical than the lower limb bones due to mechanical stressors thus comparing the humerus to the femur may assist in

assessing variations and similarities with bones when pair-matching remains and the compatibility of the mesh-to-mesh value comparison method against highly asymmetrical elements (Auerbach and Ruff, 2006).

The results obtained for the femur in this study presented high sensitivity for the Lowest Common Value (LCV) method (85,3 %) and the Receiver Operating Characteristic (ROC) curve method (84,4 %) and specificity (95,8 %) levels with Meshlab software and ROC curve statistical analysis. The results from the LCV and ROC analysis suggests that the method performs well at identifying positively matched pairs within the sample but has difficulty identifying negative pairs or non-matches when analysing with the LCV method (specificity: 63,6 %). The LCV method functions on the principle that the lowest value obtained left-right and right-left indicates a true positive pair match. The low specificity result may be related to the number of false positives that were found within the sample, the higher the number of false positives, the lower the rate of specificity within the sample.

For the femora, the results suggest that the method performs well when combining the results obtained with Meshlab and the statistical analysis of the ROC curve method. However, when applied to large, commingled assemblages such as 80 to 100 bony elements, the use of Meshlab would become tedious and laborious thus Viewbox would be better suited for large mesh-to-mesh comparisons as long as pre-alignment of all the models is performed before comparisons. While the LCV method produces high sensitivity values, the method does introduce a high number of false positives and negatives which may lead to incorrectly eliminating elements that may have positive pair-match thus complicating situations when applied to a large, commingled assemblage.

With particular attention to the results from Viewbox for the bilateral and unilateral humeri sample, the LCV method produced lower sensitivity (62,2%) and specificity (18,5%) values than previously reported by Karell *et al.* (2016), where they achieved sensitivity of 95% and specificity of 60%. The difference in results may be attributed to the sample size, the type of sample collection, differences in methodology and randomisation of data and the presence of pathologies and post-mortem damage.

The differences in methodology observed were during the pre-registration process and the process of randomisation of the data. Pre-alignment or pre-registration refers to aligning and orientating every model along the x-, y-, z-axis before importing all the models into the

software for comparison. This alignment procedure assists the program during the mesh-to-mesh model comparison process to correctly align corresponding points. For example, ensuring that proximal end of a mirrored right humerus aligns over the proximal end of a left humerus based on corresponding points, instead of proximal end of a humerus matching with the distal end of another humerus (Karell, 2019; Lynch, 2021).

Pre-alignment/pre-registration was performed for the clavicle, temporal, and calcaneus bones in the study by Karell (2019), with the exception of the humerus, for which a rough alignment was performed on Viewbox during comparison. Therefore, the difference in sensitivity and specificity levels found within this study may suggest that the pre-alignment of the models does make a difference and could be a possible factor for the decrease in the sensitivity and specificity found.

Another factor to consider is the presence of pathologies such as osteoarthritis and post-mortem damage in a few bones in this study, which makes it less diagnostic. The presence of post-mortem damage and pathologies may affect and change the surface morphology of the bone. Pathology (e.g., osteoarthritis) and post-mortem bone damage were present in a few individuals, which may increase the dissimilarity present between bilaterally paired bones, reducing the number of common feature points required to match the paired bones using the mesh-to-mesh comparison method and thus increasing the difficulty of the analysis.

The sample was substantially higher compared to the size (45) used by Karell *et al.* (2016). Their sample collection included a mix of historical and modern individuals: medieval Scottish collections around the fifteenth and seventeenth century, an archaeological Ibiza cathedral collection from the thirteenth to early nineteenth century from Spain, a modern human collection from the Frassetto Collection in Italy (these individuals died in the first decade of the twentieth century). In this study, the sample collection included a mix of individuals from at least the earliest of the 1940s of European and African descent (Dayal *et al.*, 2009). The difference in the results may be related to the high rate of diversity present among the South African population (Kruger, 2014; Liebenberg, 2014; Maass and Friedling, 2018).

There is a high degree of bilateral asymmetrical variation present between sexes and among several different population groups. This variation can greatly affect the outcome of sorting and pair matching remains in a commingled assemblage. Between males and females, the femur and the humerus are known to be larger and more robust for males and smaller and more

gracile for females. Studies performed by Kruger, (2014); Liebenberg, (2014) and Maass and Friedling, (2018) evaluated the skeletal asymmetrical differences and shape variations present among South African Black and South African White individuals for long bones. In their studies, they observed that South African White individuals' skeletal structures were significantly larger in shape and size and presented with a lower degree of sexual dimorphic variation when compared to South African Black individuals. This variation present between sexes and sex-population specific groups may contribute to the disparity noticed amongst South African White and Black individuals (Kruger, 2014; Liebenberg, 2014; Maass and Friedling, 2018).

The sexually dimorphic features that are present on long bones may also be the reason behind some of the difficulties that appeared during photogrammetrically modelling the femora and the humeri bones. This study introduces the concept and application of the Structure-from-Motion technique in pair-matching bilateral bone models with the use of the mesh-to-mesh value comparison method. During the 3D modelling process, there were difficulties in processing the left humeri bones particularly the females. The technique used performs well at capturing and modelling very asymmetrical objects since the Structure-from-Motion software uses these distinct points as references to overlap corresponding points to build the 3D generated mesh (Adamopoulos *et al.*, 2021). The more linear and simpler the object is presented, the more difficult it becomes to locate and match corresponding points to align the different sets of images for modelling, which was mainly observed among the female sample. However, the technique uses a mid-range camera and set up equipment that is affordable, easily accessible, portable, and user-friendly. The technique was able to produce high-quality mesh models with low storage file format sizes.

## **5.2. The assessment of the effects of the mesh-to-mesh value comparison method on fragmentary remains.**

In this study, it was found that the distal femur fragment performed the best with Viewbox while the shaft femur fragment performed the best with Meshlab for both the LCV and the ROC curve methods. Similar results were obtained for the humerus except for the LCV Viewbox method where the proximal humerus fragment performed the best out of the three groups.

The results observed suggests that when working with highly fragmented remains the mesh-to-mesh value comparison method performs well when working in combination with the results obtained through Viewbox and statistical analysis of the ROC curve method.

While Meshlab performs well with the ROC curve analysis, the software does require the user to match points and align the models, in highly fragmented remains this becomes more difficult when the number of corresponding points between the models becomes more difficult to locate and orientate (e.g., matching points between the anterior proximal areas between two shaft fragments). The method performed well without any pre-alignment registration being conducted suggesting that pre-alignment may not be necessary when working with fragmentary remains.

The shaft mesh fragment contradictory to the literature (McWhirter *et al.*, 2021) performed well when compared to the other fragments. The study aimed to explore the automated version of MVC with a MSCT scanner for pair matching of fragmentary or incomplete remains. The study revealed that the acromial fragments had the best performance rate, with an overall sensitivity of 87.5% and specificity of 87.9% according to the ROC analysis. The LCV analysis yielded significantly lower results, showing an overall sensitivity of 65.7% and a specificity of 40%. The improved performance of the acromial fragments can be attributed to the clavicle's morphology, which is one of the most variable regions of the clavicle, making it more diverse in shape than the midshaft or sternal fragments. The sternal area was the second-best fragment type in terms of performance. It had an average LCV sensitivity and specificity of 55.4% and 56.5% respectively, and a ROC sensitivity and specificity of 83.8% and 83.5% respectively. The mid-shaft fragments had the poorest performance with a ROC analysis of 81.3% sensitivity and 74.8% specificity. The LCV produced a sensitivity of 40.5% and a specificity of 37.8%. The LCV comparison results were low and less significant than random chance when determining a true match (McWhirter *et al.*, 2021).

Focusing on the results obtained in the current study through the ROC curve analysis and Viewbox, the shaft and proximal mesh fragments' performance was almost the same for the femur and the humerus. The results obtained for the humeri mesh fragments were considerably higher compared to the results obtained by McWhirter *et al.* (2021) for the clavicle fragments. The difference in the results obtained between the current study and the McWhirter *et al.* (2021), may be attributed to the size and surface shape morphology of the bones being tested.

All bilateral bones have a certain degree of asymmetrical differences which may be influenced by their behavioural patterns such as handedness (the directional asymmetry), environmental conditions and standard of health and living conditions (Auerbach and Ruff, 2006; Lyman, 2006; Garrido Varas, 2013). Humans have bilateral asymmetry in both the upper and lower limbs, with the right-side predominating. Human lower limbs, particularly the femur, show evidence of a less pronounced but systematic left-side preference in directional asymmetry. According to numerous studies, mechanically induced bone growth and remodelling directly link behavioural and morphological asymmetry, such as increased asymmetry between limbs with mechanical problems (Auerbach and Ruff, 2006; Lyman, 2006).

Directional bilateral asymmetry is significantly influenced by mechanical factors. In response to the same mechanical environment, various skeletal features display varying degrees of asymmetry. According to some studies, the same skeletal elements' lengths or articular dimensions exhibit less asymmetry than their diaphyseal breadths or cross-sectional dimensions. The degree of asymmetry in anatomical attributes is affected differently by genetic and environmental factors. Because different populations exhibit varying degrees of asymmetry in the same attribute, the degree of symmetry required to identify pairs determined on a modern reference collection will be unknown. Some dimensions show sexual dimorphism in asymmetry, particularly those of the upper limb, which may indicate fundamental differences in behaviour and bone growth between males and females (Auerbach and Ruff, 2006; Lyman, 2006).

### **5.3. The real-world application of the mesh-to-mesh value comparison on a small scaled commingled forensic collection.**

To assess the application of the technique and the method, it was applied to a real-world small scaled commingled forensic archaeological assemblage. The commingled assemblage presented high levels of fragmentation and taphonomy. Meyer (2016) first calculated the minimum number of individuals (MNI) using the frequency of craniums, and then femora and humeri. There were no reported bilaterally matched pairs within the forensic commingled sample based on visual pair matching of remains, and this suggests an MNI of 5 for the humeri and 6 for the femora. Pair-matching results for the case report were obtained using the methods described by Snow, (1948); Ubelaker, (2002); Byrd and Adams, (2003); L'Abbé, (2005); İşcan and Steyn, (2013).

The LCV mesh-to-mesh comparison method performed well at identifying non-matches among the femora commingled sample but performed poorly at identifying the non-matches among the humeri commingled sample. The femora results suggests that the method works well when working with fragmented and taphonomically altered femora remains and validates the results initially observed with the visual pair matching results stated in the report.

However, the humeri sample produced a high number of false positives with the results obtained through Viewbox. The high number of false positives may be related to the conditions of the humeri samples. The humeri bones were highly fragmented with distal and proximal sections of the bone missing and a high degree of taphonomical staining was present on the bones. This factor could be the reason behind the software being unable to correctly orientate and align the models during the generation of the mesh-to-mesh values.

#### **5.4. LCV mesh-to-mesh comparison method analysis vs ROC curve statistical analysis.**

For comparative statistical analysis of the mesh-to-mesh value comparison method and ROC curve analysis, ROC curve analysis provides higher statistical sensitivity and specificity rates and outputs a numerical criterion/threshold value to quantitatively understand the data with less chance of human error. The LCV mesh-to-mesh value comparison method requires a lot more observation and user input. Consequently, as the dataset increases, the number of possible pair matches increases and the chance to find a true pair match decreases. It is more likely to find a true positive or negative match within a smaller dataset using the LCV mesh-to-mesh value comparison as the chances of finding a pair among 5 bones would be considerably higher compared to 40 different bones. The probability of finding similar features among several bones increases as the sample size grows, thus increasing the likelihood of finding more than one bone for pair-matching. Smaller sample sizes enable better differentiation between elements, resulting in one distinct bilateral pair-match.

## **5.5. The potential use of 3D editing softwares: Viewbox 4.1 and Meshlab 2022.12.**

Between Viewbox and Meshlab, Meshlab generated considerably higher sensitivity and specificity values which exhibited a larger threshold value compared to Viewbox. The differences in root mean square results may be attributed to the type of ICP algorithm used for each software. Viewbox operates by using a Trimmed ICP algorithm, whereby the software automatically aligns each point in the model over the other point in the corresponding model. The algorithm generated root mean square values of  $10^{-4}$  and  $10^{-5}$  for all femora models.

Meshlab conversely uses a general ICP algorithm, in which a set of two models at a time were required to be aligned using specific points on each model. These were chosen by the user and processed. After alignment, the Hausdorff distance was determined, generating a root mean square value. The root mean square values generated were  $10^{-2}$  and  $10^{-3}$ . This variation in algorithm and software provides a substantial difference in threshold values obtained for each software. The difference in root mean square values may suggest that threshold values obtained using ROC curve analysis are dependent on the type of ICP algorithmic software used. The overall procedure utilized to generate the mesh-to-mesh values is one of the potential causes of the considerable discrepancy between the sensitivity and specificity values obtained between the two softwares.

Compared to Viewbox, which is an automatic procedure, Meshlab demands considerably more user input and control. By choosing points, the user can take control of the alignment process and reduce the likelihood of program-related misalignments. However, the method used for Meshlab also reduces the repeatability of the method as each user will perform it differently.

Viewbox is a user-friendly automated process which requires much less user input and control to perform its function. When it came to aligning and matching fragmented remains, particularly severely fragmented remains like the shafts, the software was able to perform remarkably effectively. Viewbox program is a graphics-dependent software therefore a higher-end graphics card may significantly reduce the overall duration of the program needed to run large datasets. Viewbox is a proprietary source software but can be downloaded for free while the free version only allows certain features, one of those features does allow to run the mesh similarity tool needed to complete the analysis.

Meshlab is also considered simple and user-friendly, however, it is quite dependent on user input and control to perform its function. Meshlab is independent of graphics and the overall time needed to run the algorithm is irrespective of the type of machine. Meshlab is an open-source software which means it is free and easily assessable.

## 6 Conclusion

Traditional sorting methods such as visual pair matching, the re-association of articular surfaces, the process of elimination, and the matching of bony elements based on taphonomical similarities and differences are quite effective in sorting remains. However, these methods are greatly subjective and depends substantially on the experience of the anthropologist. When working with large-scaled commingled remains, these methods may become time-consuming, laborious, and tedious. This study investigated the adaption of Structure-from-Motion technique in combination with the newly developed method, the mesh-to-mesh value comparison method in pair matching bilateral skeletal remains. The results are as following:

- For the complete cadaveric bones, the femur performed better with both softwares when compared to the humerus. Mesh-to-mesh values obtained through Meshlab and analysed with the ROC curve method generated significantly higher results and were more adept at correctly identifying and distinguishing differences between matches and non-matches. Differences in mesh-to-mesh values between sexes and different population groups were observed.
- For the fragmented remains, the distal mesh fragment and the shaft mesh fragments generated significantly high results when using the values obtained through Viewbox and statistically analysed with the ROC curve method.
- The mesh-to-mesh value comparison method was applied to real-world forensic commingled assemblage. The sample consisted of a high degree of fragmentation and different degrees of taphonomically altered bones. The Structure-from-Motion technique performed well at photogrammetrically capturing distinct details observed on the bones which greatly assisted during the 3D modelling process. The method performed well when working with the femora bone samples but performed poorly for the humeri bone sample. There were no true positive matches that could be identified since in the original case there were no individuals that could be matched with visual pair matching.

With the results obtained for the forensic commingled sample suggests that more research needs to be conducted on the performance of the method on remains with different levels of fragmentation and on different types of taphonomy.

While a separate study should be performed to assess the effectiveness of the mesh-to-mesh value comparison method on remains that have a combination of different levels of fragmentation and taphonomy on a large scaled commingled sample.

## 7. References

- Acuff, A.S., Karell, M.A., Spanakis, K.E., Kranioti, E.F. (2021). Pair-matching digital 3D models of temporomandibular fragments using mesh-to-mesh value comparison and implications for commingled human remain assemblages. In: Rea, P.M. (eds) *Biomedical Visualisation. Advances in Experimental Medicine and Biology*, vol 1317. Springer, Cham. [https://doi.org/10.1007/978-3-030-61125-5\\_1](https://doi.org/10.1007/978-3-030-61125-5_1)
- Adams, B. J. and Byrd, J. E. (2006). Resolution of small-scale commingling: A case report from the Vietnam War. *Forensic Science International*, 156: pp 63 – 69.
- Adams, B. J. and Konigsberg, L. W. (2004). Estimation of the most likely number of individuals from commingled human skeletal remains. *American Journal of Physical Anthropology*, 125: pp 138 – 151.
- Agisoft Metashape User Manual: Professional Edition, Version 1.7. (2021). Agisoft LLC.
- Auerbach, B. M. and Ruff, C. B. (2006). Limb bone bilateral asymmetry: variability and commonality among modern humans. *Journal of Human Evolution*, 50: pp 203 – 218.
- Bell, T., Li, B. and Zhang, S. (1999). Structured light techniques and applications. *Wiley Encyclopaedia of Electrical and Electronics Engineering*, pp.1-24.
- Bertsatos, A. and Chovalopoulou, M. (2019). Validation study of osteometric techniques for sorting commingled human skeletal remains in archaeological samples. *International Journal of Osteoarchaeology*, 29: pp 253 – 259.
- Bertsatos, A. and Chovalopoulou, M. (2020). Advances in osteometric sorting: Utilizing diaphyseal CSG properties for lower limb skeletal pair-matching. *Journal of Forensic Sciences*, 65(5): pp 1400 – 1405.
- Byrd, J. E. and LeGarde, C. B. (2018). Evaluation of method performance for osteometric sorting of commingled human remains. *Forensic Sciences Research*, 3(4): pp.343-349.
- Cao, Y., Ma, Y., Vieira, D. N., Guo, Y., Wang, Y., Deng, K., Chen, Y., Zhang, J., Qin, Z., Chen, F., Huang, P. (2021). A potential method for sex estimation of human skeletons using deep learning and three-dimensional surface scanning. *International Journal of Legal Medicine*, 135(6), pp.2409-2421.

Cappella, A., Affatato, L., Gibelli, D., Mazzarelli, D., Zago, M., Dolci, C., Sforza, C., Cattaneo, C. (2022). An osteometric and 3D analysis of the atlanto-occipital joint: an initial screening method to exclude crania and atlases in commingled remains. *American Journal of Biological Anthropology*, 177(3): pp 439-453.

Carew, R. M., Errickson, D. (2019). Imaging in forensic science: Five years on. *Journal of Forensic Radiology and Imaging*, 16: pp 24 – 33.

Chan, B., Auyeung, J., Rudan, J. F., Ellis, R. E., Kunz, M. (2016). Intraoperative application of hand-held structured light scanning: a feasibility study. *International Journal of Computer Assisted Radiology and Surgery*, 11: pp 1101 – 1108.

Chan, B., Rudan, J. F., Mousavi, P., Kunz, M. (2020). Intraoperative integration of structured light scanning for automatic tissue classification: a feasibility study. *International Journal of Computer Assisted Radiology and Surgery*, 15: pp 641 – 649.

Cignoni, P., Callieri, M., Corsini, M., Dellepiane, M., Ganovelli, F. and Ranzuglia, G. (2008). Meshlab: an open-source mesh processing tool. In *Eurographics Italian chapter conference*, 2008: pp 129-136.

Dayal, M. R., Kegley, A. D. T., Štrkalj, G., Bidmos, M. A., Kuykendall, K. L. (2009). The history and composition of the Raymond A. Dart Collection of Human Skeletons at the University of the Witwatersrand, Johannesburg, South Africa. *American Journal of Physical Anthropology*, 140: pp 324 – 335.

De Bruyn, C. and Meyer, A. (2018). A bioarchaeological analysis of historical human skeletal remains recovered from Lancaster Mine, Witwatersrand, South Africa. *South African Archaeological Bulletin*, 73(207): pp 4-12.

DeLong, E. R., DeLong, D. M. and Clarke-Pearson, D. L. (1988). Comparing the areas under two or more correlated receiver operating characteristic curves: a nonparametric approach. *Biometrics*, pp 837-845.

Dirkmaat, D. C., Cabo, L. L., Ousley, S. D., Symes, S. A. (2008). New perspectives in forensic anthropology. *Yearbook of Physical Anthropology*, 51: pp 33 – 52.

Fancourt, H. S. M., Lynch, J. J., Byrd, J. E., Stephan, C. N. (2021). Next-generation Osteometric sorting: Using 3D shape, elliptical Fourier analysis and Hausdorff distance to optimize osteological pair-matching. *Journal of Forensic Sciences*, 00: pp 1 – 16.

- Fawcett, T. (2006). An introduction to ROC analysis. *Pattern recognition letters*, 27(8): pp 861-874.
- Fonstad, M. A., Dietrich, J. T., Courville, B. C., Jensen, J. L., Carbonneau, P. E. (2013). Topographic structure from motion: a new development in photogrammetric measurement. *Earth surface processes and landforms*, 38 (4): pp 421 - 430.
- Franklin, D., Swift, L., Flavel, A. (2016). ‘Virtual anthropology’ and radiographic imaging in the Forensic Medical Sciences. *Egyptian Journal of Forensic Sciences*, 2(6), pp: 31-43.
- Garrido Varas, C. E. (2013). An investigation into bilateral asymmetry of the appendicular skeleton of the adult human and its use in physical and forensic anthropology.
- İşcan, M. Y., Steyn M. (2013). The human skeleton in forensic medicine. *Springfield, Illinois*: Charles C Thomas Publisher.
- Jani, G., Johnson, A., Parekh, U., Thompson, T. and Pandey, A. (2020). Effective approaches to three-dimensional digital reconstruction of fragmented human skeletal remains using laser surface scanning. *Forensic Science International: Synergy*, 2, pp.215-223.
- Joubert, L. C., Briers, N., Meyer, A. (2020). Evaluation of the enhanced computational methods of estimating age-at-death using the pubic symphyses of a white South African population. *Journal of Forensic Sciences*, 65(1): pp 37 – 45.
- Karell, M. A., Langstaff, H. K., Halazonetis, D. J., Minghetti, C., Frelat, M., Kranioti, E. F. (2016). A novel method for pair-matching using three-dimensional digital models of bone: mesh-to-mesh value comparison. *International Journal of Legal Medicine*, 130: pp 1315 – 1322.
- Karell, M. A., Lay, M., Langstaff, H. K., Kranioti, E. F. (2017). Pair-matching temporals using a digital mesh-to-mesh value comparison method. *La Revue de Médecine Légale*, 8(4): pp 185.
- Karell, M. (2019). Identifying the disappeared: testing a novel method for sorting commingled human remains. (PhD thesis).
- Keyes, C., Mahon, T. J., Gilbert, A. (2022). Human decedent identification unit: identifying the deceased at a South African medico-legal mortuary. *International Journal of Legal Medicine*, pp 1 – 8.

- Kotěrová, A., Králík, V., Rmoutilová, R., Friedl, L., Růžička, P., Velemínská, J., Marchal, F., 367 Brůžek, J. (2019). Impact of 3D surface scanning protocols on the os coxae digital data: 368 implications for sex and age-at-death assessment. *Journal of Forensic and Legal Medicine*, 68: 369 pp 1 – 10.
- Kruger, G. C. (2014). Comparison of sexually dimorphic patterns in the postcrania of South Africans and North Americans. (MSc Dissertation)
- L'Abbè, E. N. (2005). A case of commingled remains from rural South Africa. *Forensic Science International*, 151: pp 201 – 206.
- Lambacher, N., Gerdau-Radonic, K., Bonthorne, E., Valle de Tarazaga Montero, F. J. (2016). Evaluating three methods to estimate the number of individuals from a commingled context. *Journal of Archaeological Science: Reports*, 10: pp 674 – 683.
- Lee, M., Gerdau-Radonic, K. (2020). Variation within physical and digital craniometrics. *Forensic science international*, 306, p.110092.
- Liebenberg, L., L'Abbé, E. N., Stull, K. E. (2015). Population differences in the postcrania of modern South Africans and the implications for ancestry estimation. *Forensic Science International*, 257: pp 522-529.
- Loong, T. (2003). Understanding sensitivity and specificity with the right side of the brain. *British Medical Journal*, 327: pp 716 – 719.
- López-Lázaro, S., Pérez-Fernández, A., Alemán, I. and Viciano, J. (2020). Sex estimation of the humerus: A geometric morphometric analysis in an adult sample. *Legal Medicine*, 47: p 101773.
- Lucenti, S. B., Dionisio, G., Rook, L., Bigoni, F. (2021). 3D Digitalization of selected specimens of the Anthropology and Ethnology Museum of Florence with Artec Spider. *Museologia Scientifica Memorie*, pp 123 – 127.
- Lynch, J. (2021). Computerized methods for de-commingling mixed human skeletal assemblages: new automated approaches using centroid banding. (PhD Thesis)
- Lussu, P. and Marini, E. (2020). Ultra close-range digital photogrammetry in skeletal anthropology: A systematic review. *Plos One*, 15(4): pp 1 – 29.

- Nuttens, T., De Maeyer, P., De Wulf, A., Goossens, R., Stal, C. (2011). Terrestrial laser scanning and digital photogrammetry for cultural heritage: an accuracy assessment. *FIG Working Week, Marrakech, Morocco*, p.10.
- Maass, P. and Friedling, L. J. (2018). Morphometric analysis of the humerus in an adult South African cadaveric sample. *Forensic science international*, 289, pp 451-e1.
- Mahfouz, M. R., Mustafa, A., Fatah, E. E. A., Herrmann, N. P., Langley, N. R. (2017). Computerized reconstruction of fragmentary skeletal remains. *Forensic Science International*, 275: pp 212 – 223.
- Mamabolo, B., Alblas, A., Brits, D. (2020). Modern imaging modalities in forensic anthropology and the potential of low-dose X-rays. *Forensic Imaging*, 23, pp 200406.
- McCormick, K. (2016). A biologically informed structure to accuracy in osteometric reassociation. (PhD Thesis)
- McPherron, S. P., Gernat, T., Hublin, J. J. (2009). Structured light scanning for high-resolution documentation of in situ archaeological finds. *Journal of Archaeological Science*, 36(1), pp.19-24.
- McWhirter, Z., Karell, M. A., Er, A., Bozdog, M., Ekizoglu, O., Kranioti, E. F. (2021). Exploring the functionality of mesh-to-mesh value comparison in pair-matching and its application to fragmentary remains. *Biology*, 10 (12), pp 1303.
- Meyer, A., Keough, N., Nienaber, C.W. and Steyn, M. (2013). A bioarchaeological investigation into the human remains discovered in the Chloorkop area, South Africa. *International Journal of Osteoarchaeology*, 23 (5): pp 600-611.
- Meyer, A. (2016). *AFFIDAVIT IN TERMS OF SECTION 212(8) ACT 51 OF 1977. Johannesburg DR 2026/14*. Johannesburg, pp.1–38.
- Orr, K. L. (2019). Metric pair-matching of calcanei in commingled human remain cases: A case study from South Africa. (Master's dissertation).
- Palamenghi, A., De Angelis, D., Cellina, M., Sforza, C., Cattaneo, C., Gibelli, D. (2021). Does the choice of the reference model affect the results of 3D-3D superimposition procedure? A comparison of different protocols for personal identification. *International Journal of Legal Medicine*, 135(5): pp.1879-1886.

Palamenghi, A., Mazzarelli, D., Cappella, A., De Angelis, D., Sforza, C., Cattaneo, C., Gibelli, D. (2022). Digital pair-matching of iliac bones: pilot study on a three-dimensional approach with models acquired through stereophotogrammetry. *International Journal of Legal Medicine*, pp 1-9.

Palamenghi, A., Cappella, A., Cellina, M., Mazzarelli, D., De Angelis, D., Sforza, C., Cattaneo, C., Gibelli, D. (2022). 3D-3D superimposition of pubic bones: expanding the anthropological toolkit for the pair-matching of commingled skeletal remains. *Biology* 12 (30): pp 1 -10.

Puerto, M. S., Abboud, D., Baraybar, J. P., Carracedo, A., Fonseca, S., Goodwin, W., Guyomarc'h, P., Jimenez, A., Krenzer, U., Mendez, M.D.M., Prieto, J.L. (2021). The search process: Integrating the investigation and identification of missing and unidentified persons. *Forensic Science International: Synergy*, 3, p.100154.

Randolph-Quinney, P. S., Haines, S. D., Kruger, A. (2018). The use of three-dimensional scanning and surface capture methods in recording forensic taphonomic traces: issues of technology, visualisation and validation. In: Barone, P. M. and Groen, W. J. M. (eds), *Multidisciplinary Approaches in Forensic Archaeology, Soil Forensics*. Springer International Publishing AG. pp 115 – 130.

Reichert, J., Schellenberg, J., Schubert, P., Wilke, T. (2016). 3D scanning as a highly precise, reproducible, and minimally invasive method for surface area and volume measurements of Scleractinia corals. *Limnology and Oceanography: Methods*, 14: pp 518 – 526.

Rohmani, A., Shafee, M. S., Ismail, N. A. N., Hadi, H. and Nor, F. M. (2022). Sex estimation using the first lumbar vertebra by geometric morphometric analysis of 3D computed tomography in the Malaysian population. *Forensic Imaging*, 30: p 200511.

Ruotsala, A. (2016). Digital close range photogrammetry – A modern method to document forensic mass graves from the University of Helsinki, pp 1 – 65.

Schenk, T. (2005). Introduction to photogrammetry. *The Ohio State University, Columbus*, 106: pp 2005.

Siebke, I., Campana, L., Ramstein, M., Furtwängler, A., Hafner, A., Lösch, S. (2018). The application of different 3D-scans-systems and photogrammetry at an excavation – A Neolithic dolmen from Switzerland. *Digital Applications in Archaeology and Cultural Heritage*, 10: pp 1 – 11.

Snow C. E. (1948). The identification of the unknown war dead. *American Journal of Physical Anthropology* 6: 323-328.

Stull, K. E., L'Abbé, E. N., Steiner, S. (2013). Measuring distortion of skeletal elements in Lodox *Scanscan-generated images*, pp 1 – 16.

Thomas, R. M., Ubelaker, D. H., Byrd, J. E. (2013). Tables for the metric evaluation of pair matching of human skeletal elements. *Journal of Forensic Sciences*, 58 (4): pp 952 – 956.

Tsiminikaki, K., Karell, M. A., Nathana, D., Halazonetis, D., Spanakis, K., Kranioti, E. F. (2019). Three-dimensional geometry of phalanges as a proxy for pair-matching: mesh comparison using an ICP algorithm. In: Rea, P.M. (eds) *Biomedical Visualisation. Advances in Experimental Medicine and Biology*, vol 1205. Springer, Cham. [https://doi.org/10.1007/978-3-030-31904-5\\_4](https://doi.org/10.1007/978-3-030-31904-5_4)

Urbanová, P., Hejna, P., Jurda, M. (2015). Testing photogrammetry-based techniques for three-dimensional surface documentation in forensic pathology. *Forensic science international*, 250: pp 77-86.

Watson, P. F. and Petrie, A. (2010). Method agreement analysis: a review of correct methodology. *Theriogenology*, 73(9): pp 1167-1179.

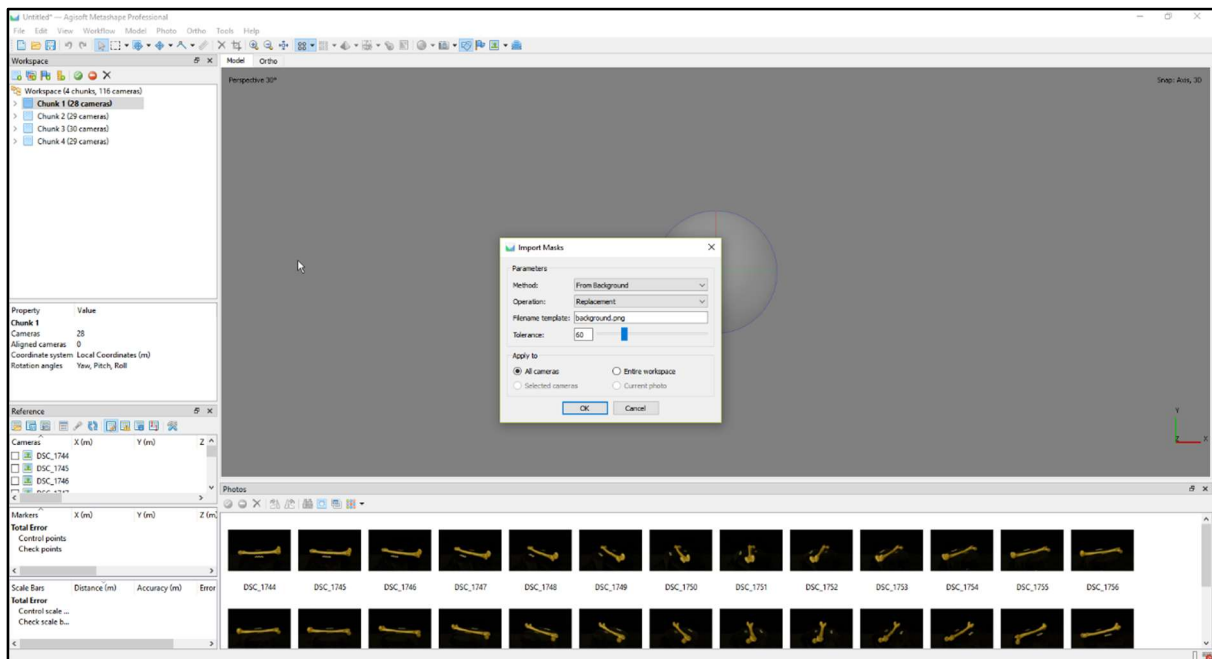
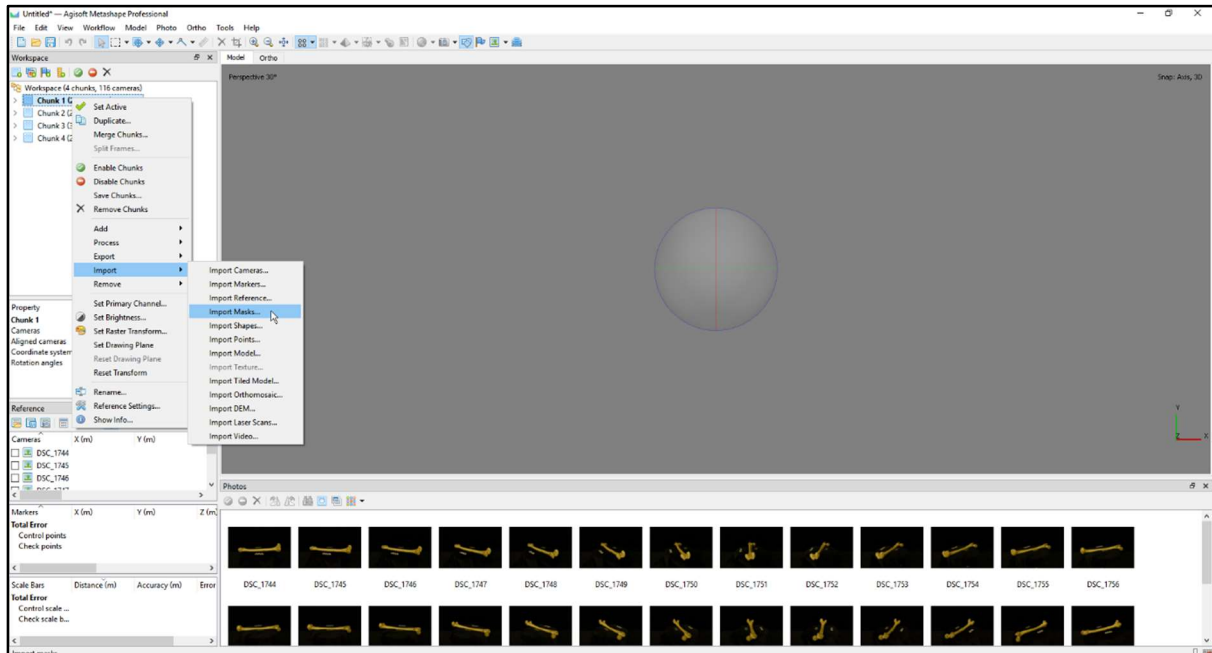
Westoby, M. J., Brasington, J., Glasser, N. F., Hambrey, M. J., Reynolds, J. M. (2012). 'Structure-from-Motion' photogrammetry: A low-cost, effective tool for geoscience applications. *Geomorphology*, 179: pp 300 - 314.

White, T. D., & Folkens, P. A. (2005). *The human bone manual*. Elsevier.

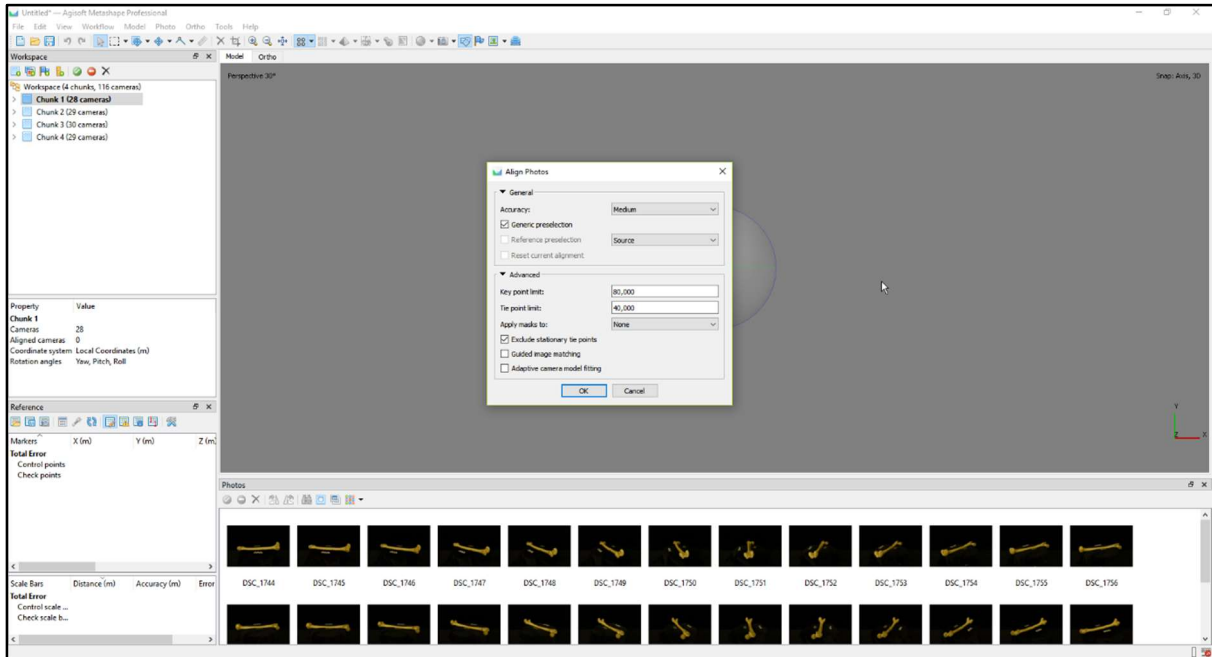
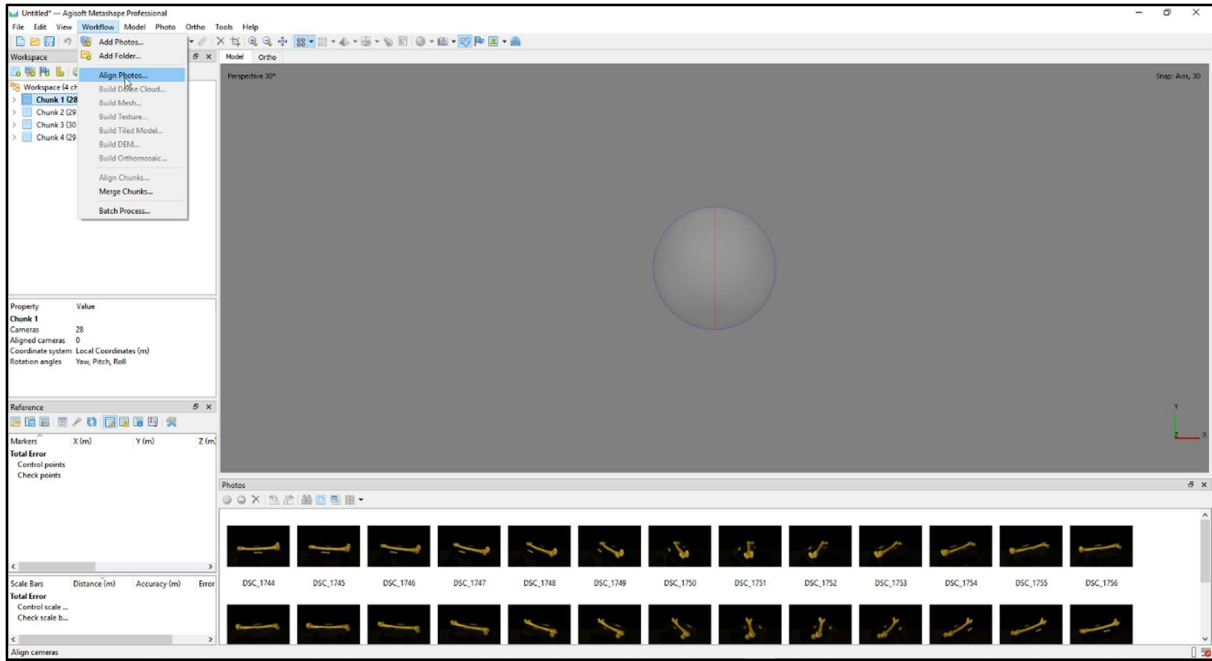
Winter, K. A., Alston-Knox, C., Meredith, M., MacGregor, D. (2021). Estimating biological sex and stature from the humerus: A pilot study using a contemporary Australian sub-population using computed tomography. *Forensic Science International: Reports*, 4: pp 100227.

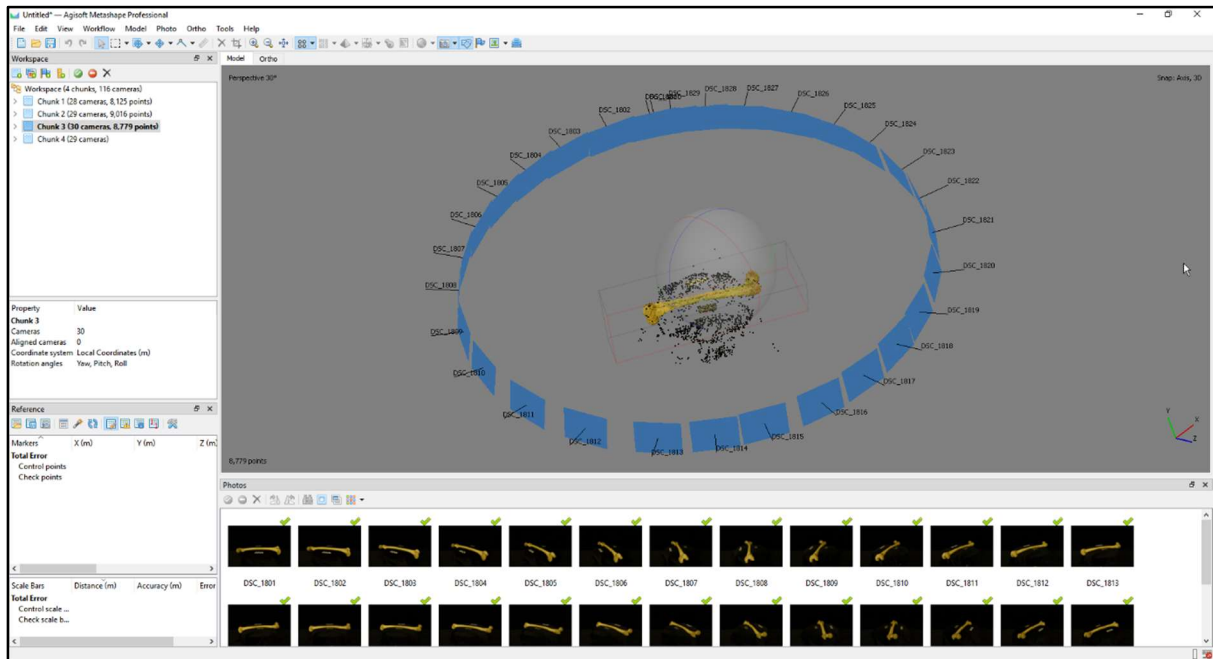
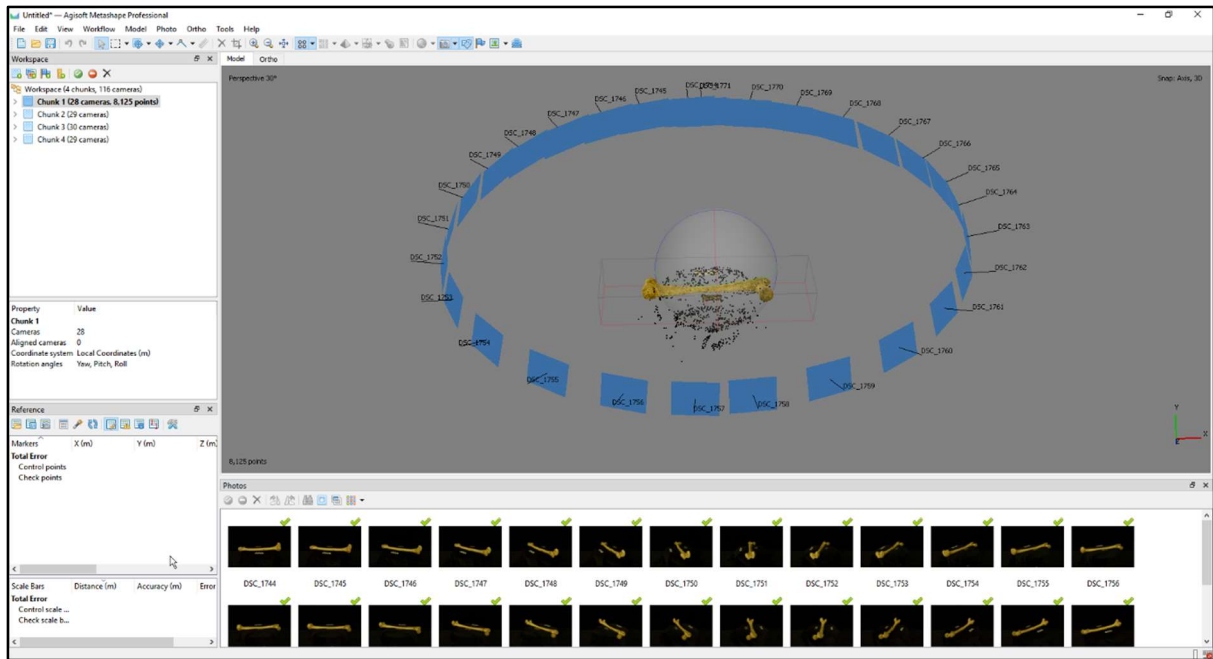
# Appendix A: Agisoft Metashape Photogrammetry Process

## Step 1 – Importing masks.

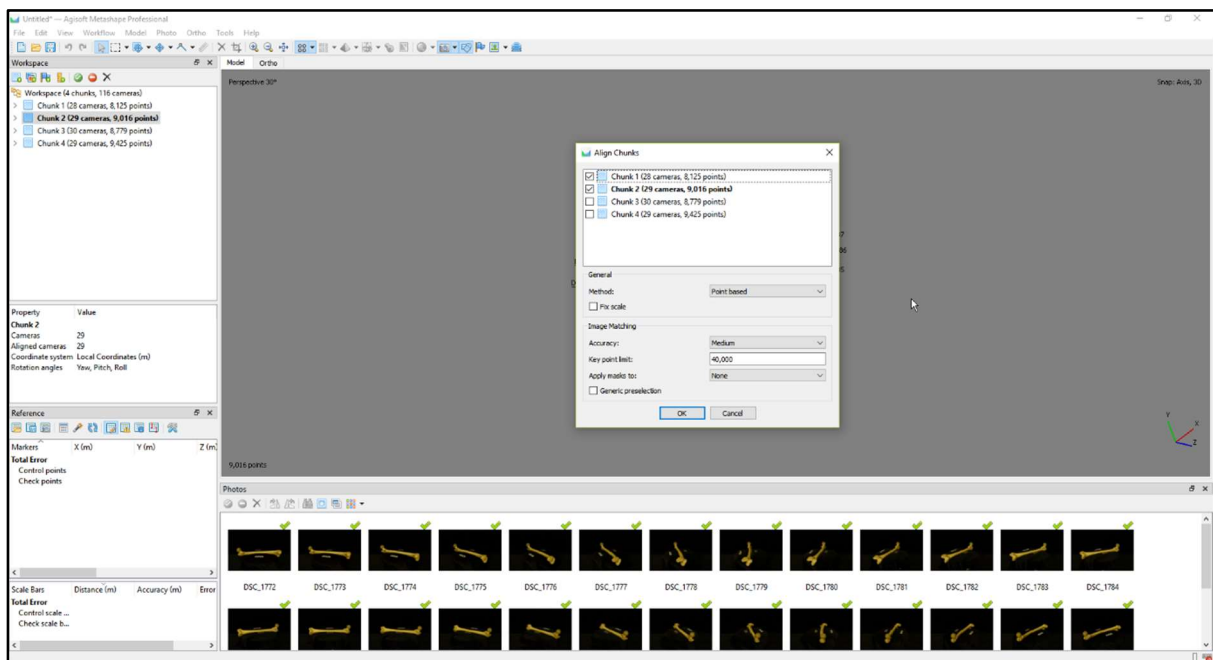
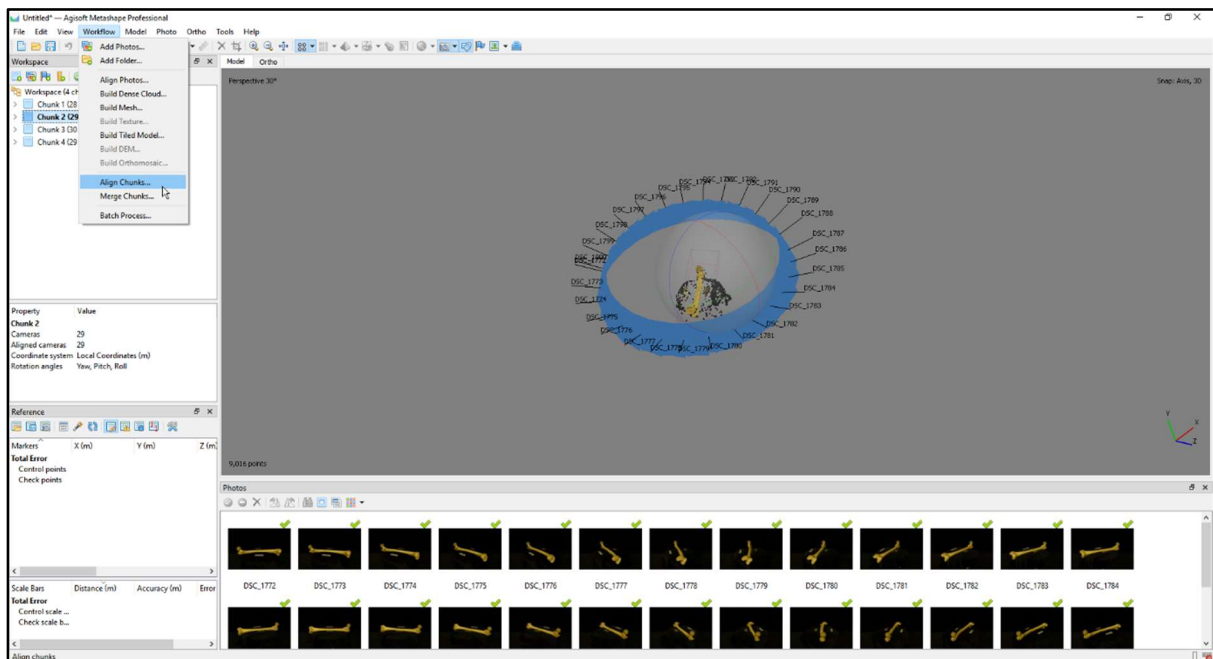


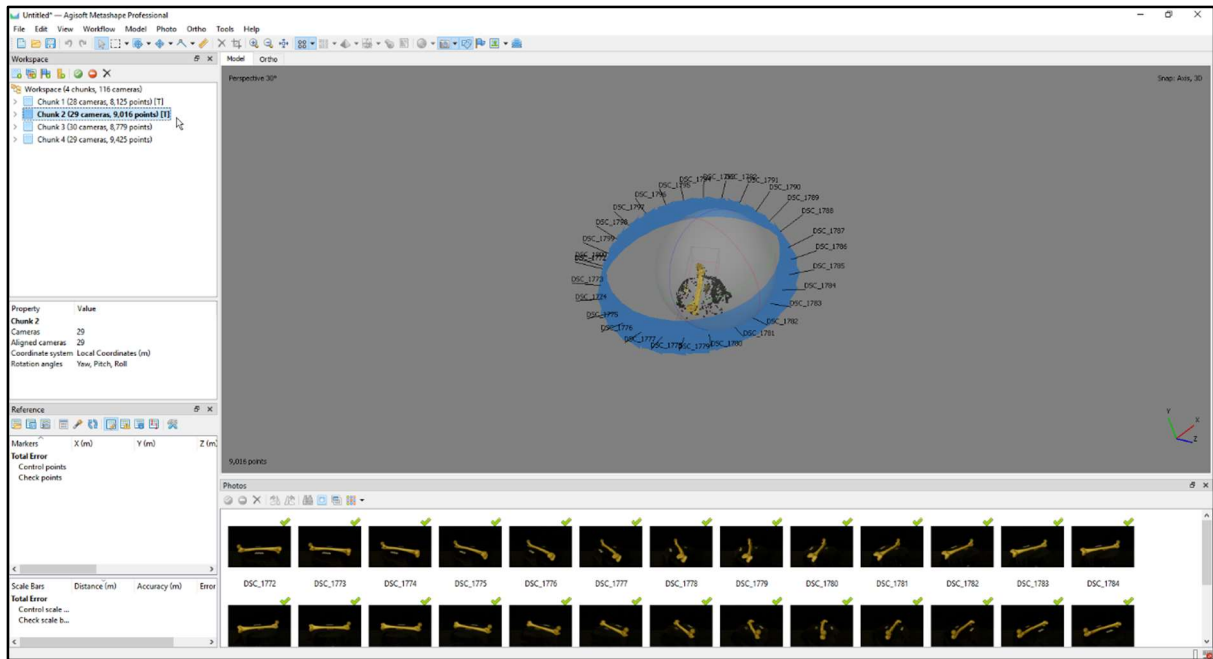
## Step 2 – Aligning photos and building the sparse point cloud.



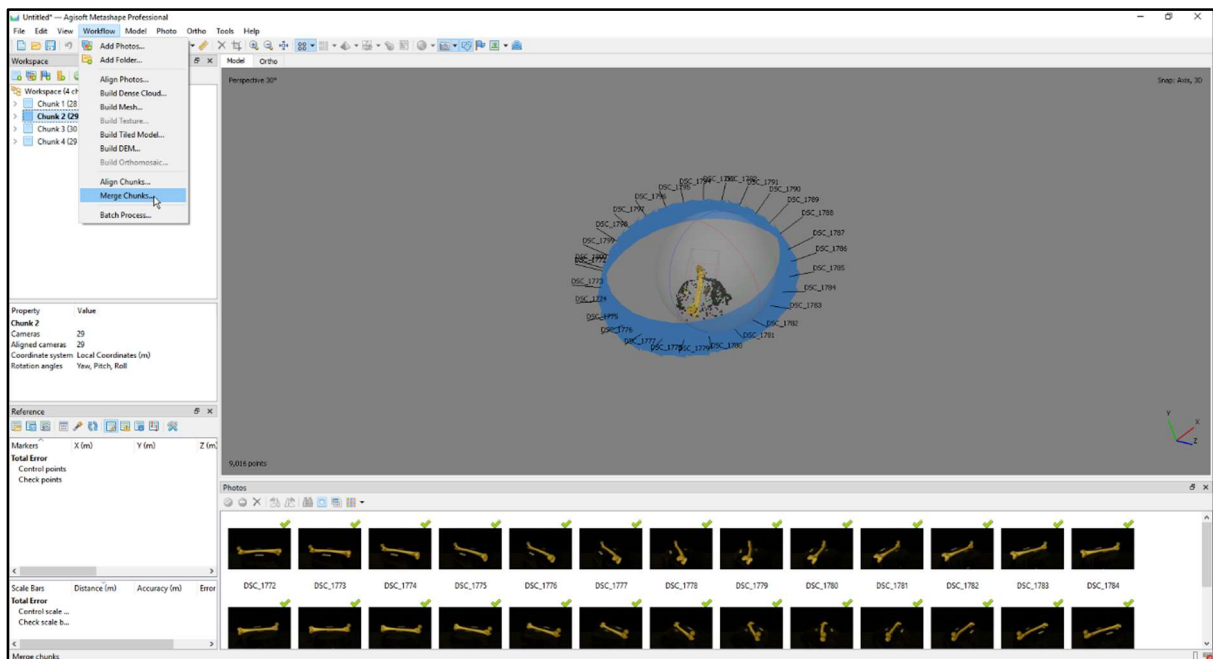


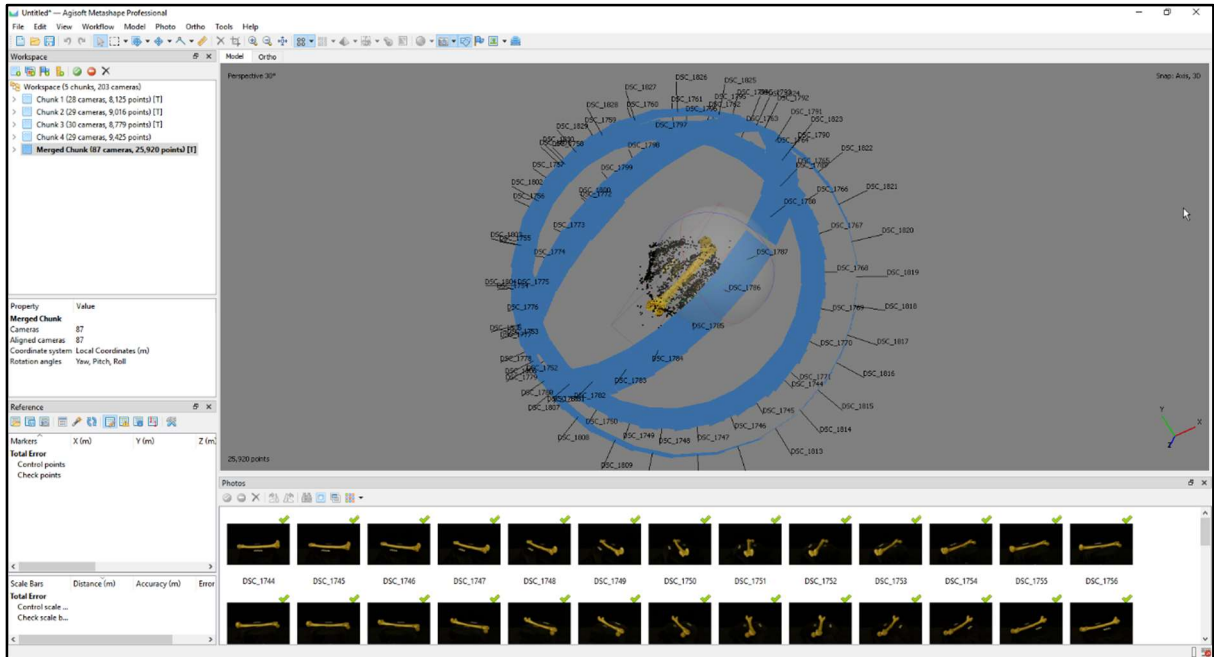
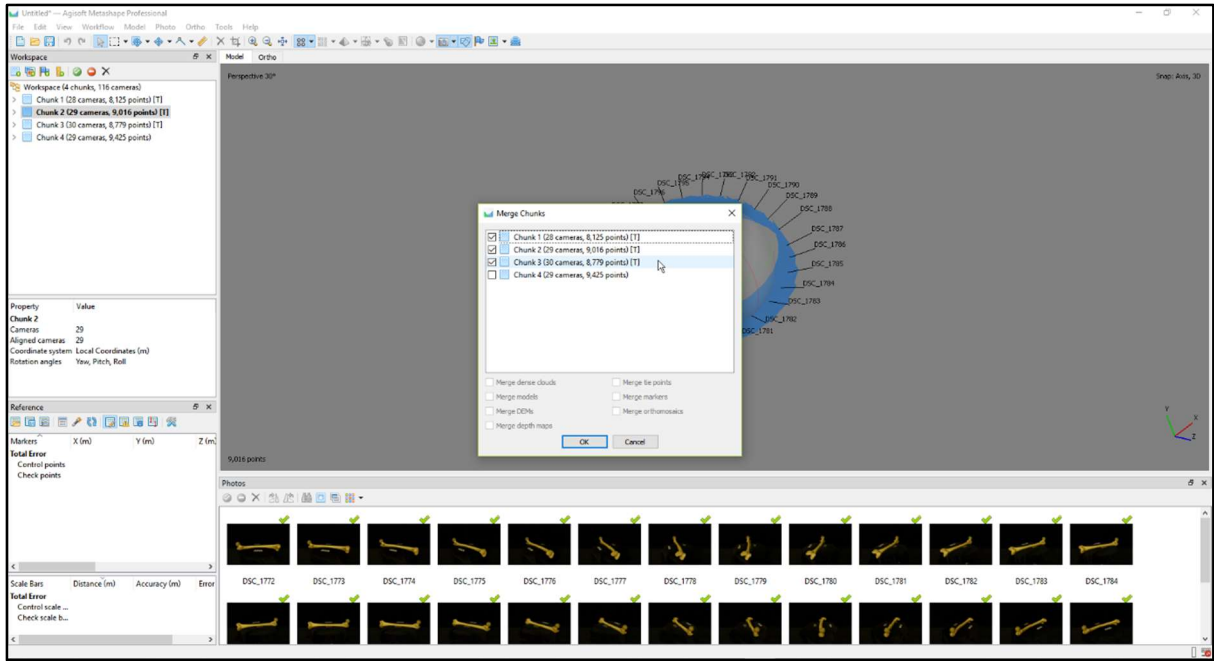
### Step 3 – Aligning chunks.



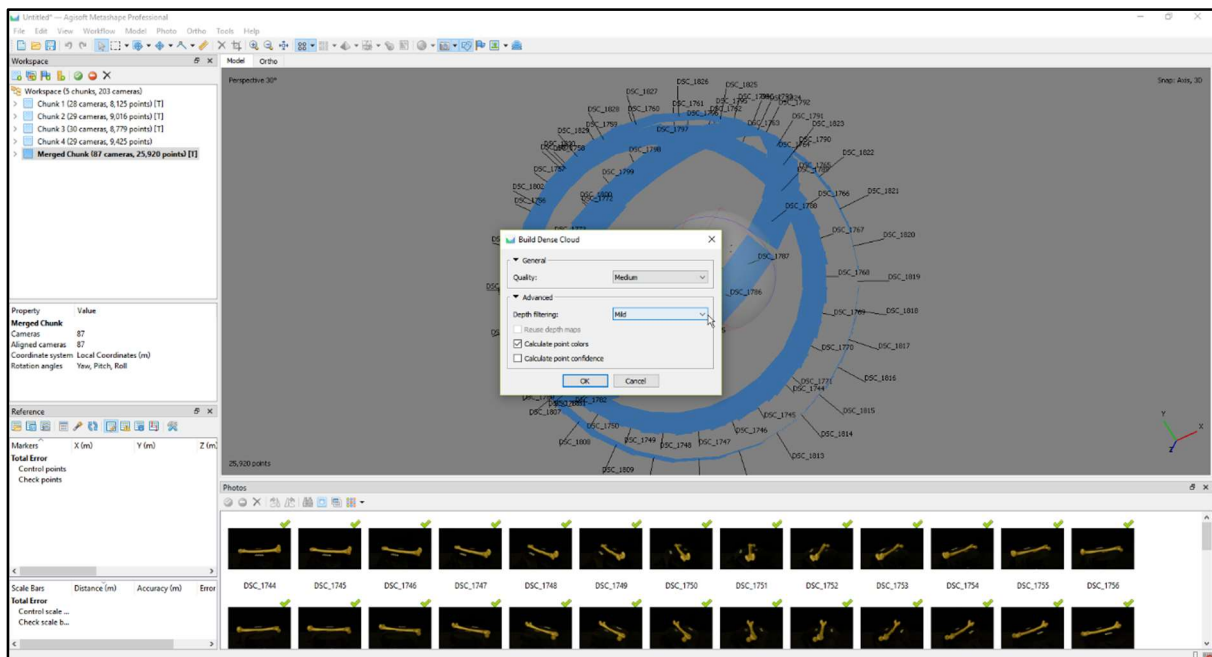
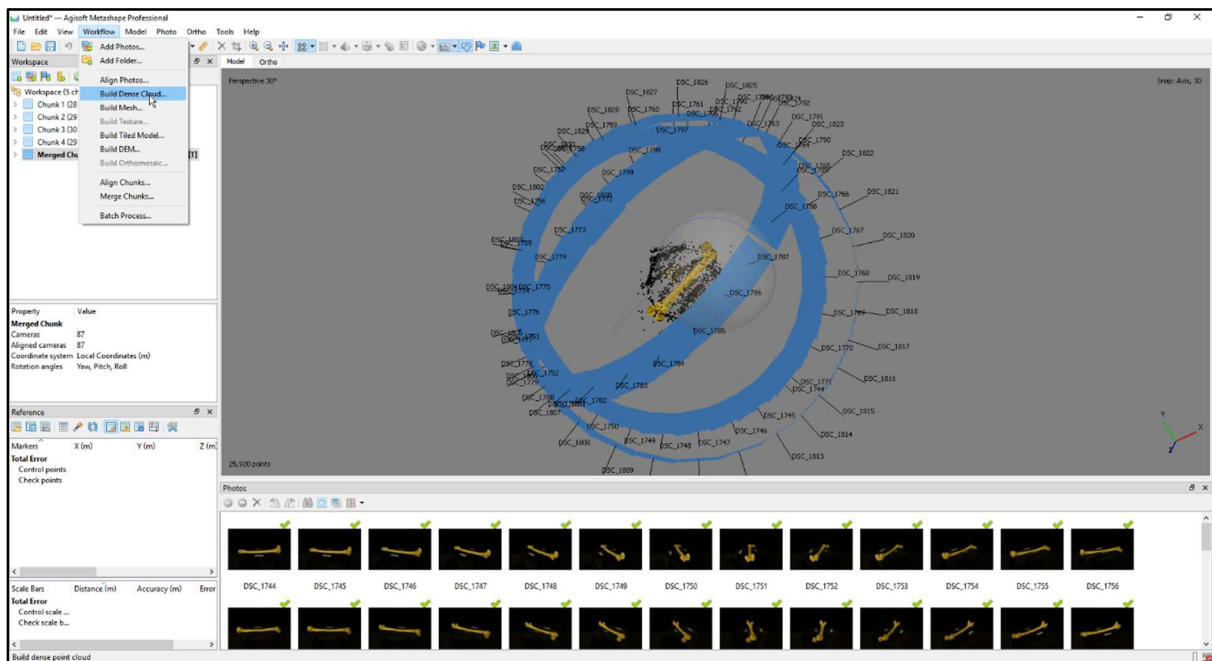


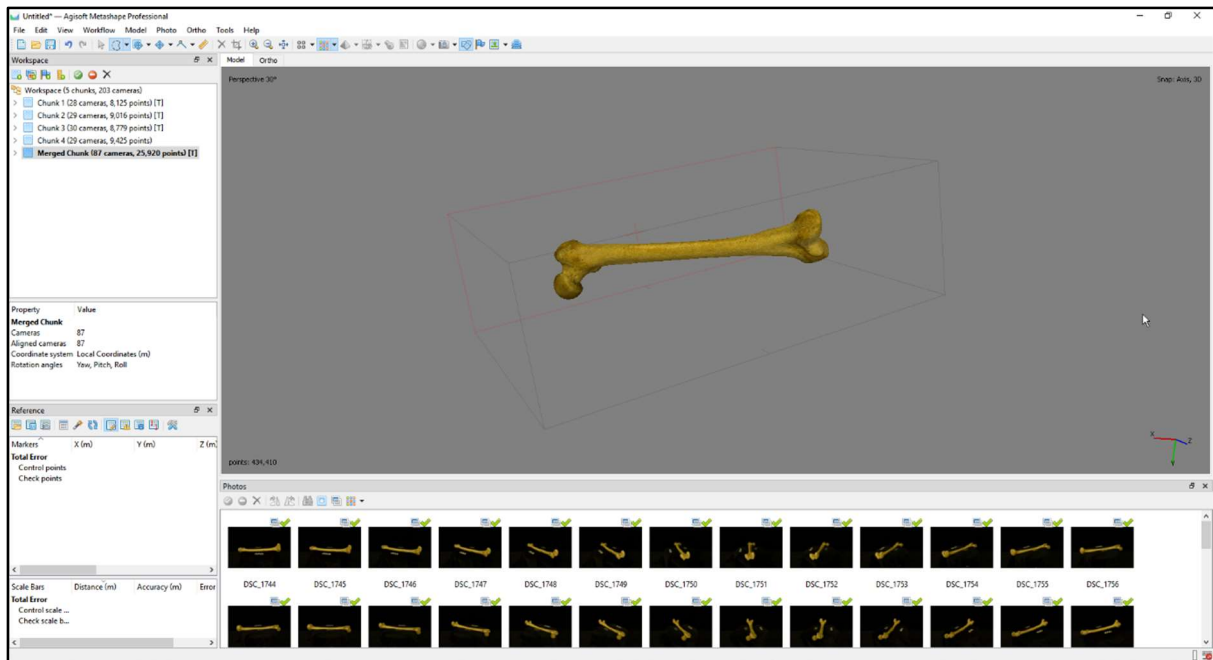
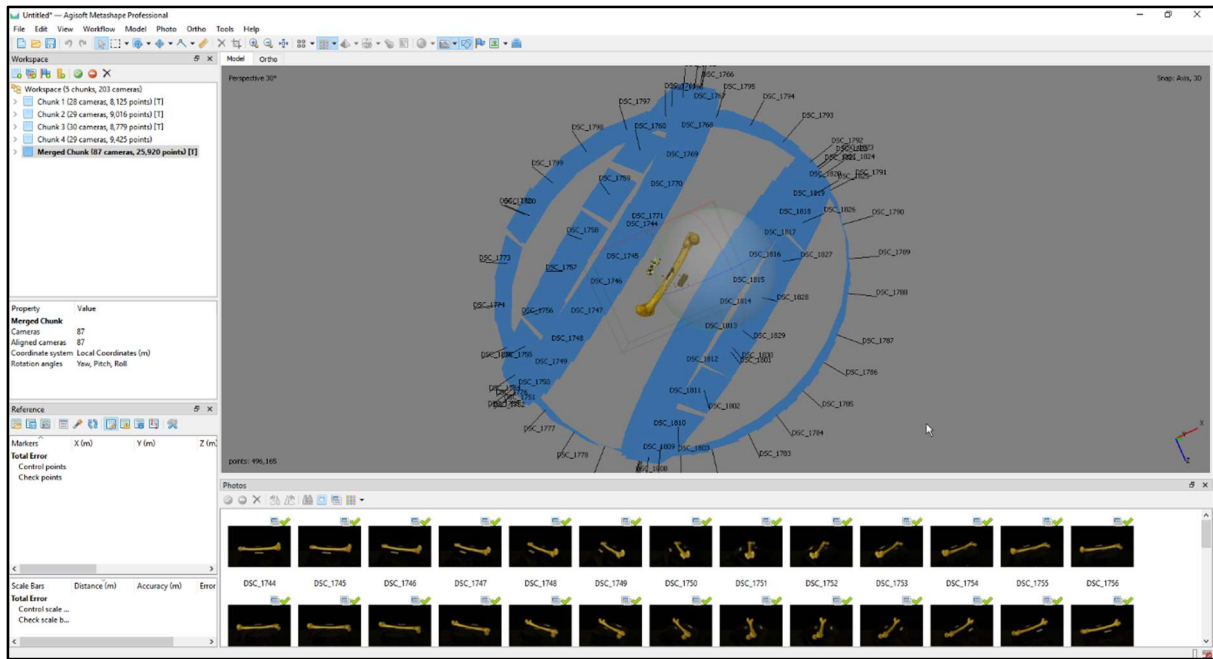
## Step 4 - Merging chunks

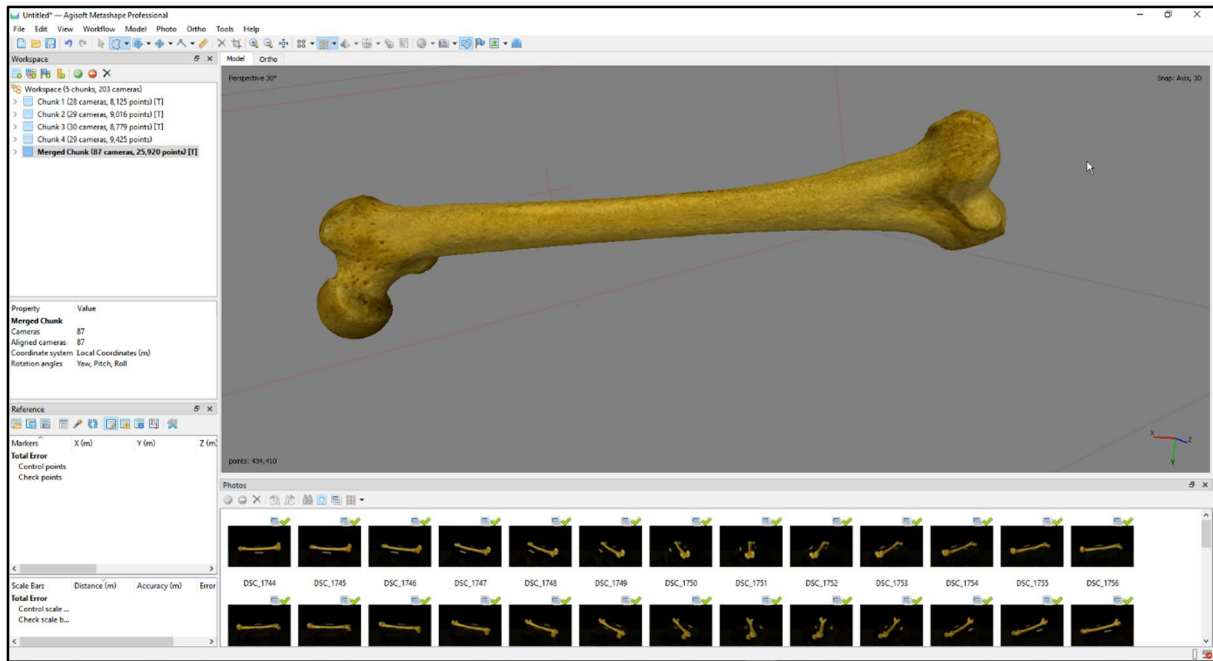




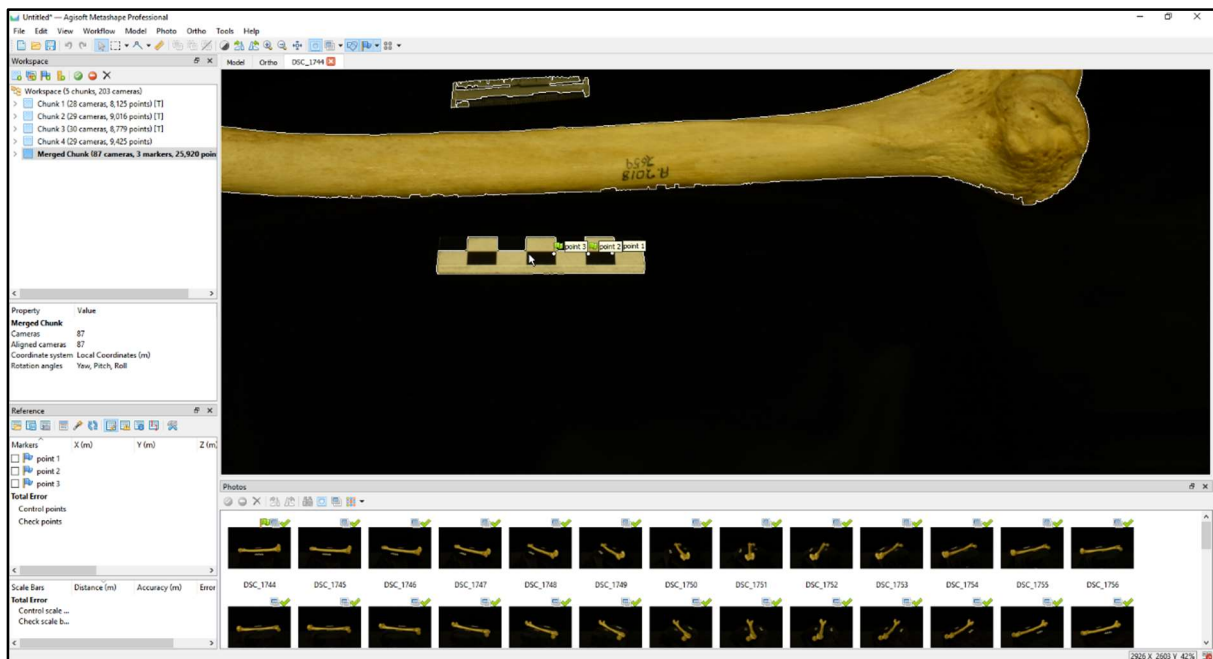
## Step 5 – Building dense point cloud.

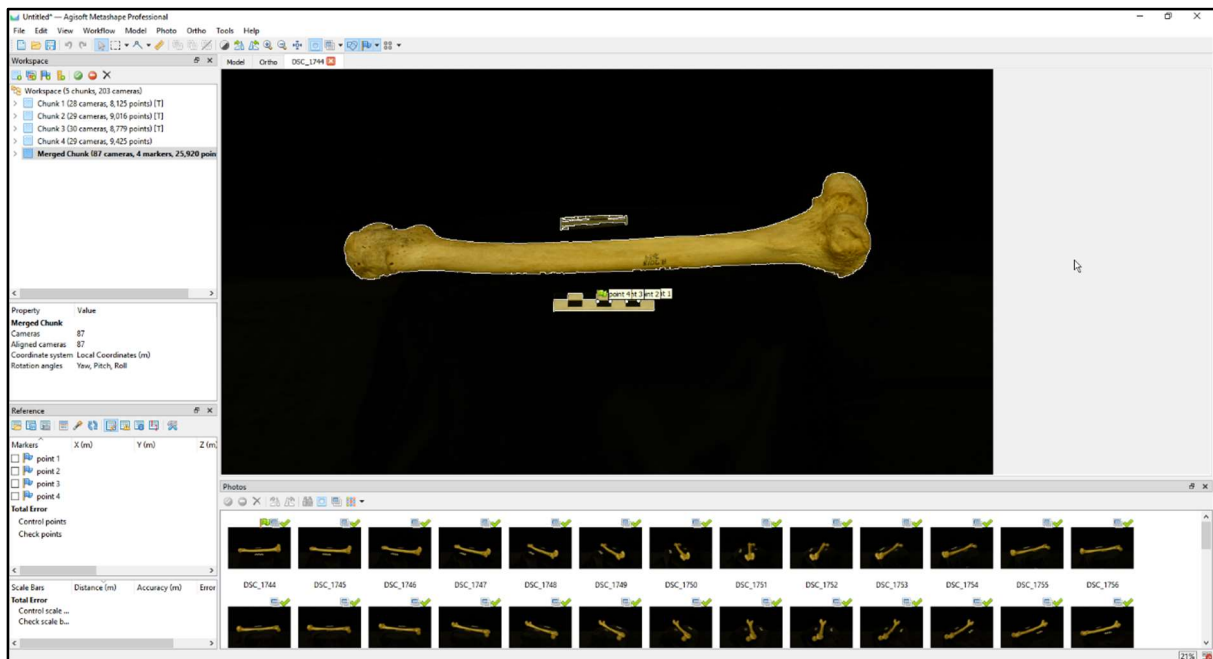
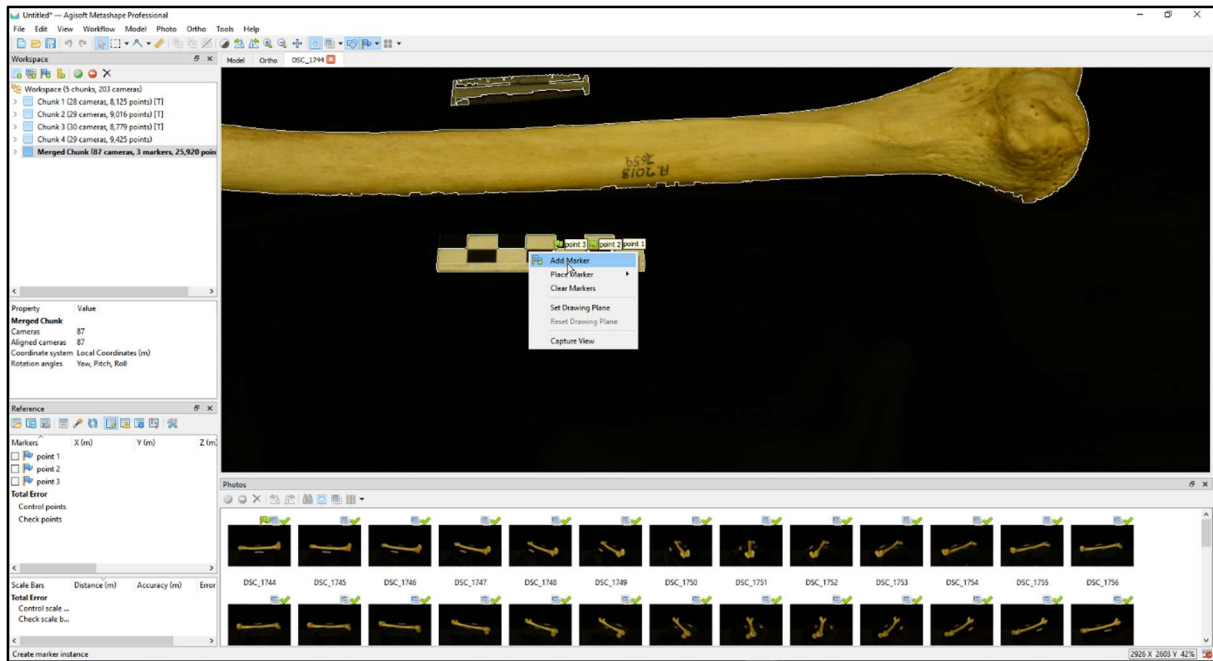


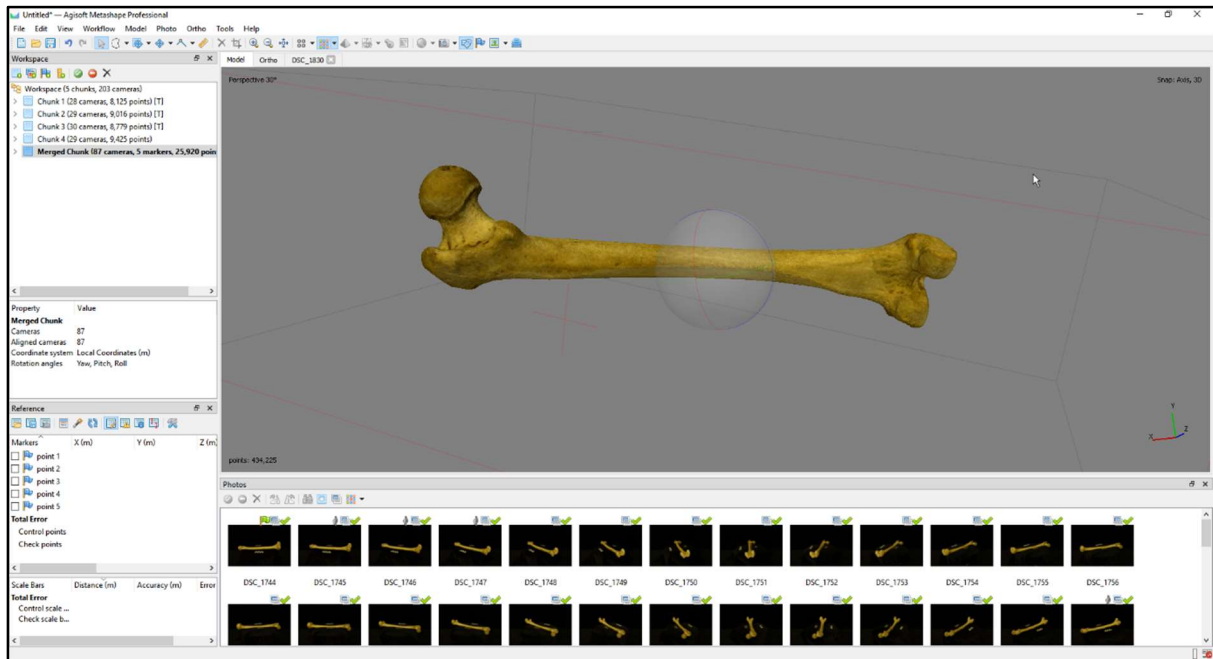


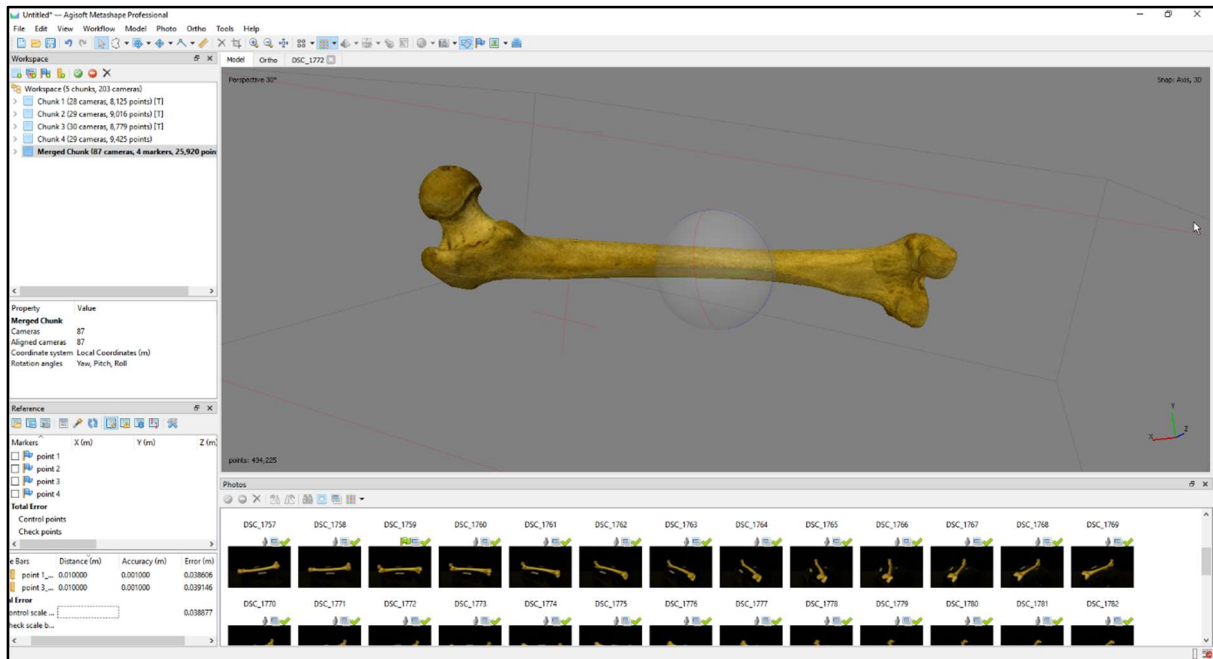
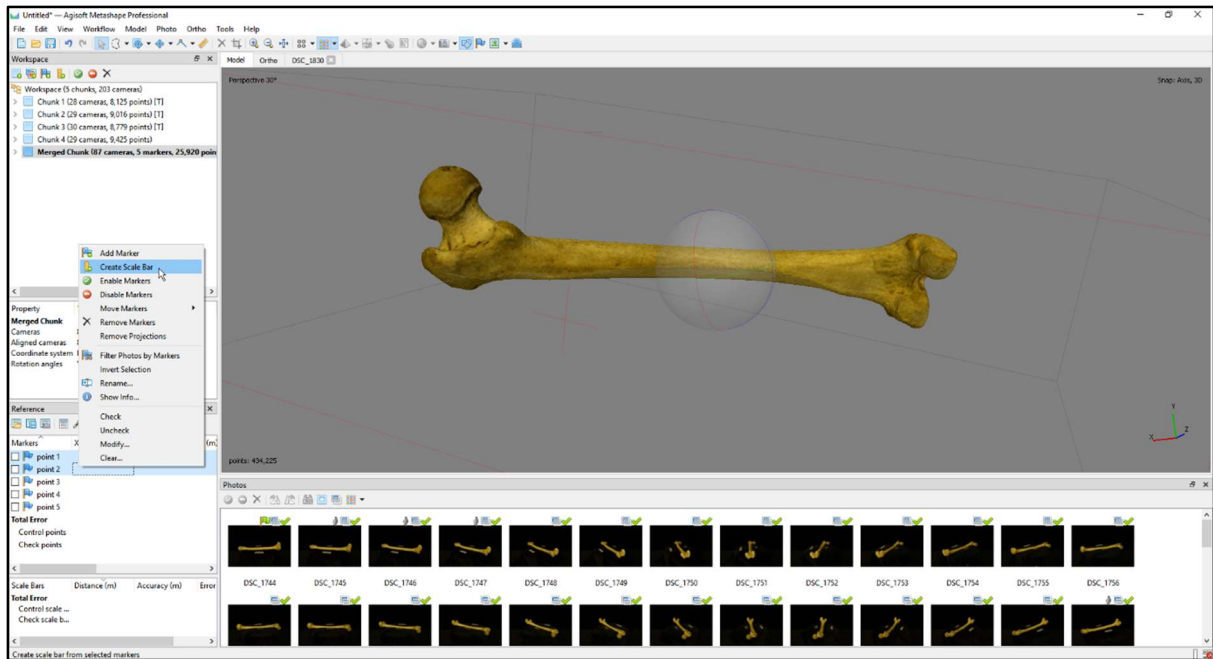


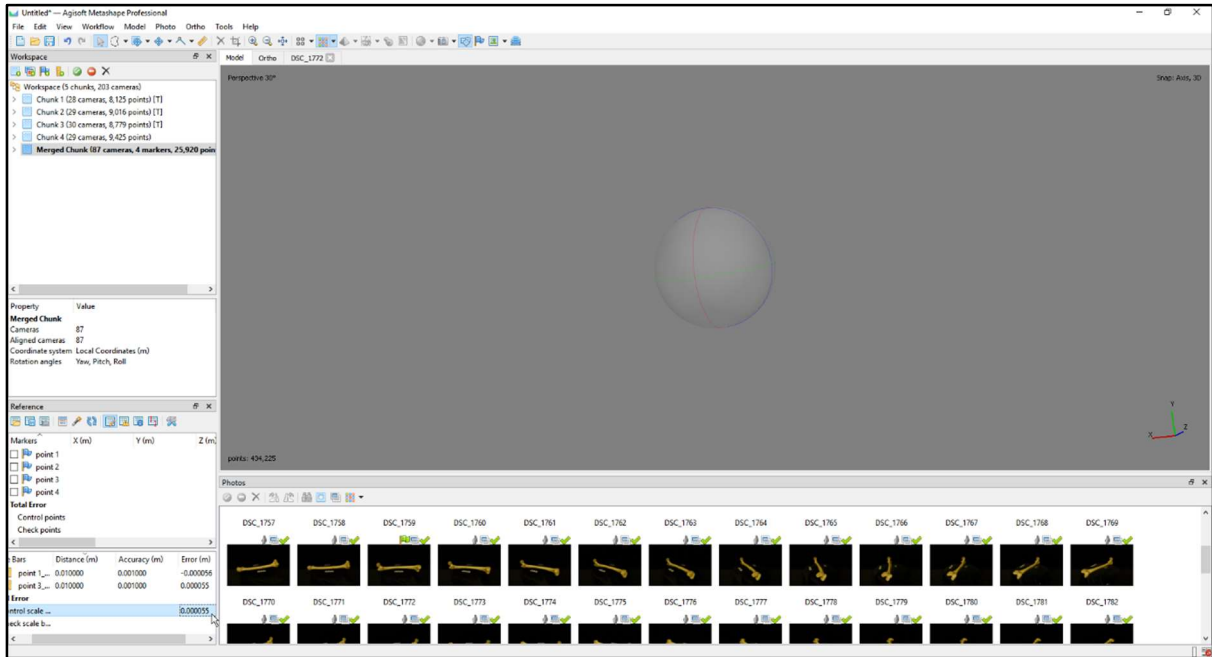
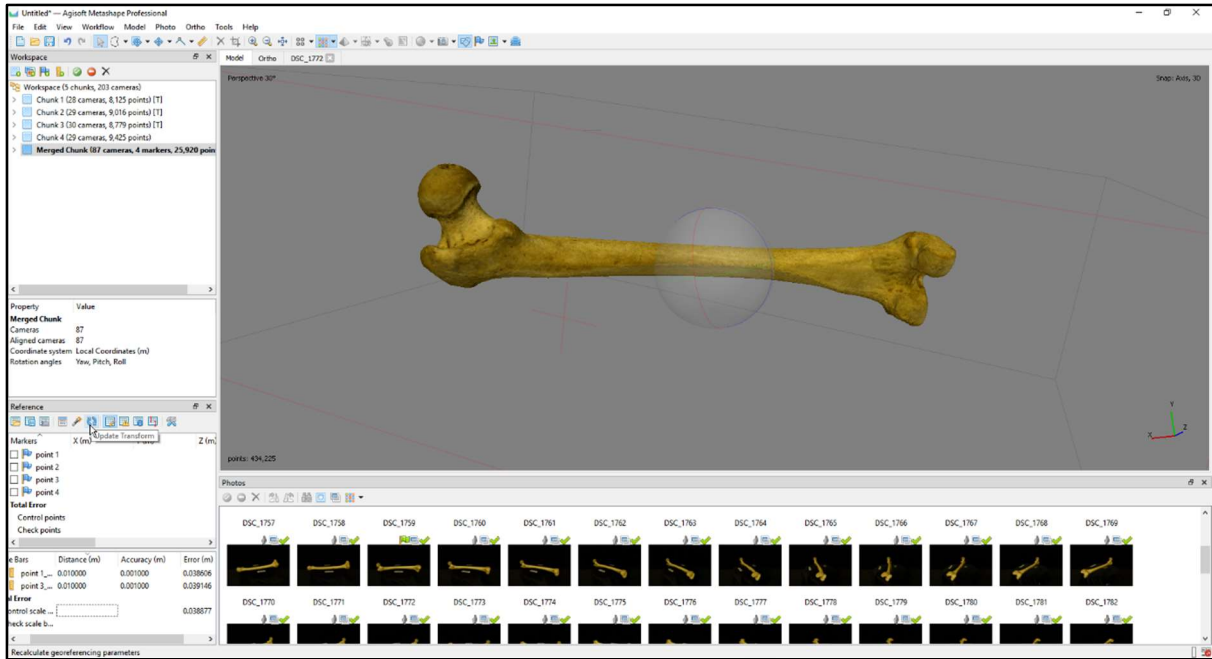
## Step 6 – Scaling model with markers



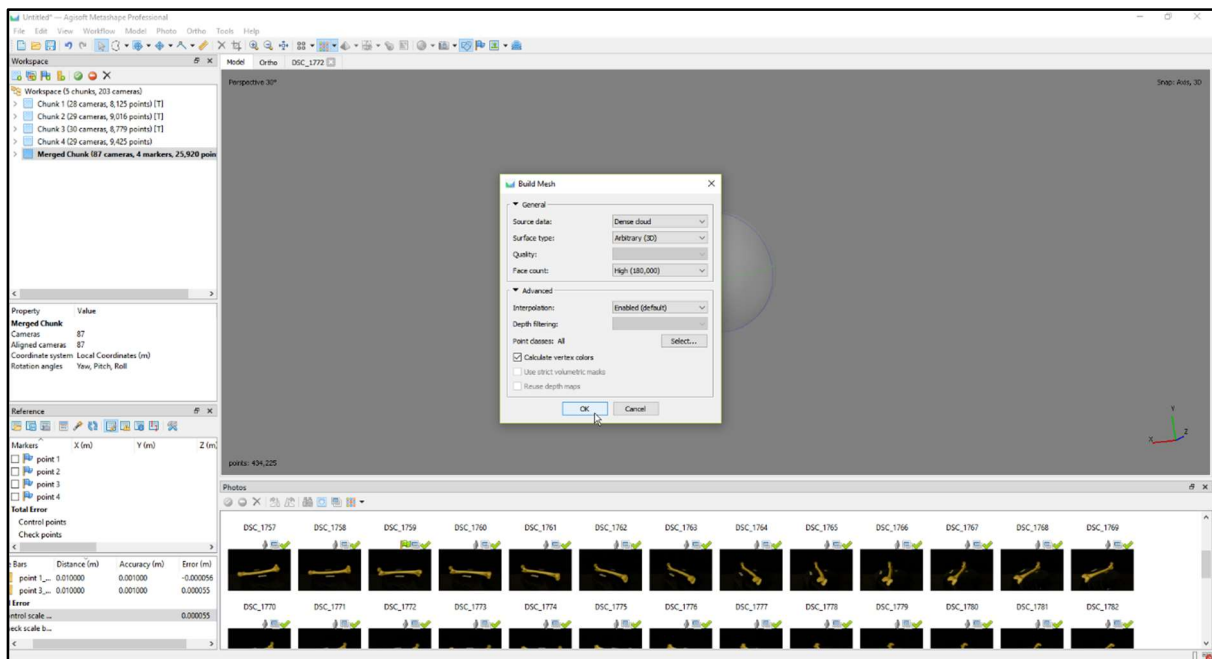
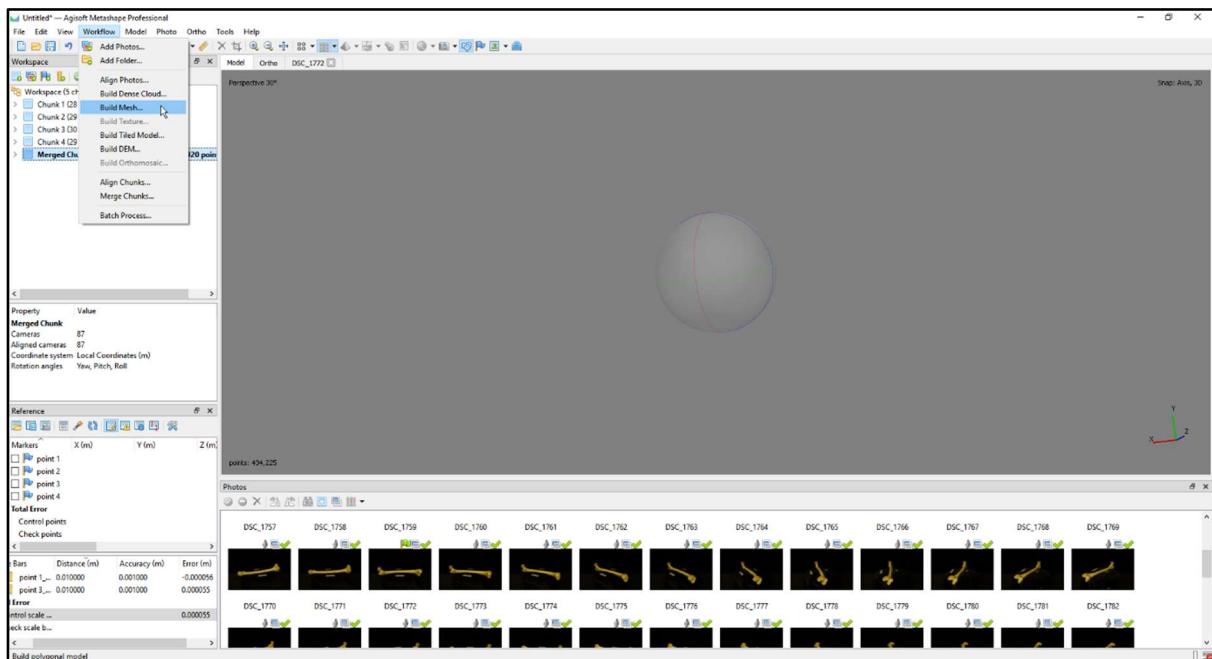


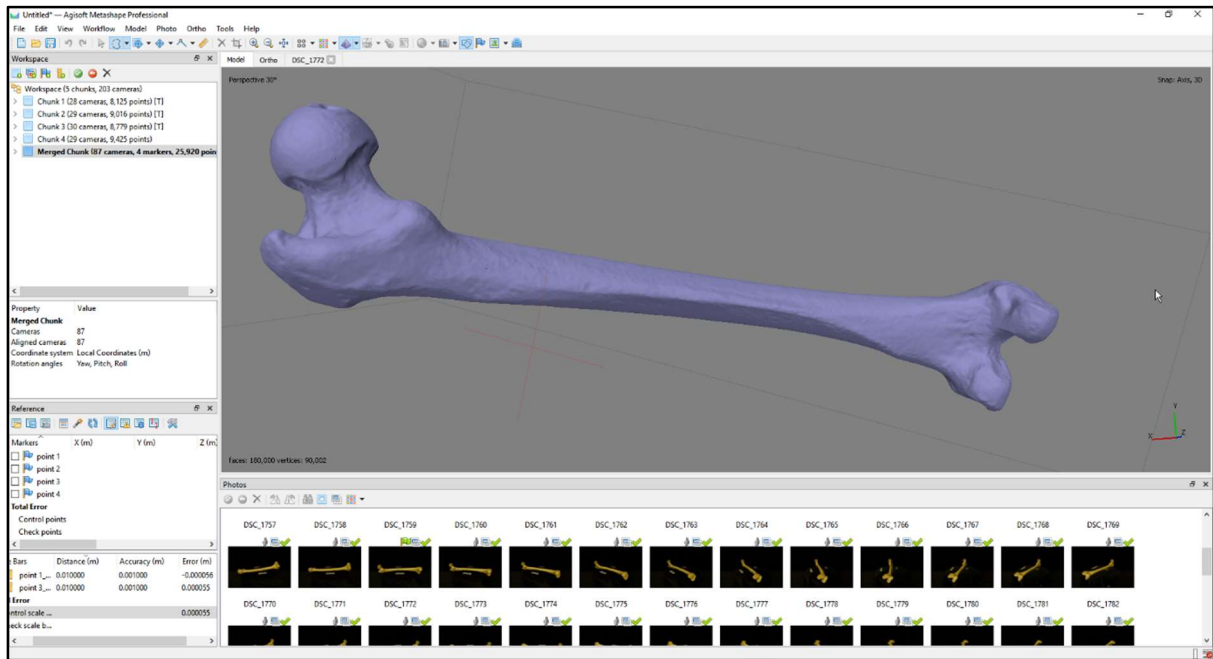
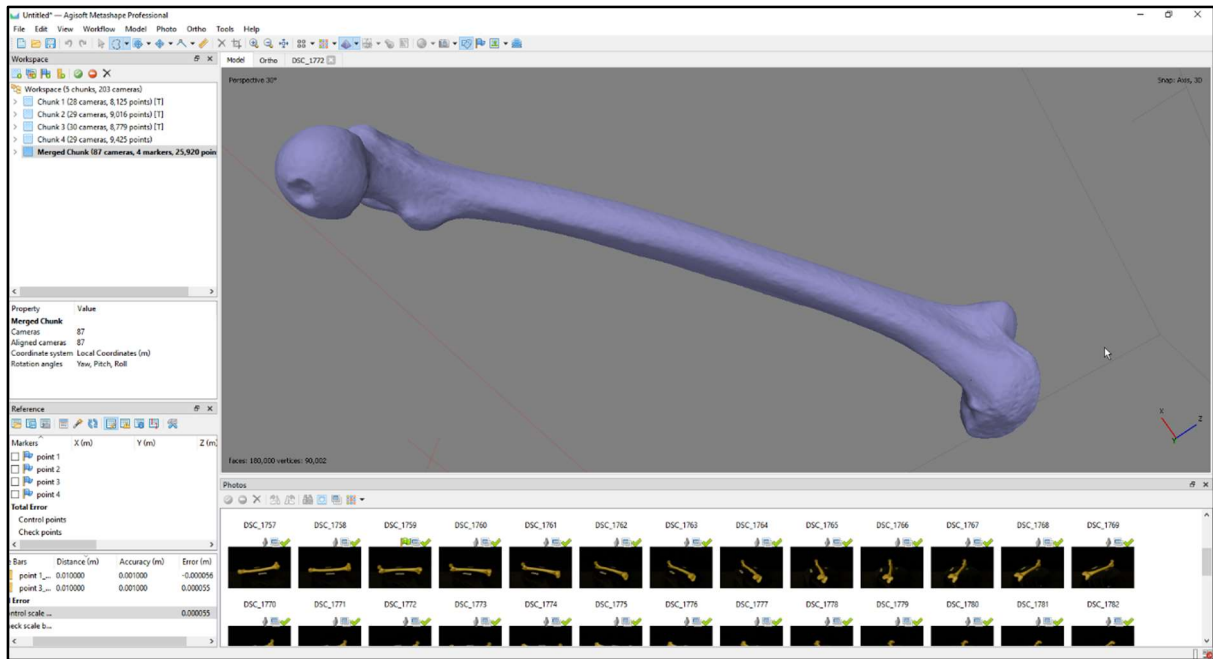




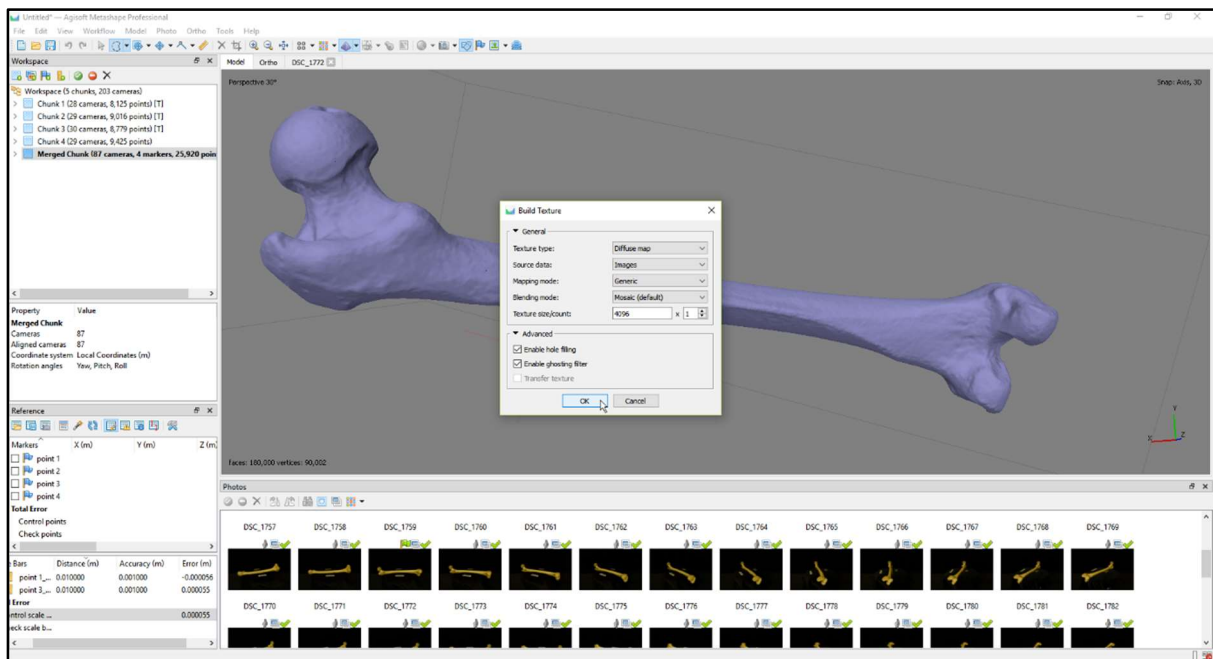
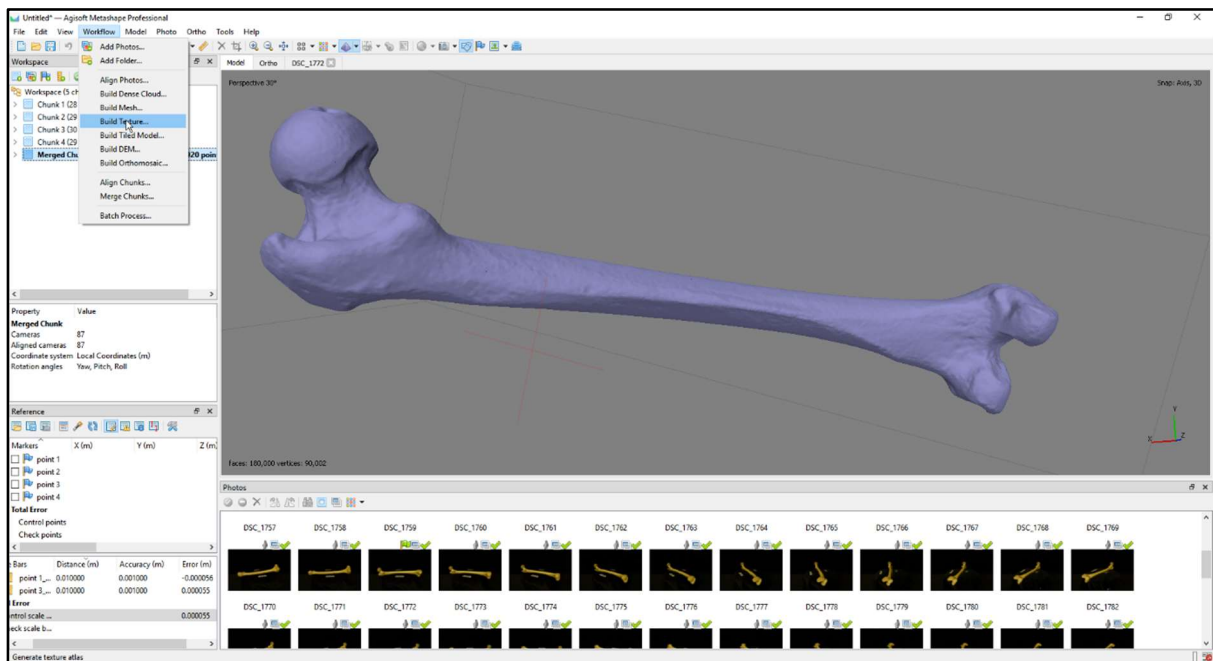


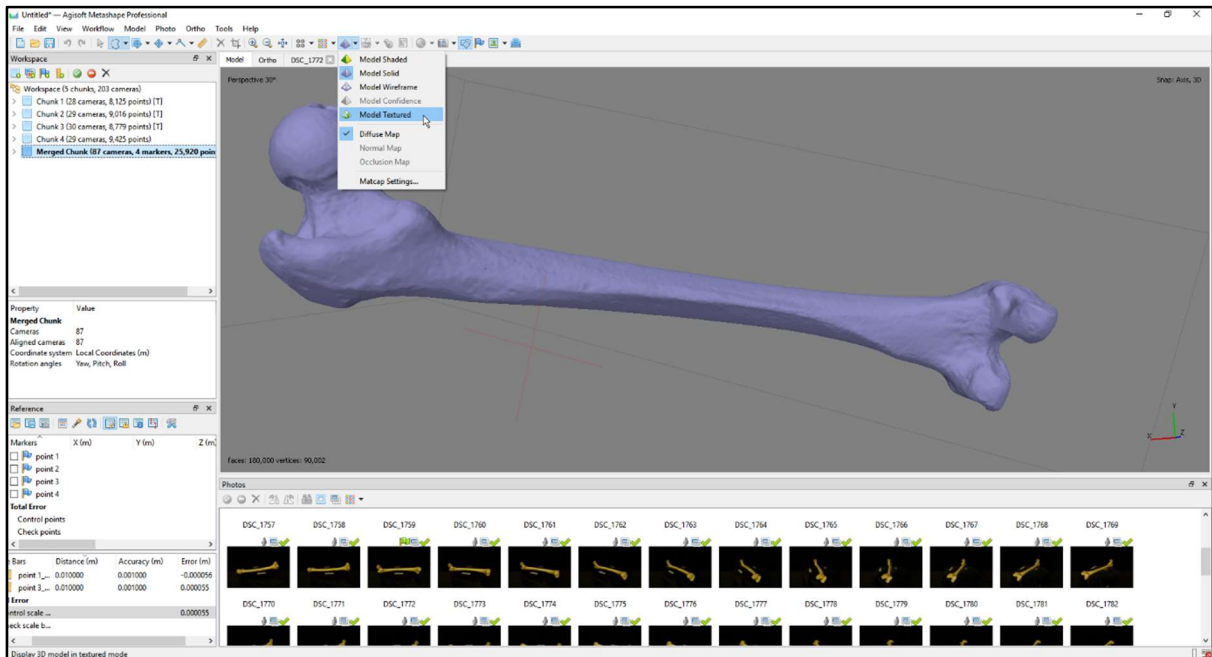
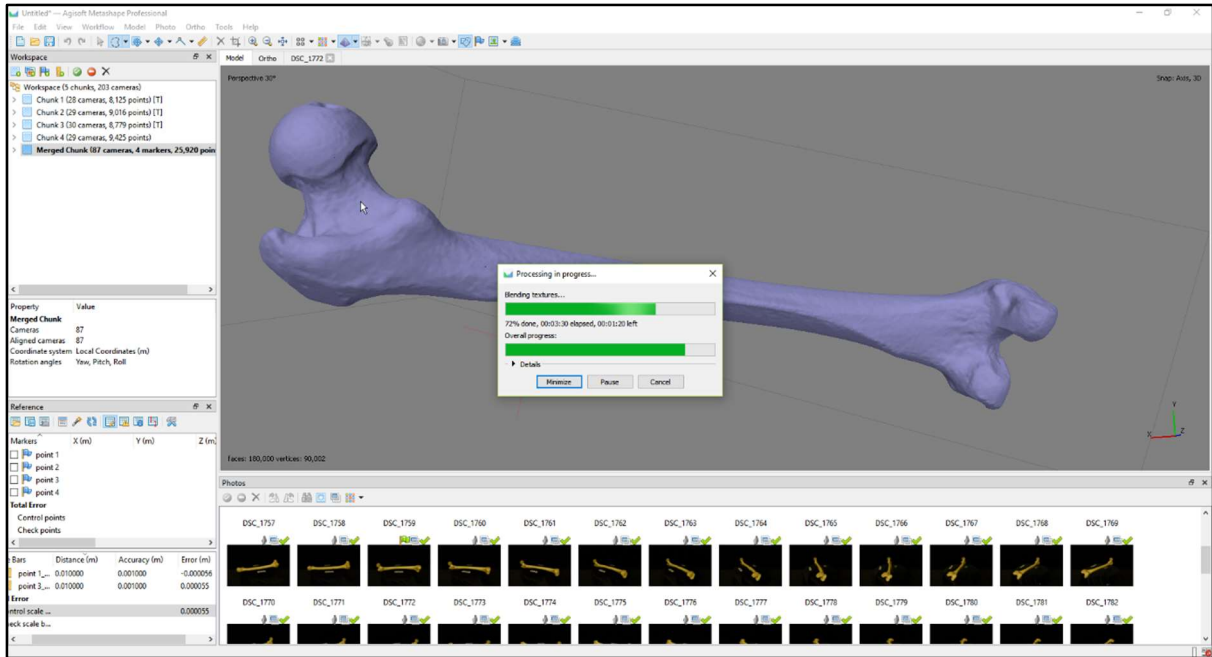
## Step 7 – Building the mesh model.

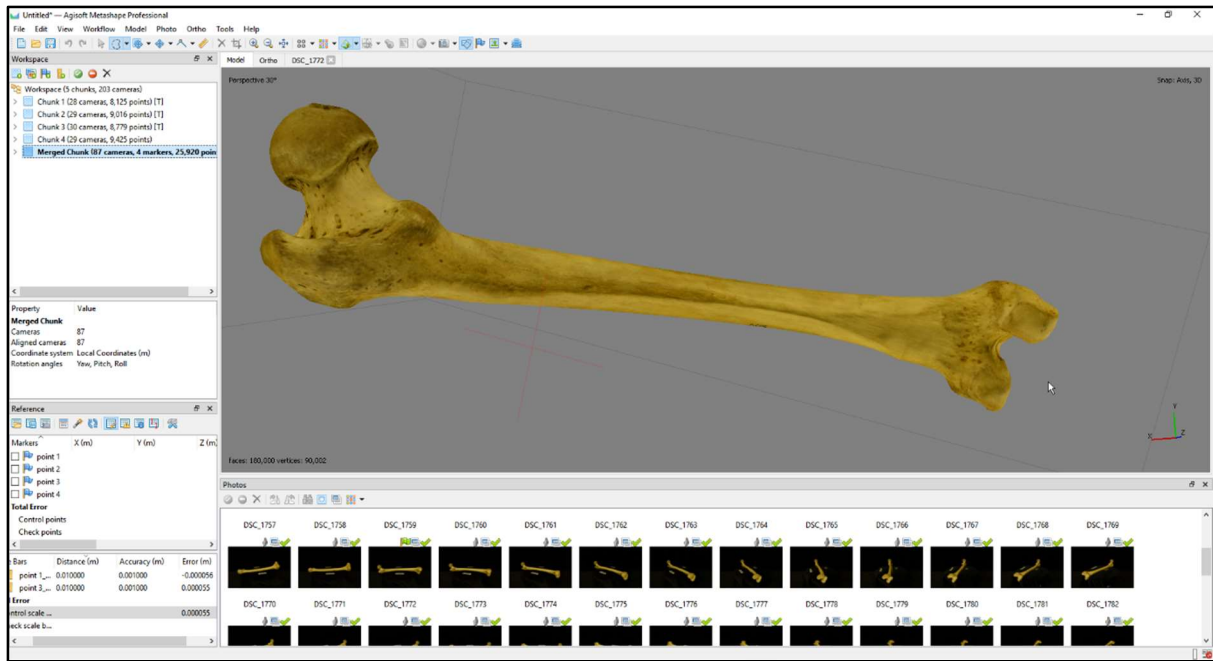


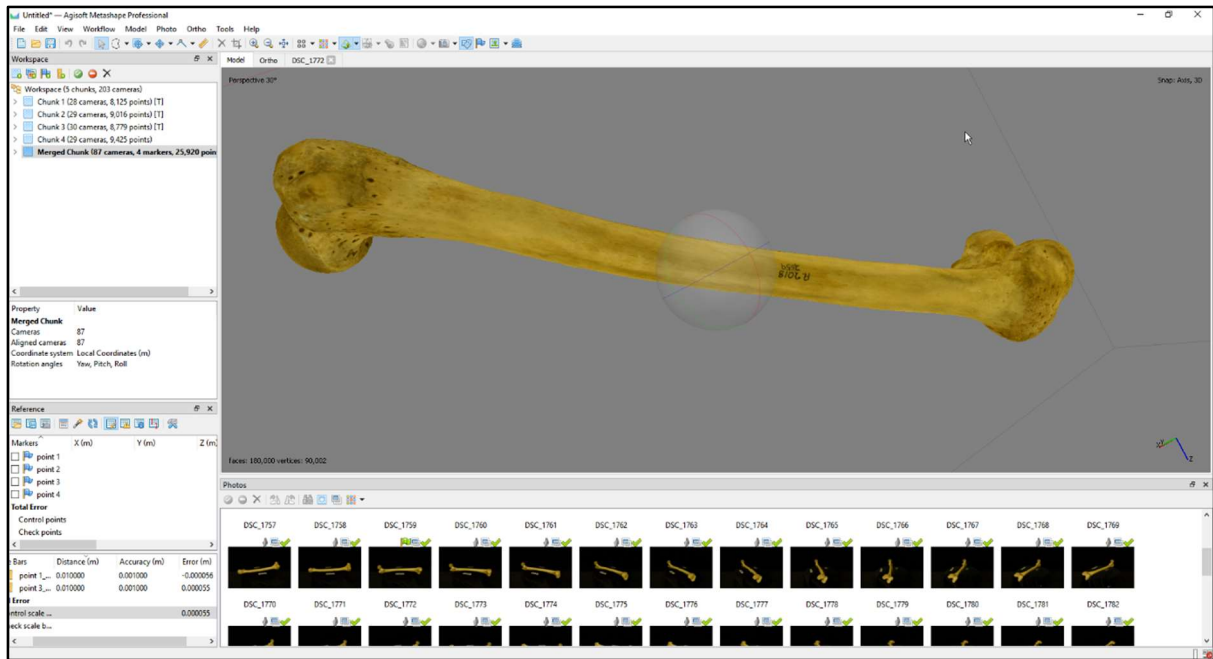


## Step 8 – Building a textured-based mesh model.

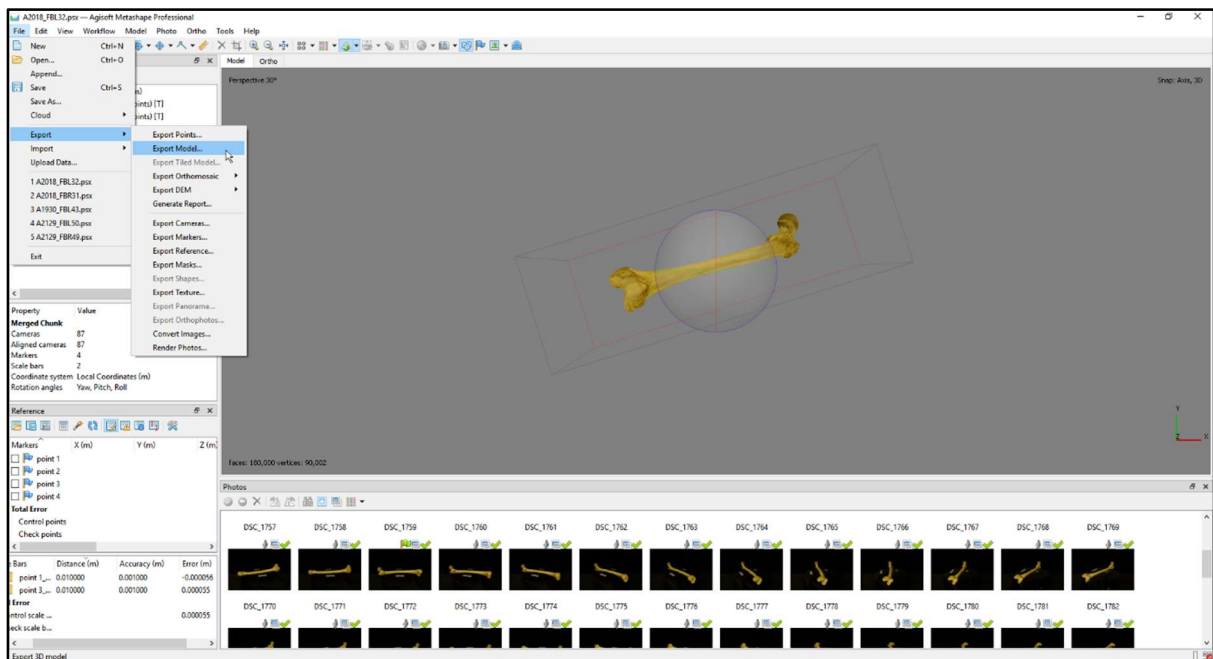




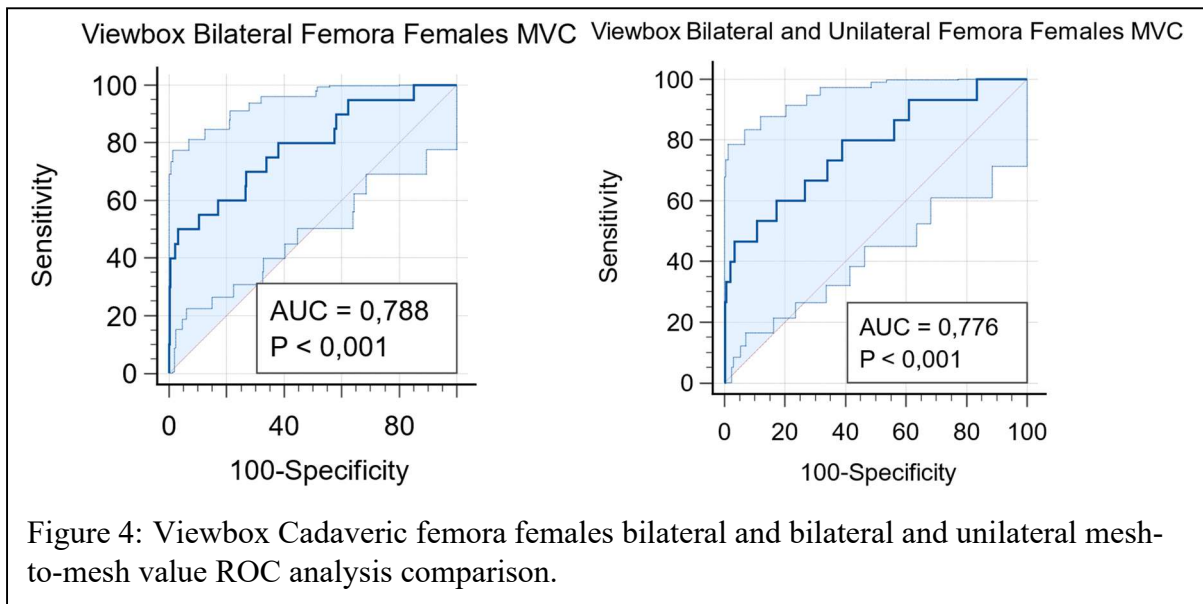
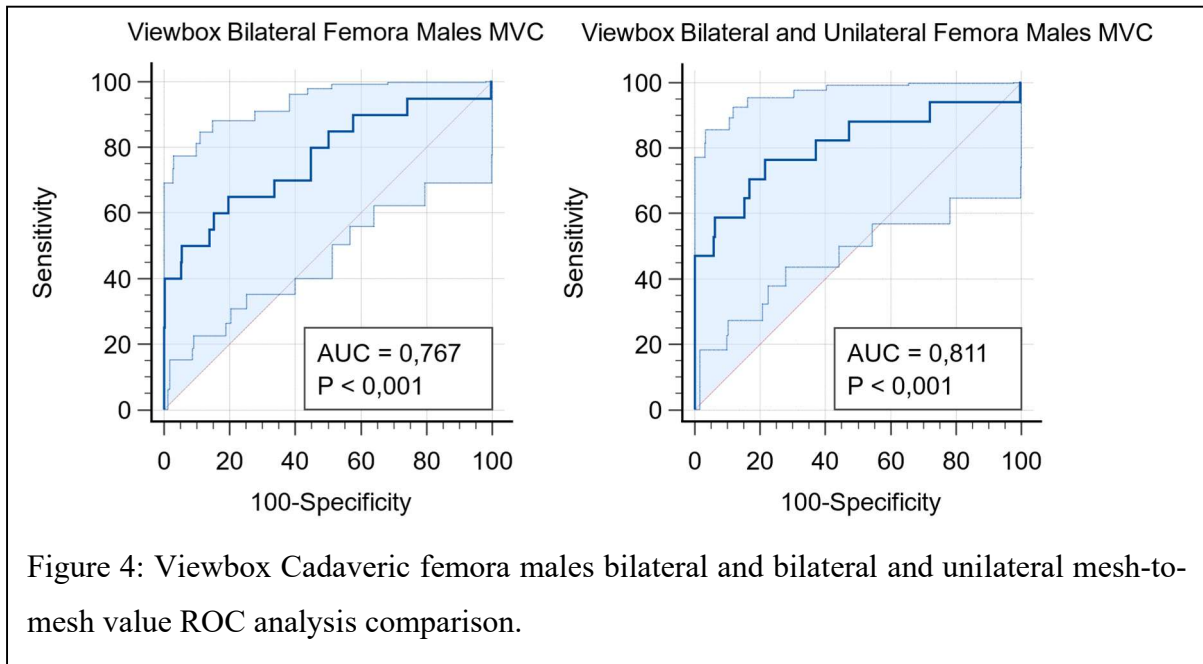


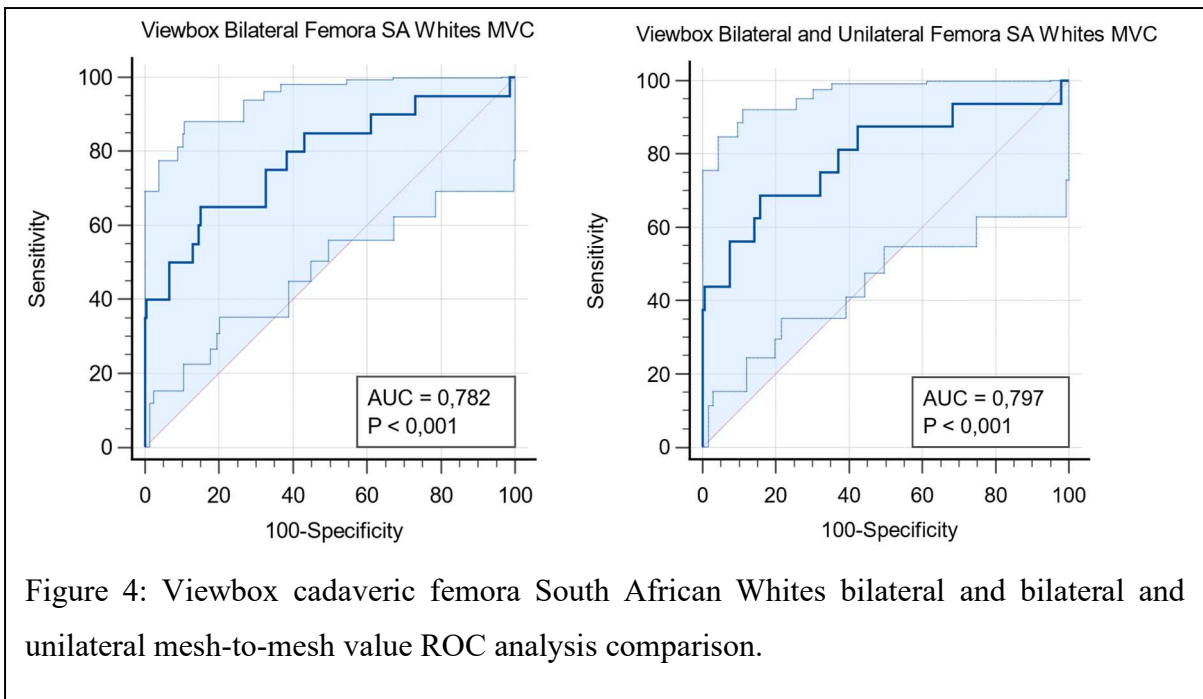
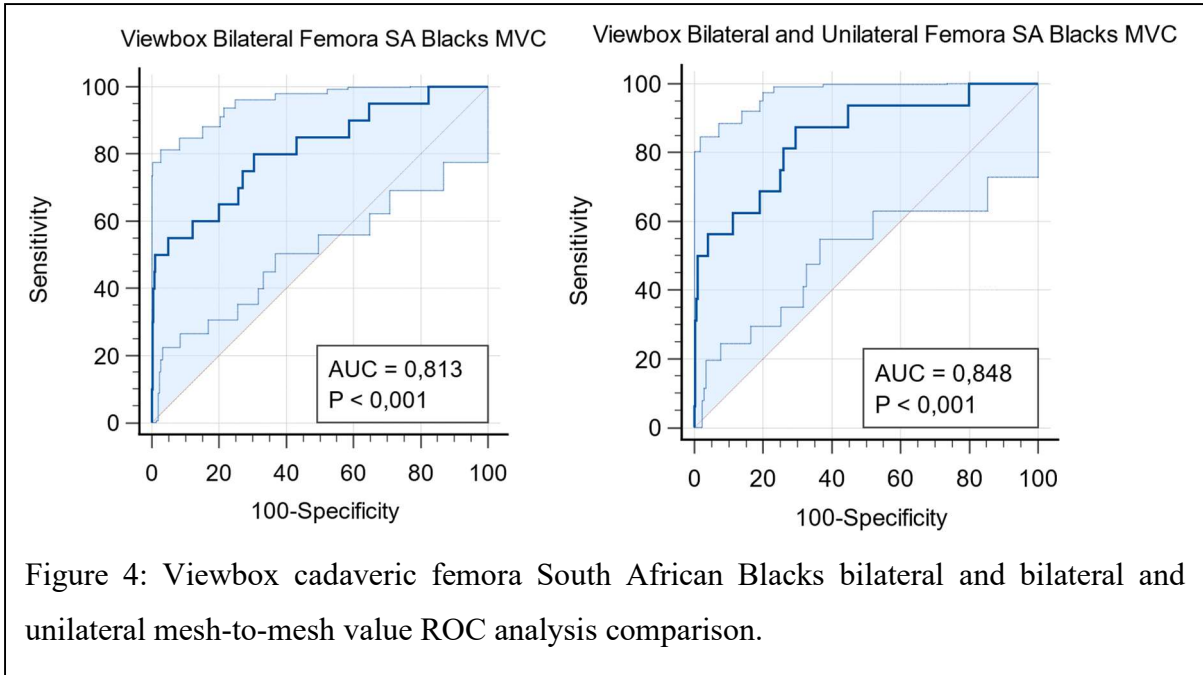


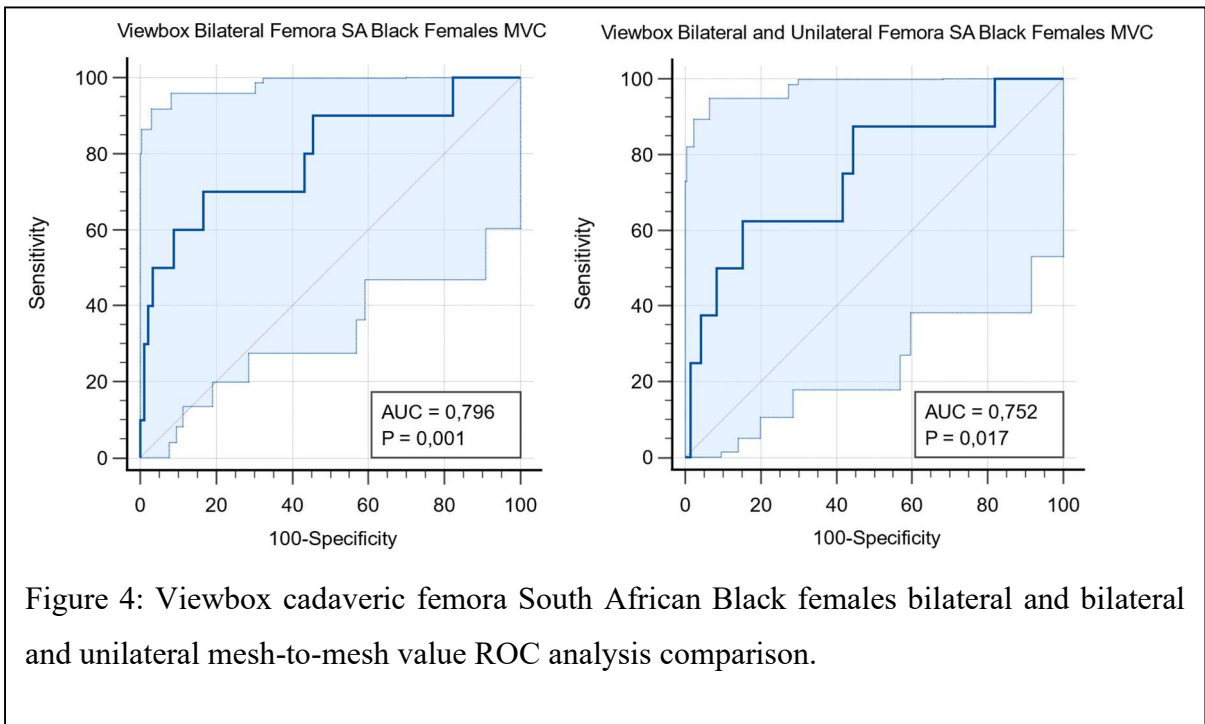
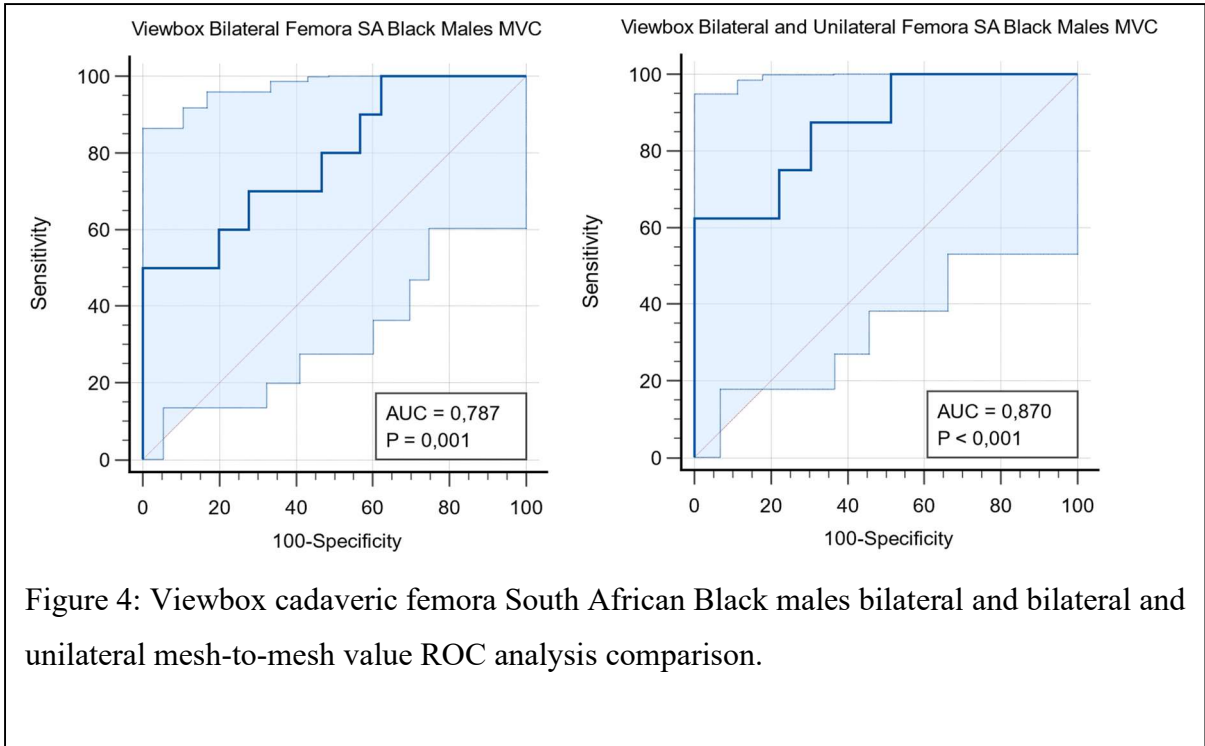
Step 9 (Final step)– Exporting the model.

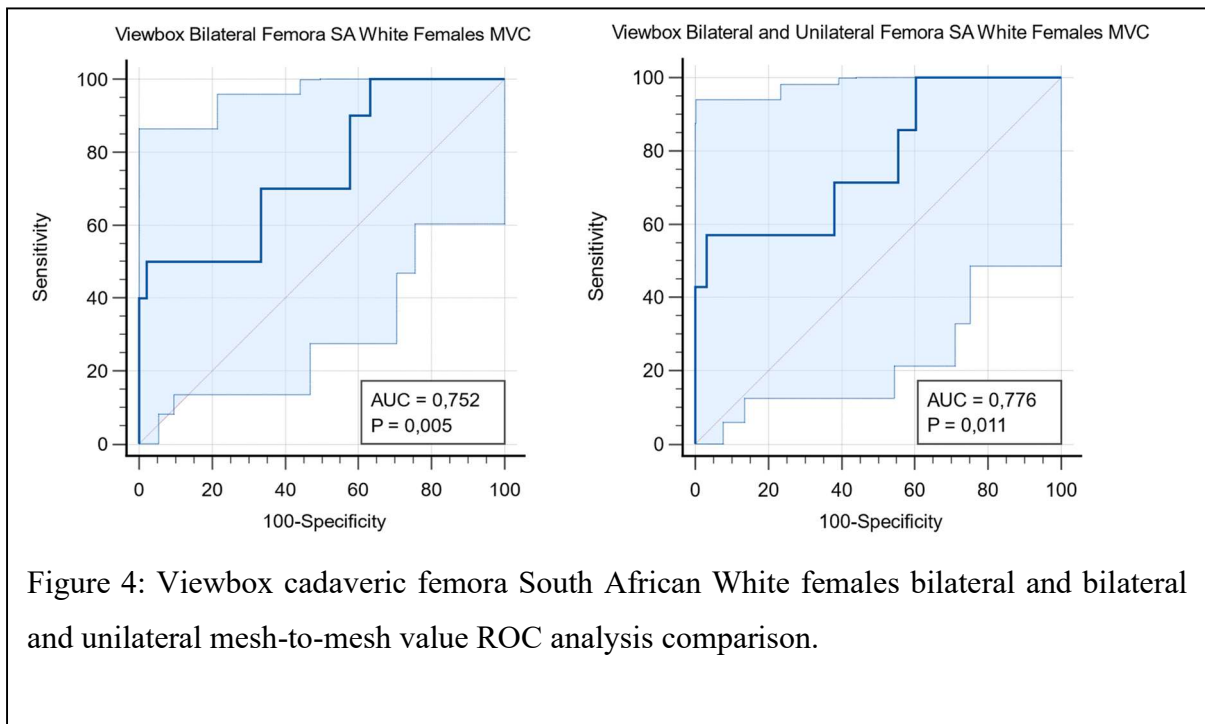
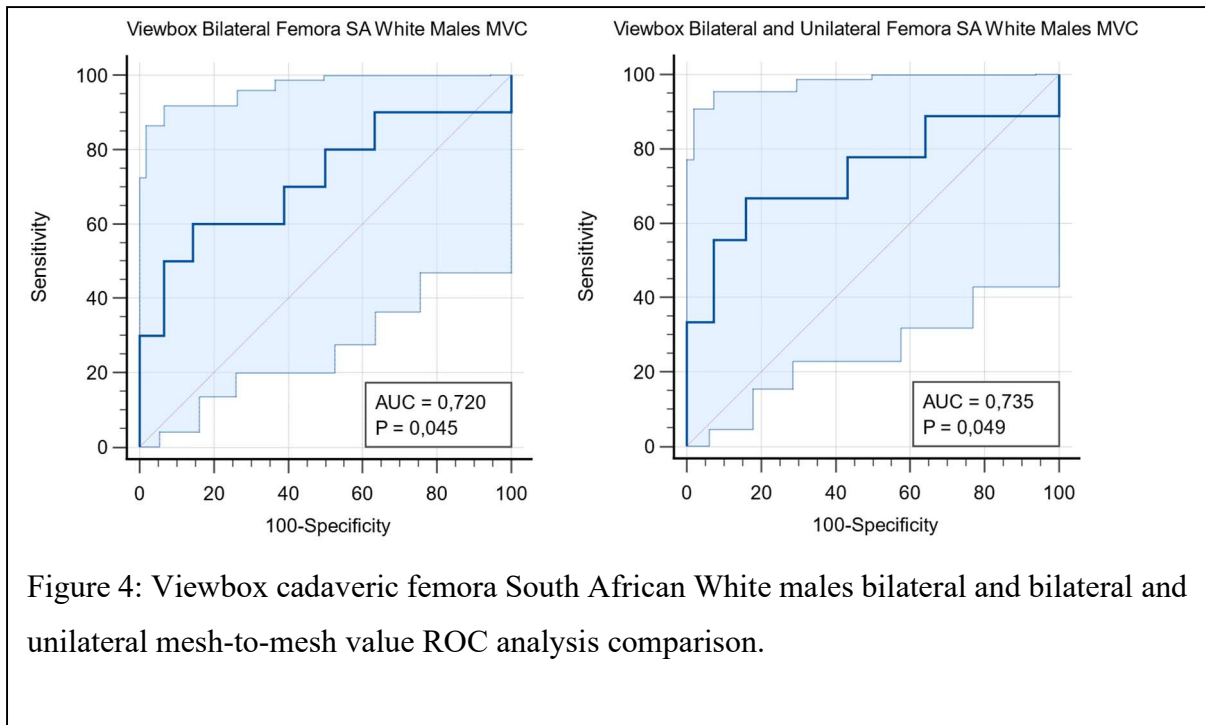


## Appendix B: Viewbox Femora ROC curve graphs

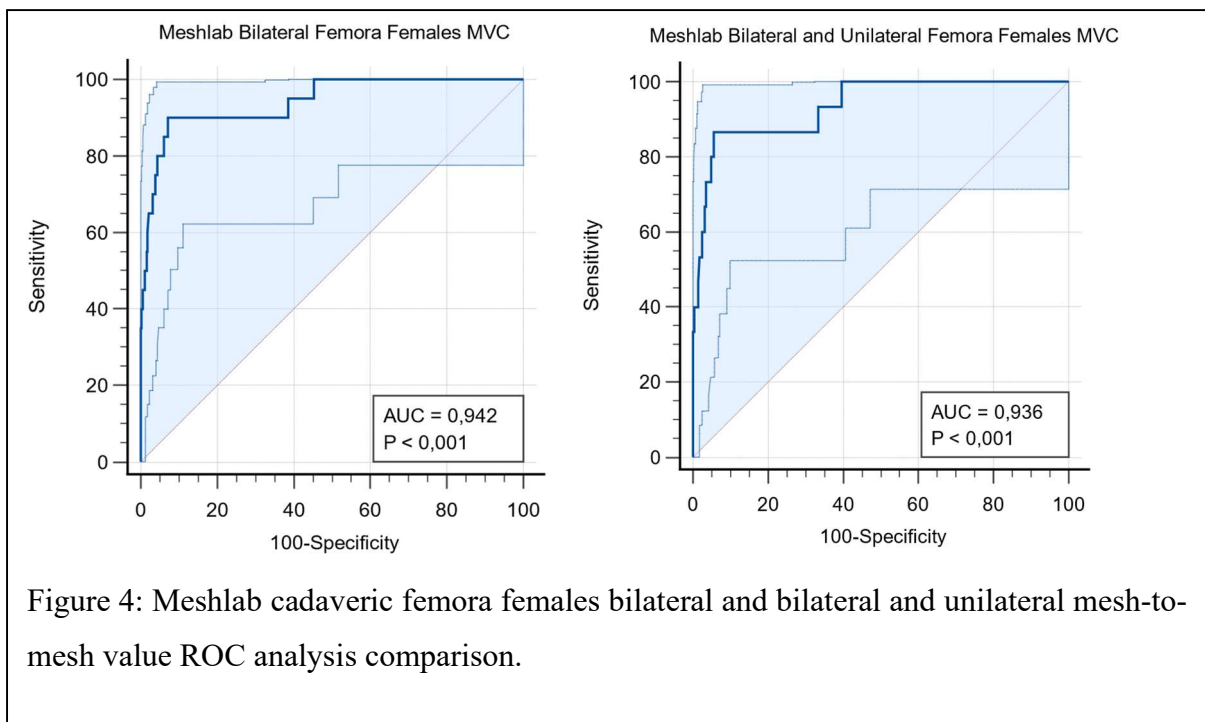
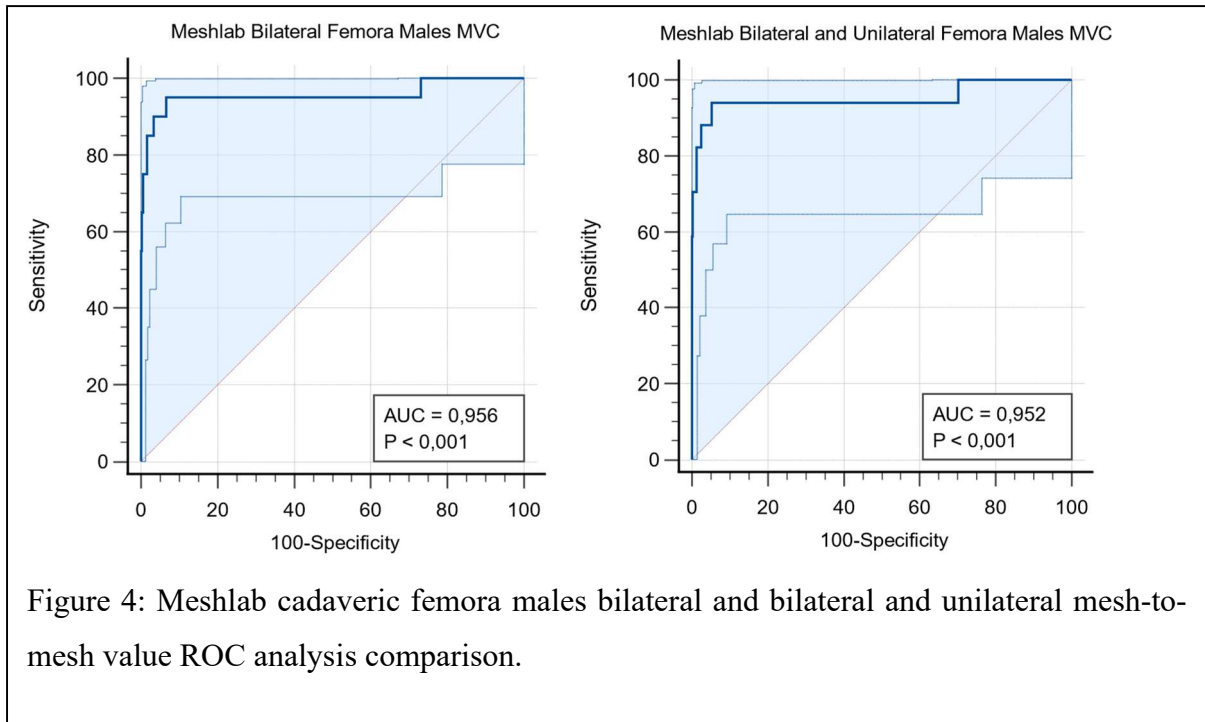


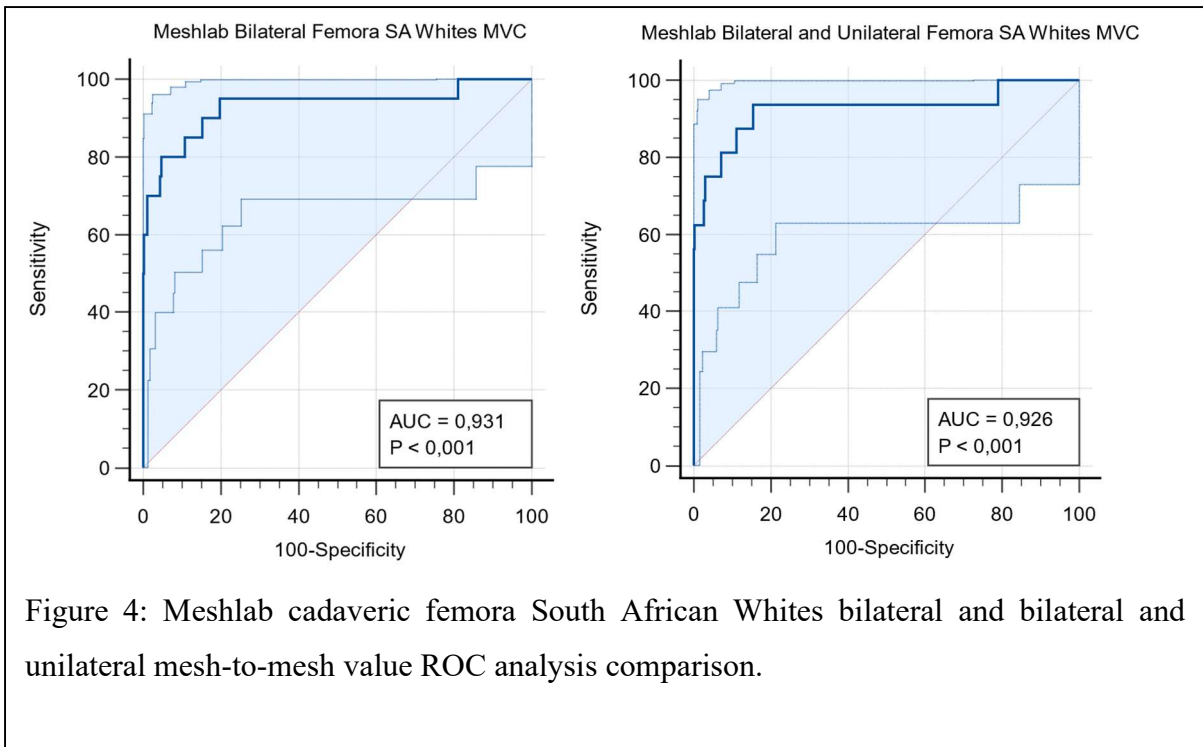
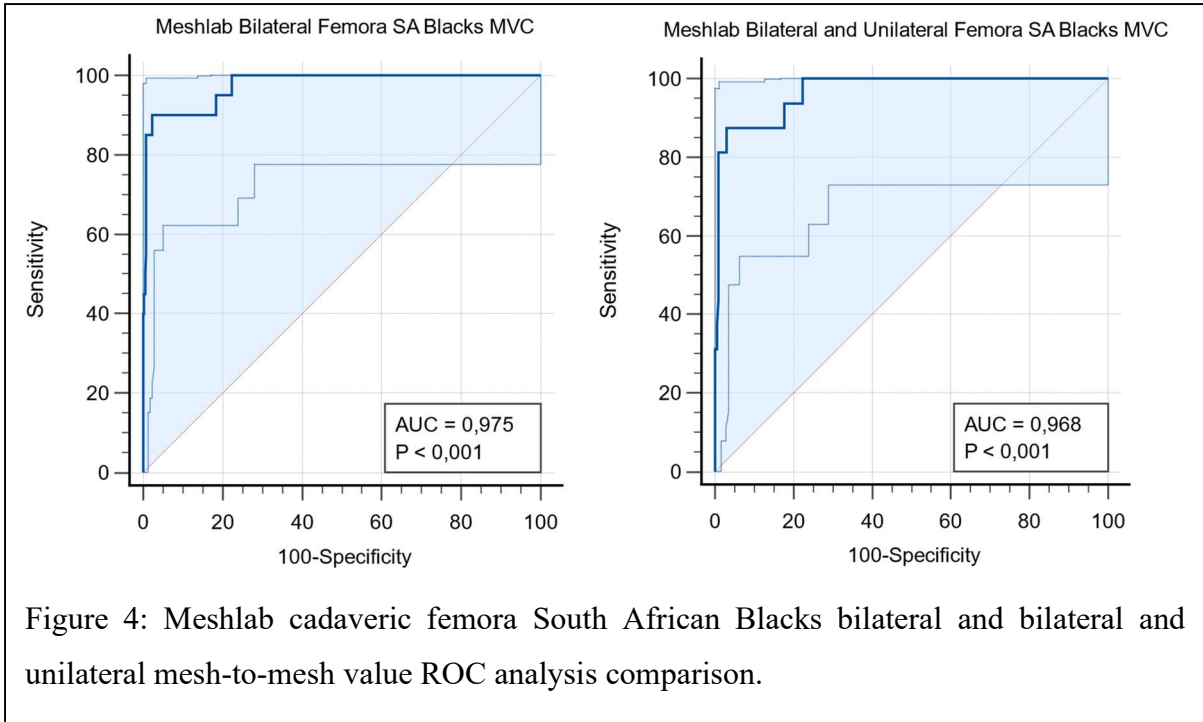


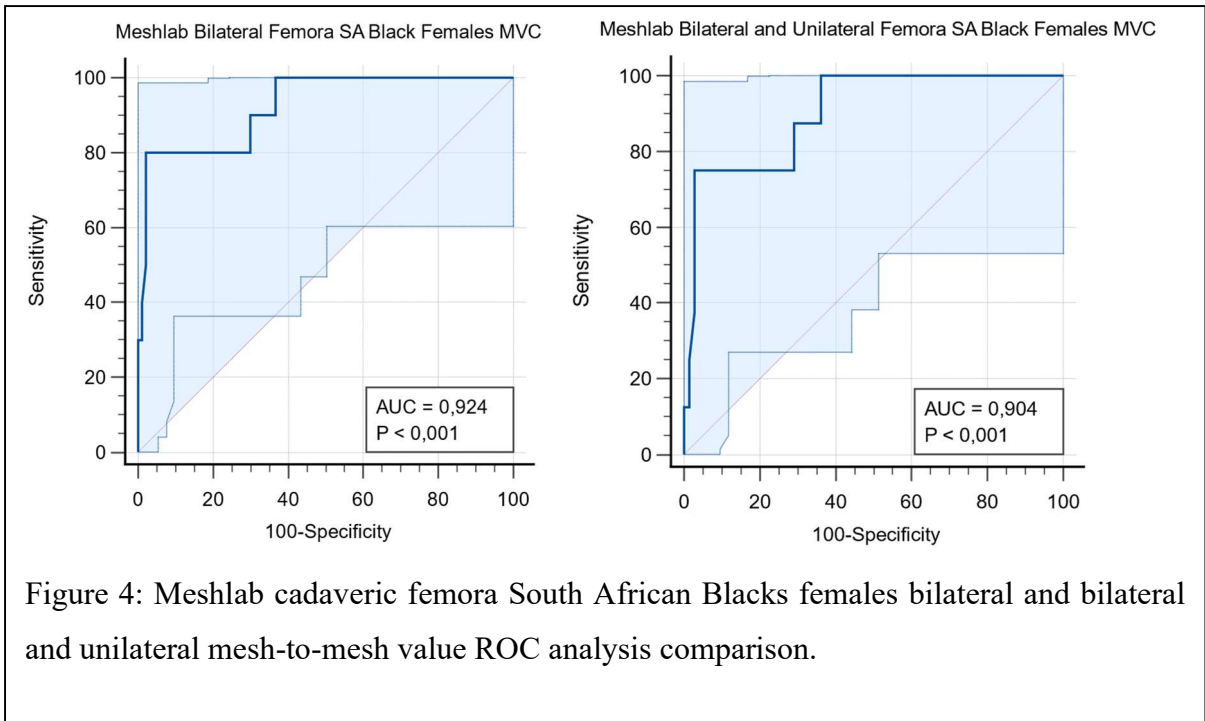
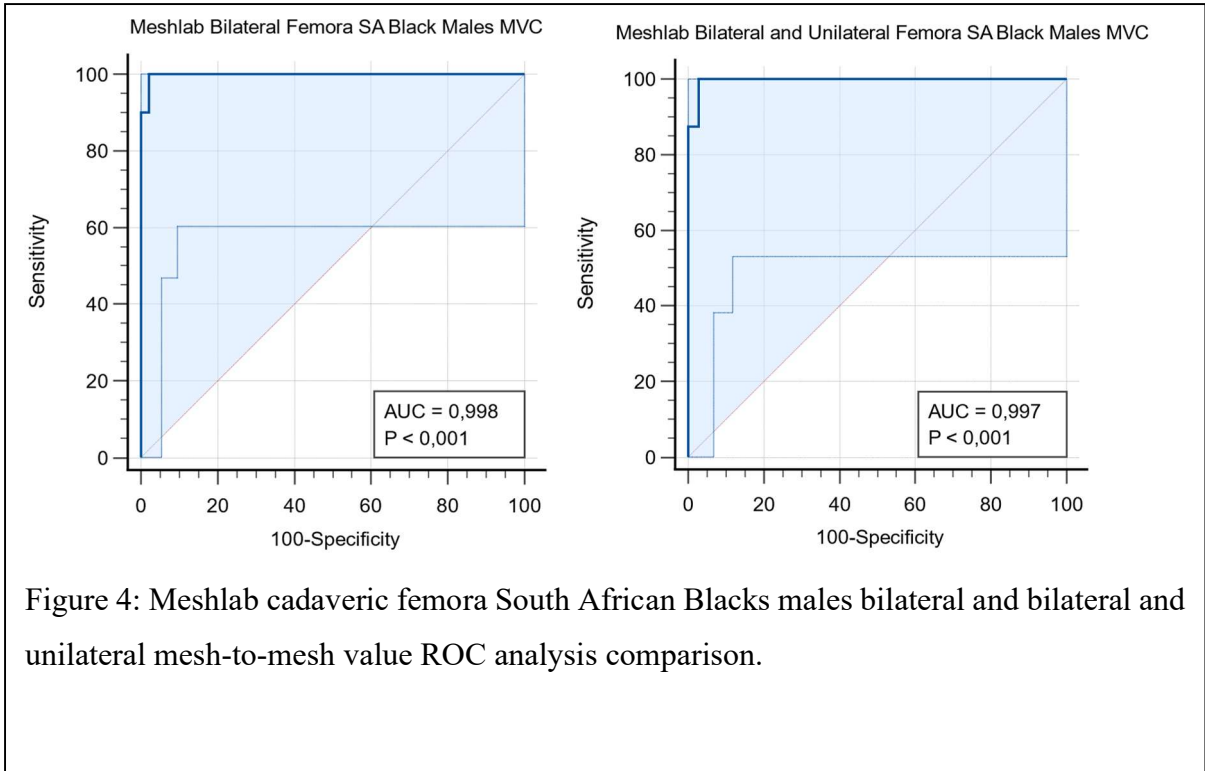


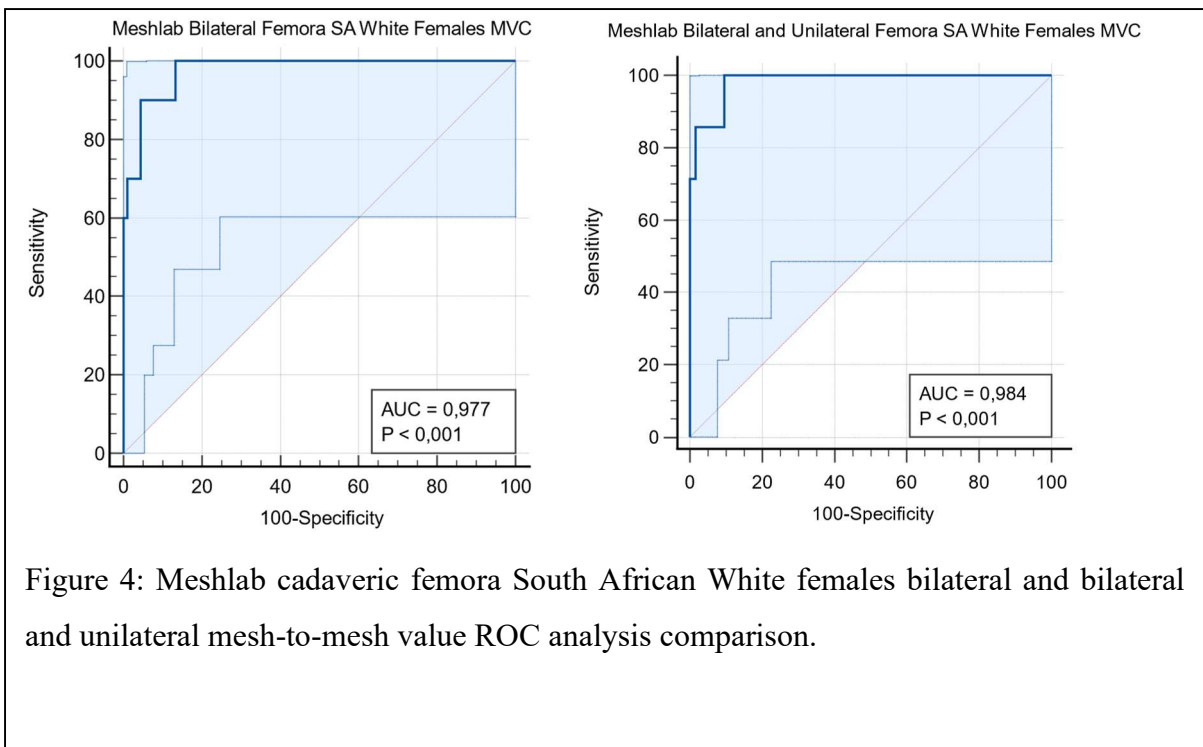
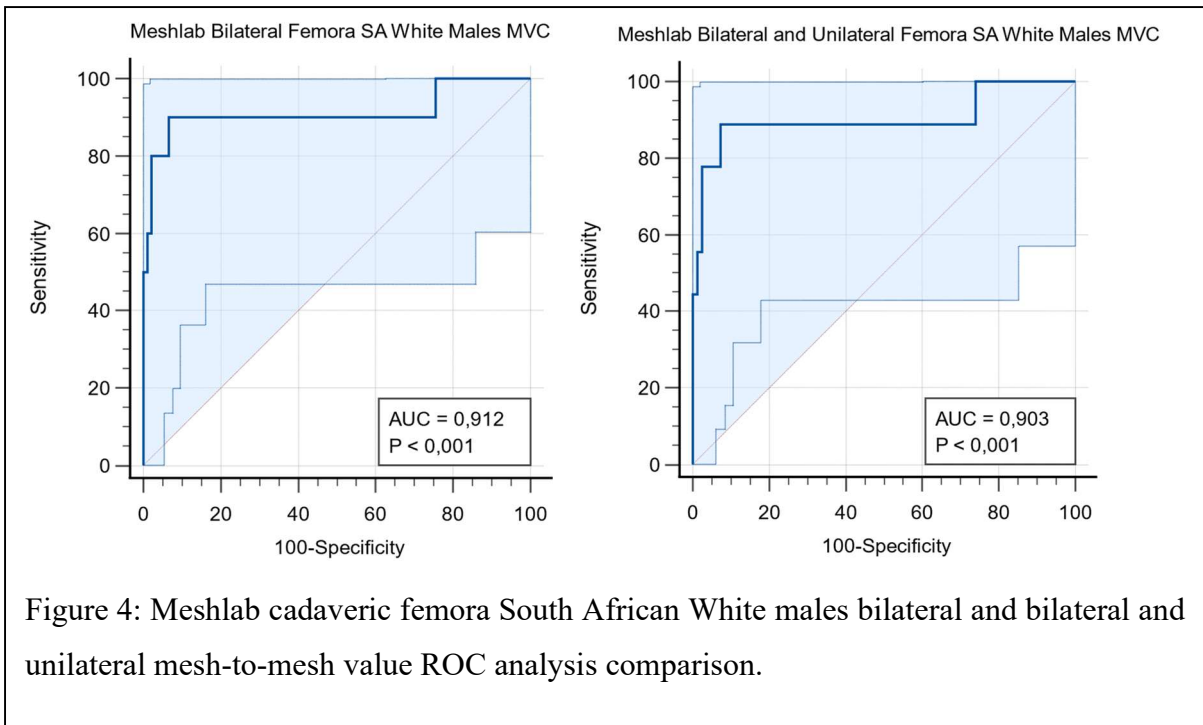


## Appendix C: Meshlab Femora ROC curve graphs

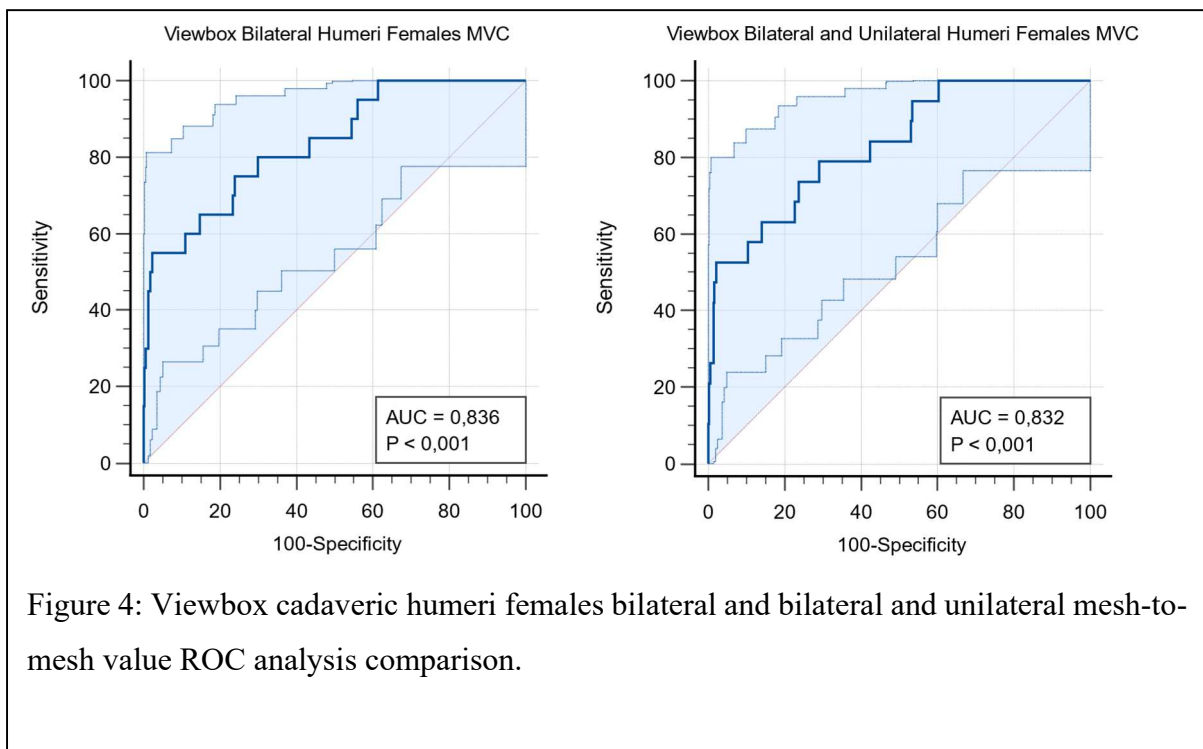
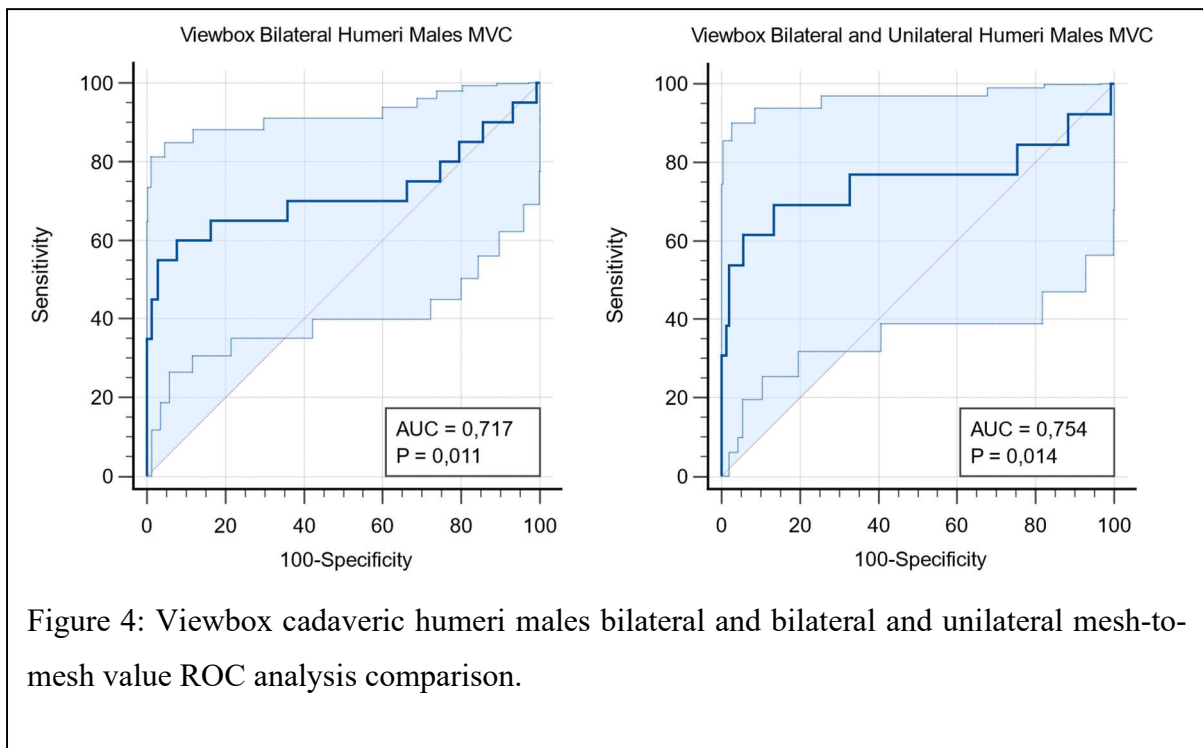


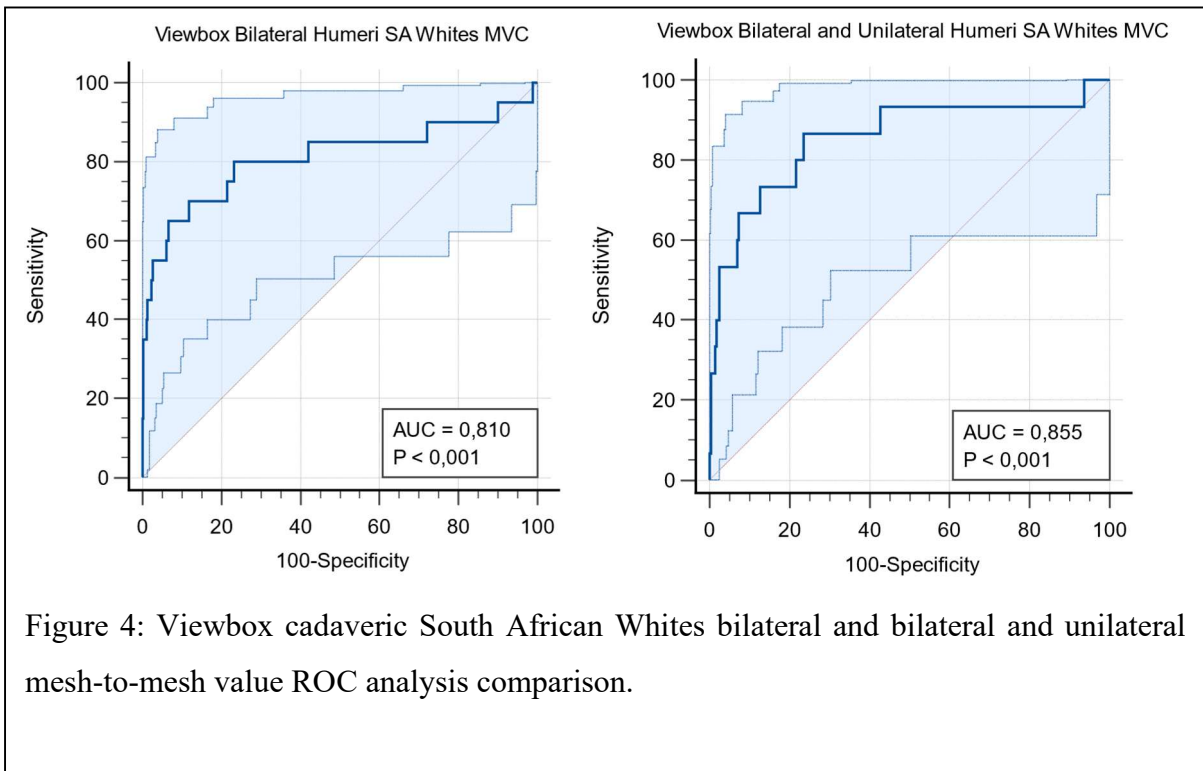
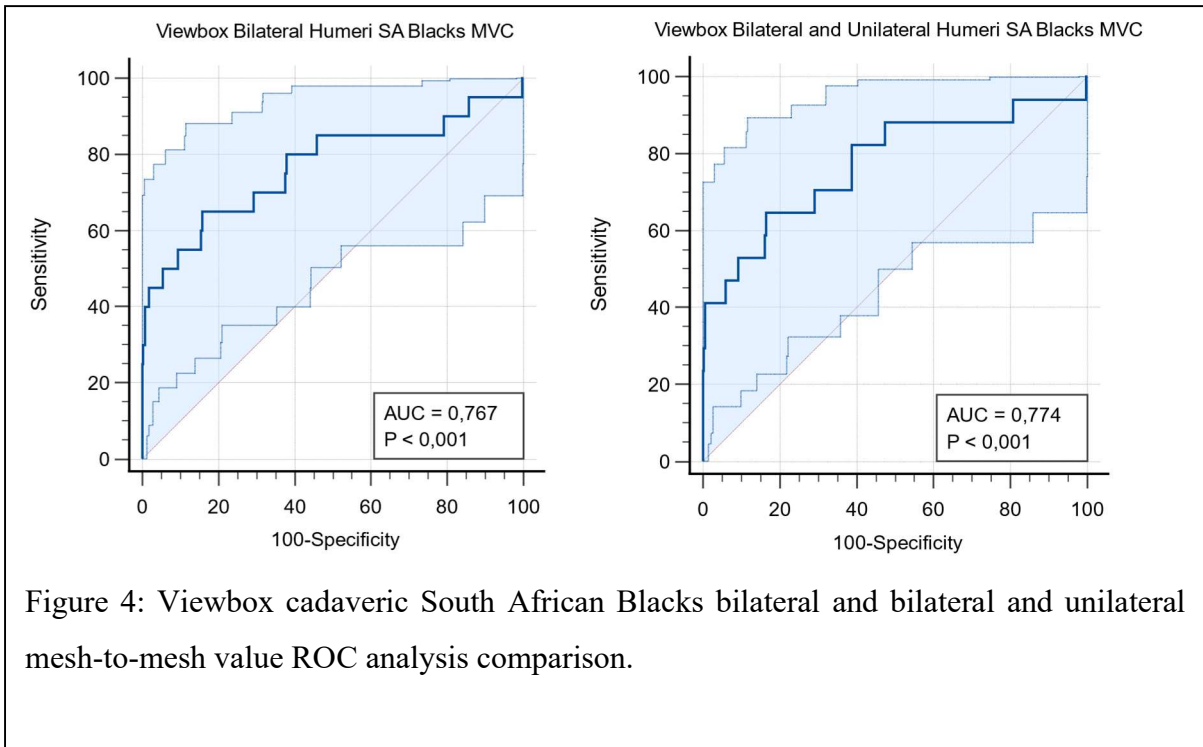


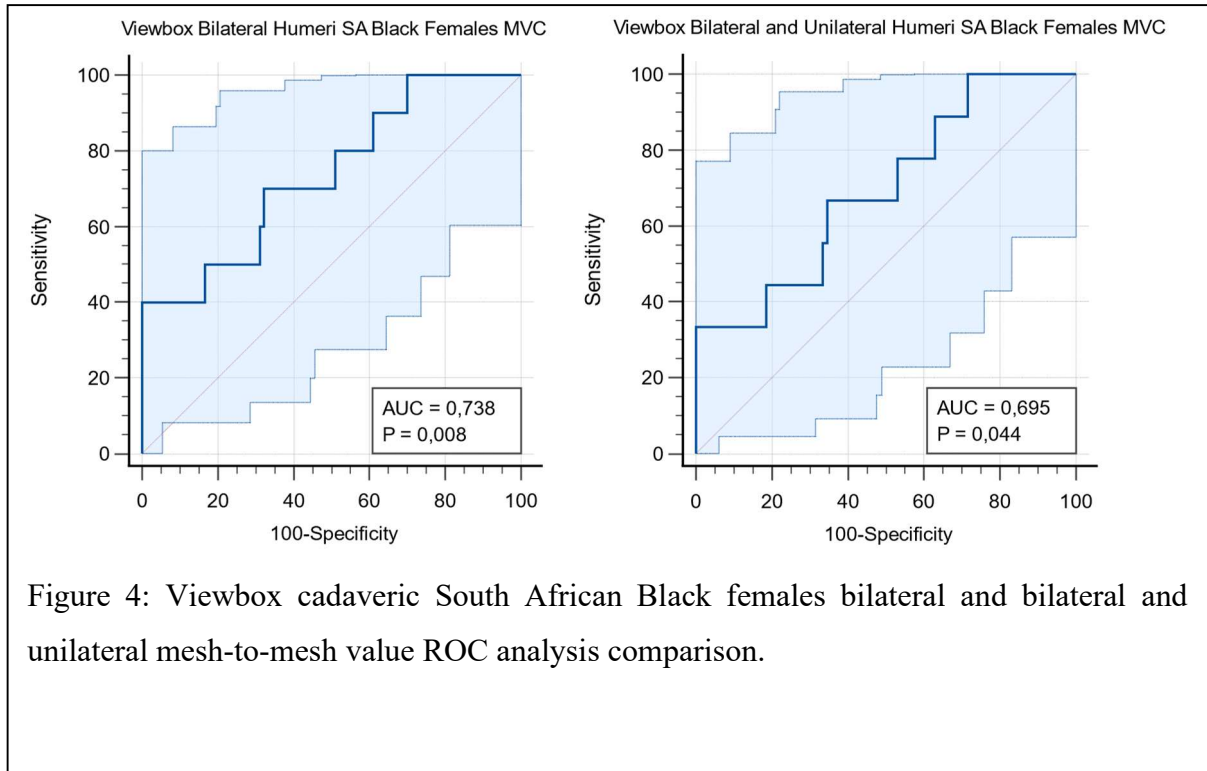
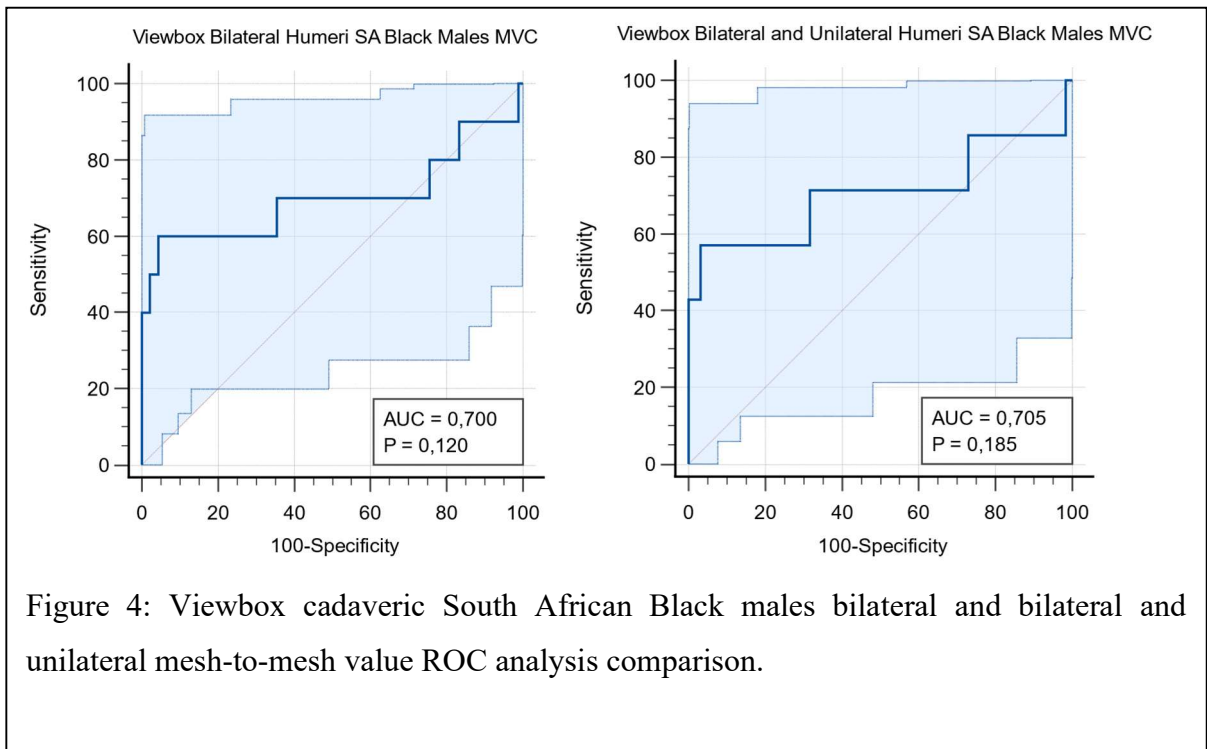


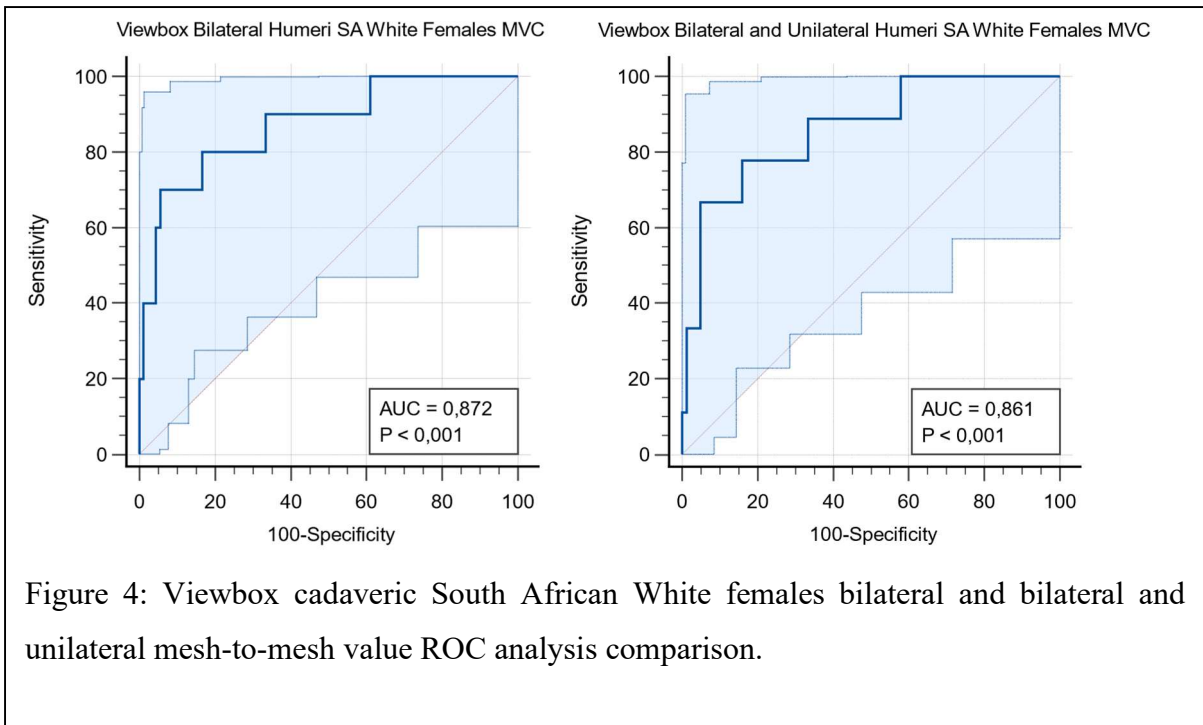
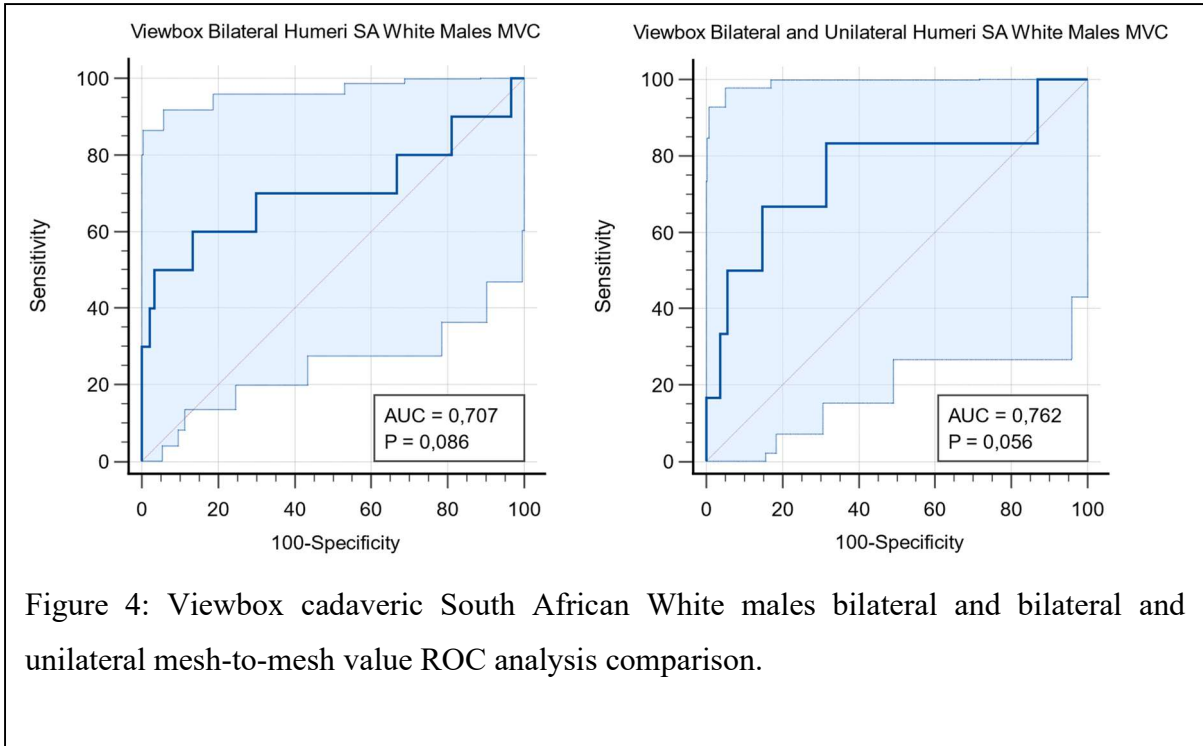


## Appendix D: Viewbox Humeri ROC curve graphs









## Appendix E: Meshlab Humeri ROC curve graphs

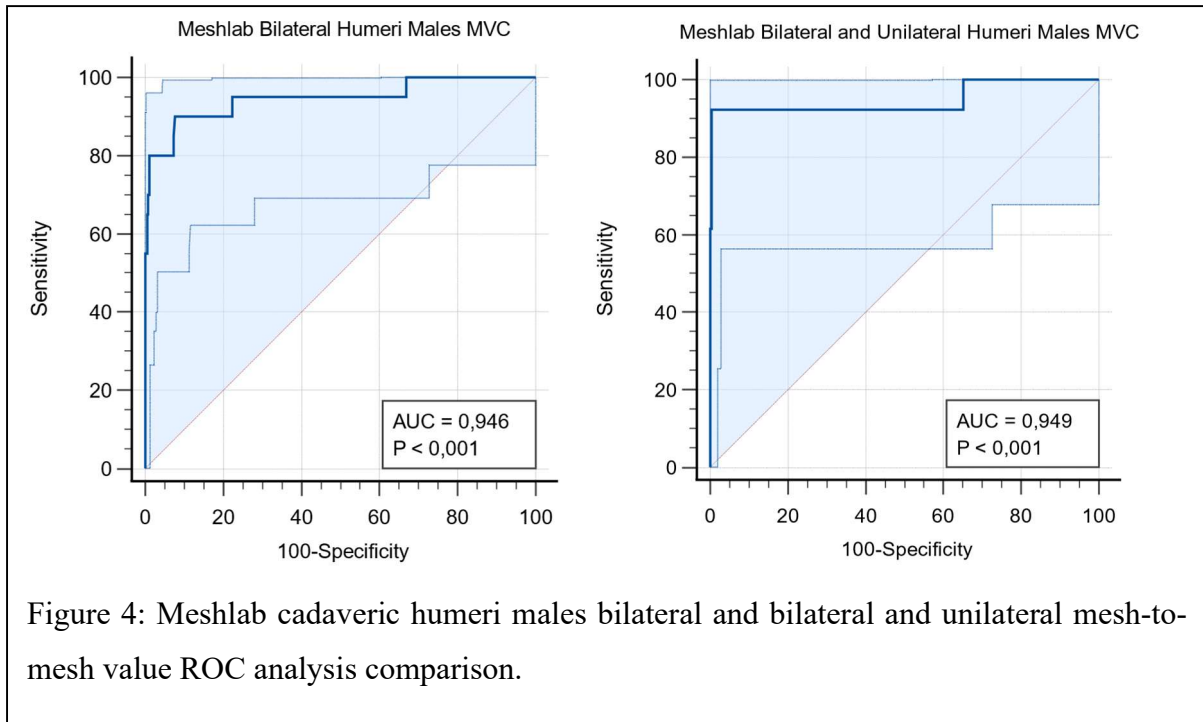


Figure 4: Meshlab cadaveric humeri males bilateral and bilateral and unilateral mesh-to-mesh value ROC analysis comparison.

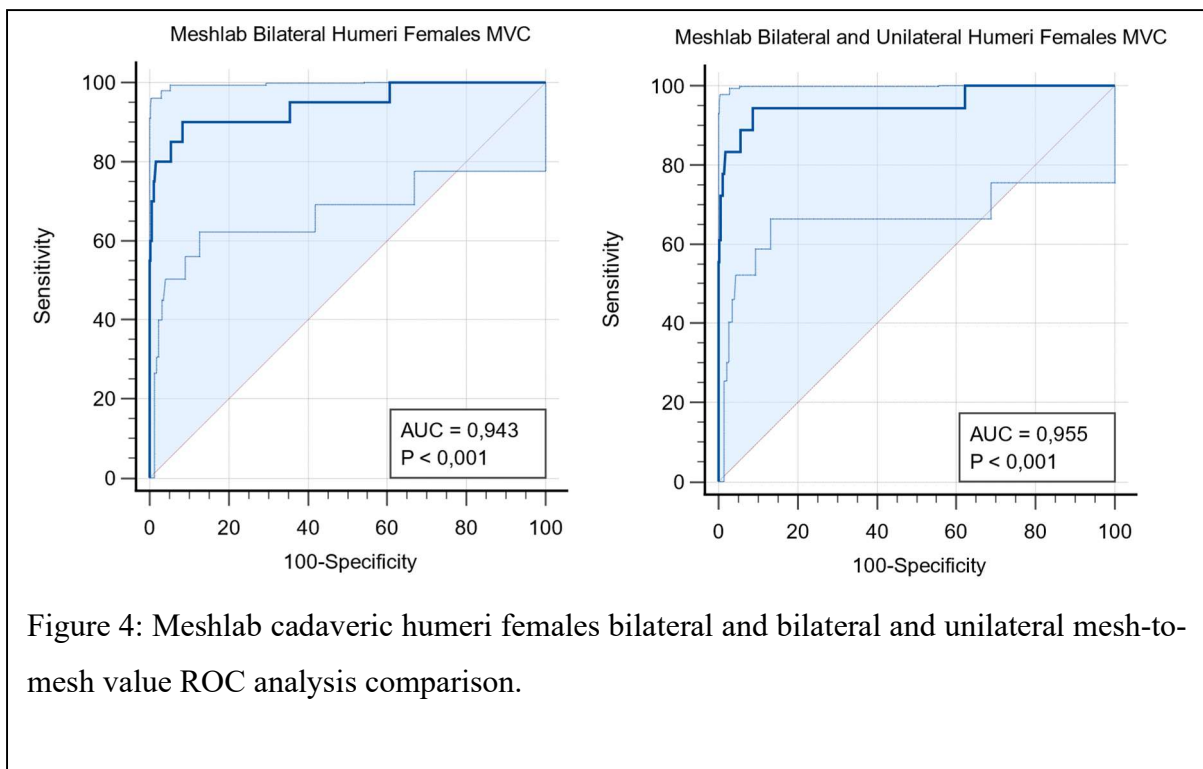
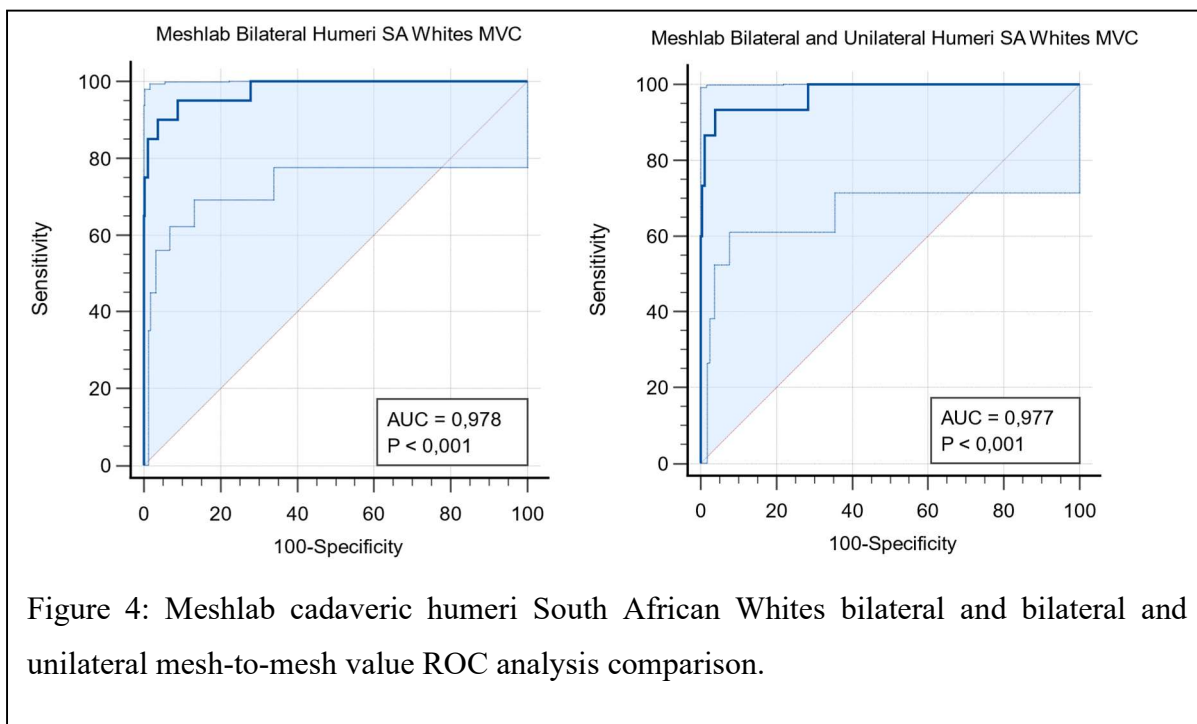
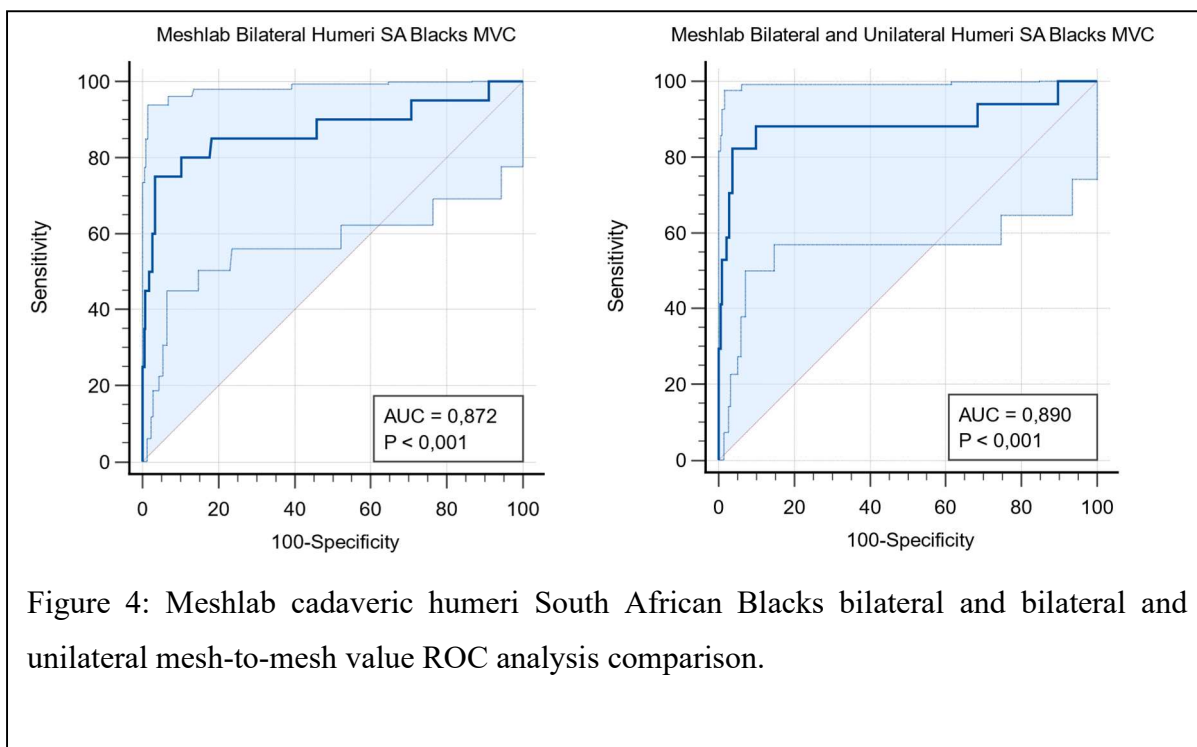
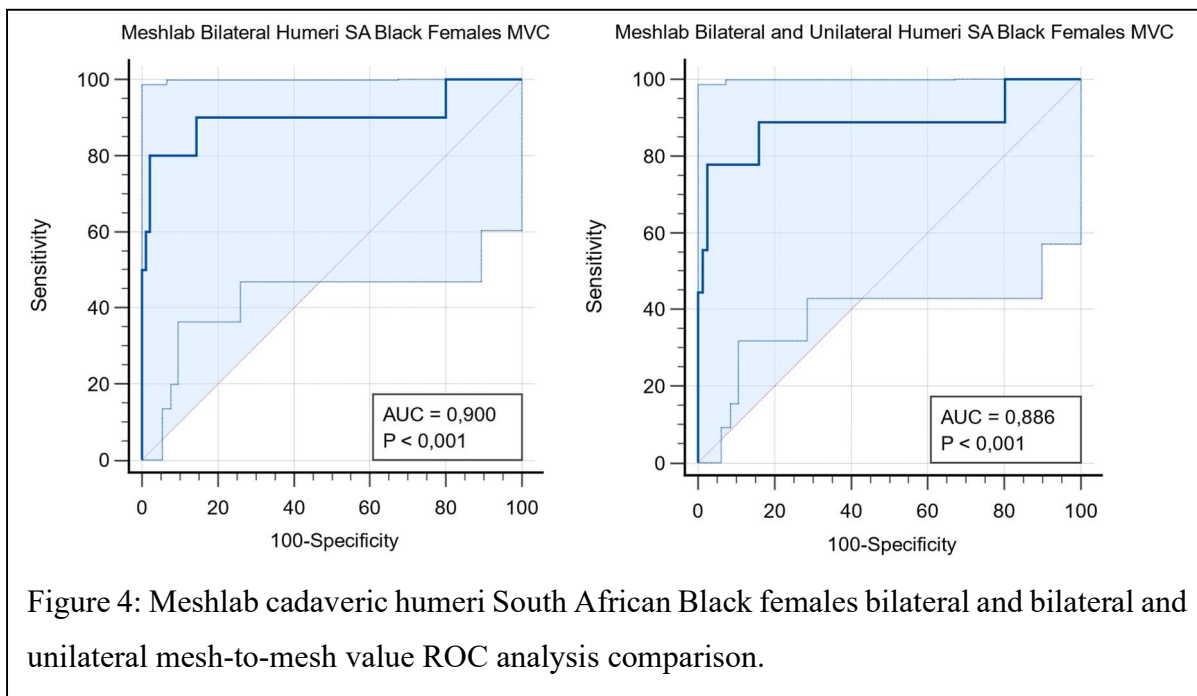
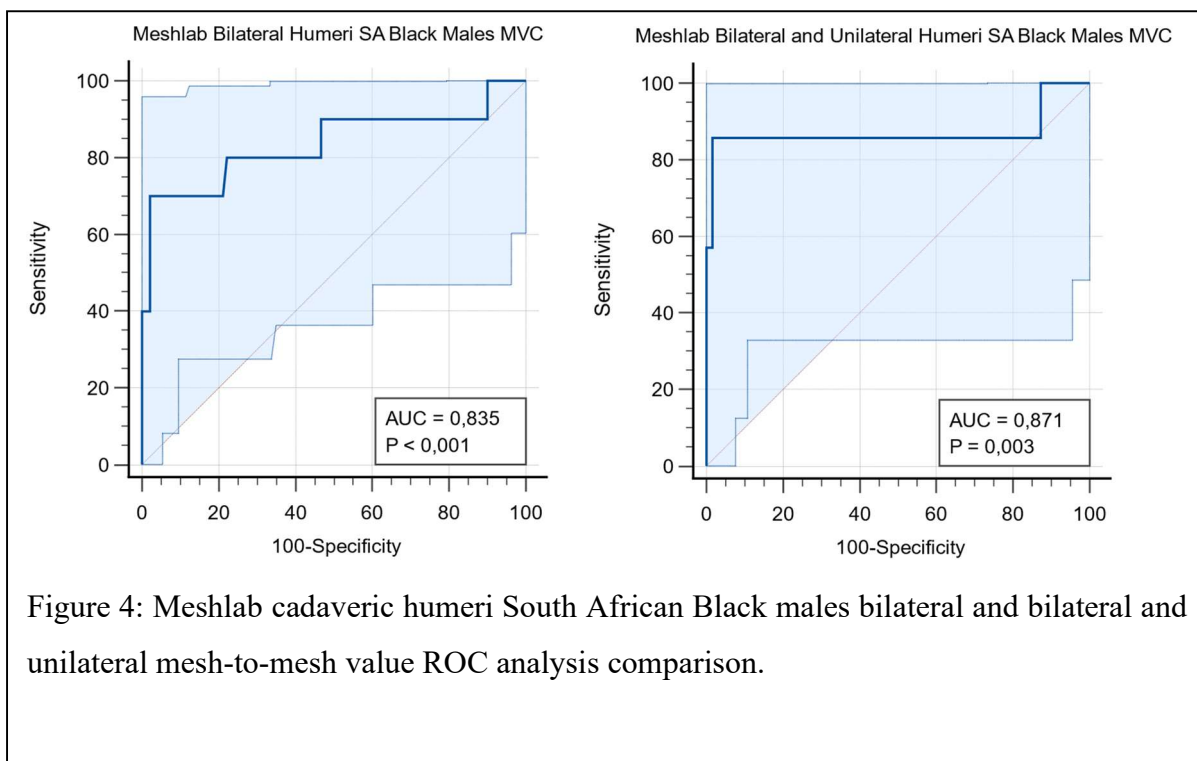


Figure 4: Meshlab cadaveric humeri females bilateral and bilateral and unilateral mesh-to-mesh value ROC analysis comparison.





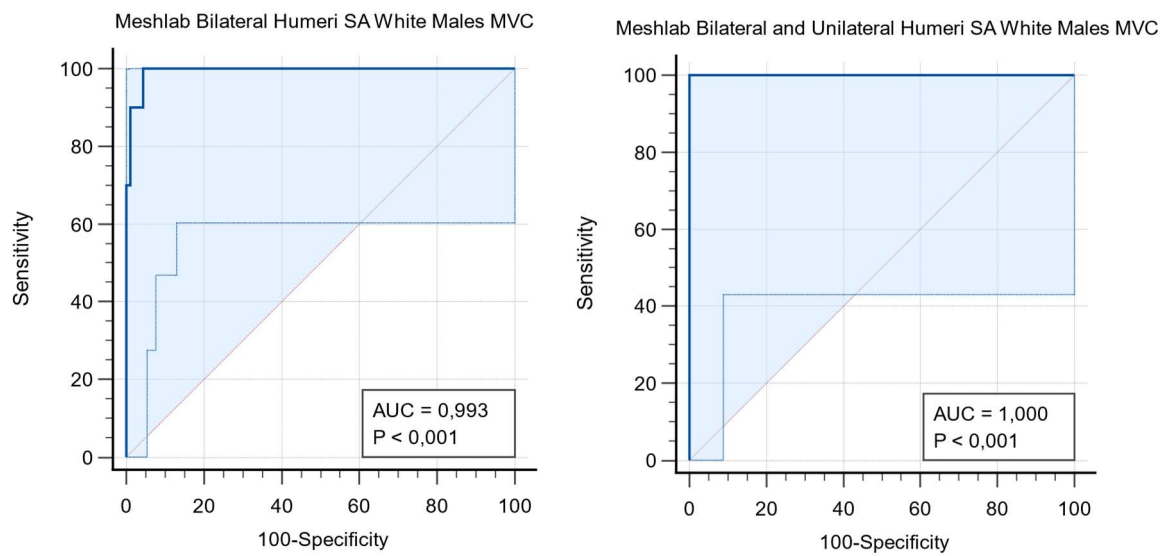


Figure 4: Meshlab cadaveric humeri South African White males bilateral and bilateral and unilateral mesh-to-mesh value ROC analysis comparison.

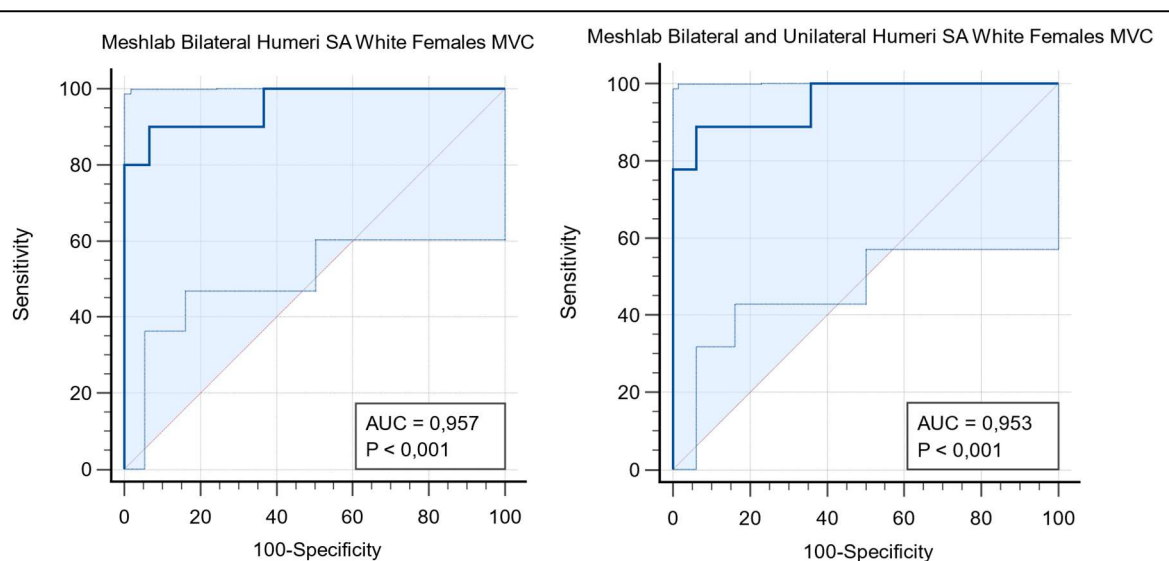
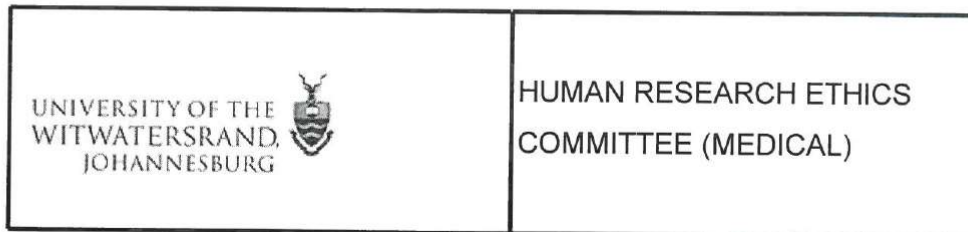


Figure 4: Meshlab cadaveric humeri South African White females bilateral and bilateral and unilateral mesh-to-mesh value ROC analysis comparison.



Office of the Deputy Vice-Chancellor (Research and Innovation)

**TO:** Ms K Pillay  
School of Anatomical Sciences  
Medical School  
University

E-mail: [2373351@students.wits.ac.za](mailto:2373351@students.wits.ac.za)

**CC:** Supervisor: Dr A Meyer and Mr R van der Merwe  
[Anja.Meyer@wits.ac.za](mailto:Anja.Meyer@wits.ac.za)  
and <[HREC-Medical Research Office@wits.ac.za](mailto:HREC-Medical Research Office@wits.ac.za)>

**FROM:** Mr Iain Burns  
Human Research Ethics Committee (Medical)  
Tel: 011 717 1252

E-mail: [Iain.Burns@wits.ac.za](mailto:Iain.Burns@wits.ac.za)

**DATE:** 2021/08/30

**REF:** R14/49

**PROTOCOL NO:** **M210715** (This is your ethics application reference number. Please quote it in all enquiries, oral or written, relating to this study.)

**PROJECT TITLE:** *Three-dimensional surface rendering and mesh-to-mesh comparisons as a method of pair-matching commingled human skeletal remains*

Please find attached the Clearance Certificate for the above project. I hope it goes well and that an article in a recognized publication comes out of it. This will reflect well on your professional standing and contribute to Government funding of the University.



MSWorks2000/Iain0007/Clearscan.wps

**SCHOOL OF ANATOMICAL SCIENCES ETHICS WAIVER CLEARANCE LETTER**

Faculty of Health Sciences  
School of Anatomical Sciences  
University of the Witwatersrand  
Johannesburg

Re: In terms of Chapter 8, sections 62-64 of the National Health Act No 61 of 2003, donated bodies and their tissues may be used for, among other purposes, health and research. Use of such material is subject only to permission from the responsible person in the School of Anatomical Sciences – the Head or person designated by the Head.

Human Research Ethics Committee (Medical) Clearance Certificate:

**W-CBP-210401-01**

This letter serves to confirm that the signatory of the ethics waiver as well as the Head of School, both based in the School of Anatomical Sciences, Faculty of Health Sciences, have reviewed the research proposal entitled: “Three-dimensional surface rendering and mesh-to-mesh comparisons as a method of pair-matching commingled human skeletal remains” and have granted clearance to access the blanket ethics waiver to conduct the abovementioned research study for materials held in the Raymond A Dart Collection of Human Skeletons.



**Professor M Steyn**  
Signatory: Ethics waiver

5 August 2021  
Dated



**Professor LA Schepartz**  
Head of School (acting)  
School of Anatomical Sciences

# Kamini Pillay\_2373351\_Final dissertation.pdf

## ORIGINALITY REPORT

<b>11</b> %	<b>10</b> %	<b>7</b> %	<b>2</b> %
SIMILARITY INDEX	INTERNET SOURCES	PUBLICATIONS	STUDENT PAPERS

## PRIMARY SOURCES

<b>1</b>	<b>era.ed.ac.uk</b> Internet Source	<b>1</b> %
<b>2</b>	<b>Submitted to University of Edinburgh</b> Student Paper	<b>1</b> %
<b>3</b>	<b>link.springer.com</b> Internet Source	<b>1</b> %
<b>4</b>	<b>www.researchgate.net</b> Internet Source	<b>&lt;1</b> %
<b>5</b>	<b>open.uct.ac.za</b> Internet Source	<b>&lt;1</b> %
<b>6</b>	<b>doi.org</b> Internet Source	<b>&lt;1</b> %
<b>7</b>	<b>docs.oracle.com</b> Internet Source	<b>&lt;1</b> %
<b>8</b>	<b>www.science.gov</b> Internet Source	<b>&lt;1</b> %
<b>9</b>	<b>Submitted to University of Witwatersrand</b> Student Paper	<b>&lt;1</b> %